FLUOROCARBON DERIVATIZATION OF SURFACE-INITIATED POLYMER FILMS VIA POST-POLYMERIZATION REACTIONS

By

Eric Lee Brantley

Dissertation

Submitted to the Faculty of the

Graduate School of Vanderbilt University

in partial fulfillment of the requirements

for the degree of

DOCTOR OF PHILOSOPHY

in

Chemical Engineering

December, 2005

Nashville, Tennessee

Approved:

Professor G. Kane Jennings

Professor Bridget Rogers

Professor Ken Debelak

Professor David Hercules

Professor Peter Cummings

To my parents, Stan and Lynne Brantley,

and my grandparents.

ACKNOWLEDGMENTS

I would like to thank my advisor, Dr. Kane Jennings, for his helpful guidance and support throughout my graduate work. I am appreciative of everything he has done for me, particularly for overseeing my professional development as a chemical engineering researcher, and am grateful for the three years I was able to work under his supervision. He has my utmost respect and admiration. I am also appreciative to the faculty members that comprised my Ph.D. committee: Dr. Bridget Rogers, Dr. Peter Cummings, Dr. Ken Debelak, and Dr. David Hercules. Each committee member provided constructive insight during my defense that served to make this work more complete, and I thank each of them for their time.

For financial support that made it possible to work with Dr. Jennings on this project, I acknowledge the National Science Foundation for a Graduate Research Fellowship. The experiments conducted in this work utilized equipment from outside sources. I would like to acknowledge Dr. Bridget Rogers for use of an ellipsometer, Dr. Tomlinson Fort for use of a contact angle goniometer, and the Vanderbilt Institute of Nanoscale Science and Engineering (VINSE) for use of AFM.

For the many people I have met during my career at Vanderbilt and who made life during these past four years very enjoyable, I am deeply grateful. Since I attended Vanderbilt for both my undergraduate and graduate degrees, I have gotten to know the faculty and staff of the chemical engineering department very well. I thank all of them for putting up with me all these years, aiding me numerous times in various ways, and for always being supportive of my efforts. Fellow graduate students and especially fellow

members of my research group have always been willing to help me in whatever way possible and have been a joy to work with. I am particularly grateful for the help of the following Jennings group members for their direct contributions to this research project: graduate students Mayker Bantz and Dongshun Bai and undergraduate students Tracy Holmes and Ian Snyder. Along with these four, I am grateful to Vorakan "Ten" Burapatana, Sean Hartig, John Hutson, Adam Broslat, Helen Kincaid, and Brad Berron for making my time in graduate school at Vanderbilt very memorable. I am grateful to God for having given me the opportunity to work with and meet these and many other wonderful people at Vanderbilt, and I wish all of you the best.

Finally, and most importantly, I am grateful for the unending support of my family, especially my parents. They raised me to strive to be the best at whatever I do but to be humble, recognizing that anything I accomplished was a gift from God. My academic career has now been completed with their full love and encouragement each step of the way. Thank you and may God continue to bless all of you.

TABLE OF CONTENTS

LIST OF TABLES

LIST OF FIGURES

CHAPTER I

INTRODUCTION

Polymeric Thin Films

With the tremendous recent focus on nanoscale science and engineering, an increasing need exists for high performance ultrathin films for use as coatings on surfaces.[1] Several obstacles must be addressed in order to provide new, engineered materials for various applications in this field. The ability to coat objects of any shape, not just flat surfaces, is important when considering the wide range of surfaces (nanoparticles, microchannels, etc) currently being used.[2-4] Along these lines, the ability to pattern films at interfaces in a straightforward manner can impact surface-directed or templated processes. Precise control over film thickness at the nanometer level, surface properties at the molecular level, and selectivity as to which materials are modified and the composition and placement of chemical moieties within the film represent ideal processing capabilities for molecularly engineered surfaces.[5] Films and coatings are used to alter surface and barrier properties of materials and can potentially meet the processing requirements for nanoscale science and engineering.[6] Thin polymer films offer an ideal tool for these purposes due to the large array of available polymers that can be used depending upon the specific application.[6] Tailoring bulk and surface properties of polymers, by either choosing an appropriate polymer initially or introducing desirable moieties by reaction with an existing polymer film, can enhance the use of these materials in separations[7] or in the protection or modification of metal surfaces.[8]

Fluorinated Polymer Films

Fluorinated polymer films are of particular interest due to the unique and useful properties they exhibit, including low critical surface energy, low dielectric constant, reduced friction, and enhanced chemical resistance.[9-12] Fluorinated polymers already have found use in a variety of applications including various coatings,[10] integrated circuit interconnects,[13] and biomedical materials.[14,15] They comprise a significant economic market, with approximately 100 million kg consumed annually.[9] For all of their desirable attributes and use in applications, however, fluorinated polymers are limited by difficult processibility and high expense.[10,16,17] Perfluoropolymers, polymers made up entirely of carbon and fluorine (i.e. poly(tetrafluoroethylene), or PTFE) are especially limited by these two issues. Furthermore, the precursor of PTFE is C_2F_4, a known carcinogen that is regulated by the Clean Air Act of 1990 (Section 112(r)). For these reasons, other avenues to harnessing the desirable properties of fluorinated polymers have been sought.

Processing of Partially Fluorinated Polymer Films

The most common method for circumvention of perfluoropolymer processibility issues is the use of partially fluorinated polymers. Since the most desirable fluoropolymer properties are typically the surface characteristics, only a small proportion of fluorocarbon need be introduced into a film in the interfacial region to affect surface properties. Furthermore, placing the expensive fluorocarbon groups only at the outer interface dramatically reduces production cost as compared to a perfluoropolymer. Fluorinated groups tend to phase separate from other chemical functionalities (including hydrocarbons) so that when in reasonable proximity to a surface, these groups

spontaneously migrate away from the bulk polymer and preferentially partition at the air-film interface, thus yielding fluoropolymer-like properties at very low overall concentrations.[9,10] Films that take advantage of partial fluorination are generally prepared by spin-coating,[18,19] solution-casting,[17,20,21] direct surface polymerization with fluorinated monomers,[16] plasma deposition,[22,23] or chemical adsorption.[24] These methods produce films with the properties of fluorinated polymers but often in a relatively uncontrolled fashion. Chemical adsorption produces only polymer monolayers.[24] Solution casting, spin coating, and plasma deposition are all limited to flat surfaces and result in films that are only physisorbed to the surface.[19,21,22] Spin-coating, unlike solution casting, does offer some control over film thickness in the sub-micron range, however. Plasma deposition offers greater control over film growth but requires low pressure and specialized equipment.[22] These methods often require curing at high temperatures after deposition to bring fluorocarbon moieties to the interface to enhance surface properties.

Surface-Initiated Polymerization of Partially Fluorinated Polymer Films

Surface-initiated polymerizations do not have many of the drawbacks encountered by these other film application methods. Surface-initiated polymerization, as the name implies, involves the following two steps: 1) anchoring of an initiator (typically a good leaving group that produces a radical or ion under proper conditions) and 2) polymerization directly from the surface-tethered initiator to grow the polymer film. Since these polymerizations occur directly from the surface, film thickness is readily controlled simply by varying polymerization time or other reaction conditions, and the

resulting polymer films are covalently anchored to the substrate. Finally, the method is applicable to both flat and rough substrates since single molecule diffusion is utilized to fill in all surface sites. Surface-initiated polymerization with a fluorinated monomer, however, results in only very thin fluorinated films and can be quite expensive.[16,25,26] To extend the applications of fluorinated polymer films, further developments in the ability to produce and use these films in numerous applications must be sought. Herein, an untapped method for enhancing and altering film properties by introduction of fluorocarbon (and similarly hydrocarbon) groups will be explored in great detail.

New Approach to Partially Fluorinated, Engineered Films

This research introduces a new methodology (Figure 1.1) for the preparation of well-defined polymer thin films and enables engineering of surfaces for different applications. In this new approach, we first grow surface-initiated polymer films by means of a controlled polymerization technique. The robust, covalently attached films can be grown on surfaces of any geometry and to desired thickness with nanometer-level control. Second, these polymer films contain side chains that can be modified chemically to add functionality to the films. Many different film compositions—fluorocarbons and hydrocarbons, for instance—may be employed and used in combination with one another to gain molecular-level control over film surface properties as well as bulk properties. Furthermore, unlike polymerizations in solution, there are no separations issues after reaction since the polymer film is anchored to the surface and unreacted species are simply washed away by rinsing. The numerous possibilities for growth and modification

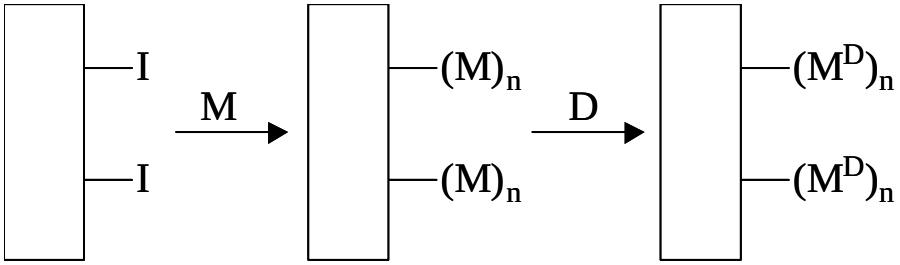

Figure 1.1. A general surface-initiated film preparation scheme is shown. I represents an initiator adsorbed to a surface. Upon exposure to a monomer, M, a polymer is grown from the initiated surface. If M has reactive sites, it may be reacted with a derivatizing species, D, to form a polymer film having derivatized repeat units, M^D.

of these films provide a direct avenue to molecularly engineered polymer films on surfaces.

This work will address the creation of relatively thick (up to 200 nm) polymer films through the use of a controlled surface-initiated polymerization followed by simple post-polymerization reactions. In light of the fact that fluorocarbons are generally useful for surface and bulk hydrophobicity, attaching fluorocarbon side chains via post-polymerization derivatization yields the ability to direct surface properties (wettability) or bulk structuring and hydrophobicity (barrier properties) of the films. The base idea of this work details the effect of side chain composition and length on the surface and barrier aspects of the resulting films. A variety of both fluorocarbon and hydrocarbon modifications can be made to direct and even tune film properties. Once a fundamental understanding of modification-properties relationships are developed, these same ideas can be transferred into engineering film properties in more advanced ways. As specifically demonstrated in this work, fluorocarbon-modified films may be hydrolyzed to retain a bulk fluorocarbon composition while allowing surface properties to be tuned using any of the modifications already characterized. Finally, microcontact printing may be used to pattern these engineered surfaces at a much smaller scale.

References

1. Lüning, J.; Yoon, D. Y.; Stöhr, J. "Importance of Structural Order for the Low Surface Energy of Perfluoroalkyl Substituted Polymethacrylates," *Journal of Electron Spectroscopy and Related Phenomena* **2001**, *121*, 265-279.

2. Bontempo, D.; Tirelli, N.; Masci, G.; Crescenzi, V.; Hubbell, J. A. "Thick Coating and Functionalization of Organic Surfaces Via ATRP in Water," *Macromolecular Rapid Communications* **2002**, *23*, 418-422.

3. Pyun, J.; Kowalewski, T.; Matyjaszewski, K. "Synthesis of Polymer Brushes Using Atom Transfer Radical Polymerization," *Macromolecular Rapid Communications* **2003**, *24*, 1043-1059.

4. Belder, D.; Ludwig, M. "Surface Modification in Microchip Electrophoresis," *Electrophoresis* **2003**, *24*, 3595-3606.

5. Matyjaszewski, K. "Macromolecular Engineering by Controlled/Living Ionic and Radical Polymerizations," *Macromolecular Symposia* **2001**, *174*, 51-67.

6. Edmondson, S.; Osborne, V. L.; Huck, W. T. S. "Polymer Brushes Via Surface-Initiated Polymerizations," *Chemical Society Reviews* **2004**, *33*, 14-22.

7. Balachandra, A. M.; Baker, G. L.; Bruening, M. L. "Preparation of Composite Membranes by Atom Transfer Radical Polymerization Initiated from a Porous Support," *Journal of Membrane Science* **2003**, *227*, 1-14.

8. Yasuda, H.; Yu, Q. S.; Chen, M. "Interfacial Factors in Corrosion Protection: An EIS Study of Model Systems," *Progress in Organic Coatings* **2001**, *41*, 273-279.

9. Grainger, D. W.; Stewart, C. W. "Fluorinated Coatings and Films: Motivation and Significance" In *Fluorinated Surfaces, Coatings, and Films*; Castner, D. G.; Grainger, D. W., Eds.; American Chemical Society: Washington, D.C., 2001; Vol. 787, pp 1-14.

10. Anton, D. "Surface-Fluorinated Coatings," *Advanced Materials* **1998**, *10*, 1197-1205.

11. Schmidt, D. L.; Coburn, C. E.; Dekoven, B. M.; Potter, G. E.; Meyers, G. F.; Fischer, D. A. "Water-Based Nonstick Hydrophobic Coatings," *Nature* **1994**, *368*, 39-41.

12. Kang, E. T.; Zhang, Y. "Surface Modification of Fluoropolymers Via Molecular Design," *Advanced Materials* **2000**, *12*, 1481-1494.

13. Mocella, M. T. "Fluorinated Compounds for Advanced IC Interconnect Applications: A Survey of Chemistries and Processes," *Journal of Fluorine Chemistry* **2003**, *122*, 87-92.

14. Tarnowski, D. J.; Bekos, E. J.; Korzeniewski, C. "Oxygen-Transport Characteristics of Refunctionalized Fluoropolymeric Membranes and Their Application in the Design of Biosensors Based Upon the Clark-Type Oxygen Probe," *Analytical Chemistry* **1995**, *67*, 1546-1552.

15. Bekos, E. J.; Ranieri, J. P.; Aebischer, P.; Gardella, J. A.; Bright, F. V. "Structural-Changes of Bovine Serum-Albumin Upon Adsorption to Modified Fluoropolymer Substrates Used for Neural Cell Attachment Studies," *Langmuir* **1995**, *11*, 984-989.

16. Jung, D. H.; Park, I. J.; Choi, Y. K.; Lee, S. B.; Park, H. S.; Rühe, J. "Perfluorinated Polymer Monolayers on Porous Silica for Materials with Super Liquid Repellent Properties," *Langmuir* **2002**, *18*, 6133-6139.

17. Li, K.; Wu, P. P.; Han, Z. W. "Preparation and Surface Properties of Fluorine-Containing Diblock Copolymers," *Polymer* **2002**, *43*, 4079-4086.

18. Genzer, J.; Sivaniah, E.; Kramer, E. J.; Wang, J. G.; Korner, H.; Xiang, M. L.; Char, K.; Ober, C. K.; DeKoven, B. M.; Bubeck, R. A.; Chaudhury, M. K.; Sambasivan, S.; Fischer, D. A. "The Orientation of Semifluorinated Alkanes Attached to Polymers at the Surface of Polymer Films," *Macromolecules* **2000**, *33*, 1882-1887.

19. Tirelli, N.; Ahumada, O.; Suter, U. W.; Menzel, H.; Castelvetro, V. "Investigation on the Wettability Properties of Thin Films of Methacrylic Polymers with Partially Fluorinated Side Chains," *Macromolecular Chemistry and Physics* **1998**, *199*, 2425-2431.

20. van Ravenstein, L.; Ming, W.; van de Grampel, R. D.; van der Linde, R.; de With, G.; Loontjens, T.; Thune, P. C.; Niemantsverdriet, J. W. "Low Surface Energy Polymeric Films from Novel Fluorinated Blocked Isocyanates," *Macromolecules* **2004**, *37*, 408-413.

21. Sivakumar, C.; Wen, T. C.; Gopalan, A.; Teng, H. "Electroactive Conducting Blends of Poly(O-Toluidine) and Poly(Vinylidene Fluoride) and Characterisation," *Synthetic Metals* **2003**, *132*, 219-226.

22. Mackie, N. M.; Castner, D. G.; Fisher, E. R. "Characterization of Pulsed-Plasma-Polymerized Aromatic Films," *Langmuir* **1998**, *14*, 1227-1235.

23. Feichtinger, J.; Galm, R.; Walker, M.; Baumgartner, K. M.; Schulz, A.; Rauchle, E.; Schumacher, U. "Plasma Polymerized Barrier Films on Membranes for Direct Methanol Fuel Cells," *Surface & Coatings Technology* **2001**, *142*, 181-186.

24. Fukushima, H.; Seki, S.; Nishikawa, T.; Takiguchi, H.; Tamada, K.; Abe, K.; Colorado, R.; Graupe, M.; Shmakova, O. E.; Lee, T. R. "Microstructure, Wettability, and Thermal Stability of Semifluorinated Self-Assembled Monolayers (SAMs) on Gold," *Journal of Physical Chemistry B* **2000**, *104*, 7417-7423.

25. Granville, A. M.; Boyes, S. G.; Akgun, B.; Foster, M. D.; Brittain, W. J. "Synthesis and Characterization of Stimuli-Responsive Semifluorinated Polymer Brushes Prepared by Atom Transfer Radical Polymerization," *Macromolecules* **2004**, *37*, 2790-2796.

26. Granville, A. M.; Boyes, S. G.; Akgun, B.; Foster, M. D.; Brittain, W. J. "Thermoresponsive Behavior of Semifluorinated Polymer Brushes," *Macromolecules* **2005**, *38*, 3263-3270.

CHAPTER II

BACKGROUND

Surface-Initiated Polymerizations

Major advances in the solution-phase synthesis of polymers have yielded unprecedented control over macromolecular composition, molecular weight, and polydispersity index (PDI) to enable the preparation of extremely well-defined polymeric materials.[1-3] Within the past few years, many of these advances have been extended to surfaces in the creation of polymer films and coatings. To form robust attached films, one end of the polymer chains must be functionalized to adhere to the surface. If polymer chains have been grown in solution and then are applied to a substrate, both steric effects and diffusional limitations arise when trying to pack the chains on a surface.[4] Once several of the chains attach to the surface, they prevent the subsequent diffusion and placement of more chains, and the packing density is greatly limited. If, however, the polymer chains are simultaneously grown from the entire surface, the chain density can be maximized and diffusional effects minimized since the monomer must only be present at the outer, growing chain end. Hence, only a procedure involving direct, surface-initiated growth of a polymer film can achieve well-packed, covalently attached surface films. This so-called surface-initiated polymerization strategy offers several advantages over traditional methods for preparing polymer films and coatings, including (1) improved adhesion due to a chemical coupling of the initiator/polymer chain to the substrate, (2) the ability to prepare uniform, conformal coatings on objects of

any shape,[5] (3) excellent control over film thickness,[6] from a few nanometers up to the micron level[5] in some cases, (4) tunable grafting densities, based on the surface coverage of the initiator, (5) simplified separations issues, since the polymer is grown from a support, and (6) good control over depth-dependent composition by growing additional blocks to prepare copolymer films.[7-9] Due to these processing advantages, surface-initiated polymerizations have been utilized to functionalize or modify nanostructures and particles,[10-17] chromatography media,[18-23] and porous supports,[24-26] to prepare environmentally responsive brushes that alter their conformation upon exposure to a stimulus,[8,24,27-30] to provide a barrier against etching,[31,32] to serve as a dielectric layer in a device,[5] and to prevent or reduce biological adsorption.[33,34]

In general, surface-initiated polymerizations require the immobilization of appropriate initiator groups onto the surface prior to polymerization, typically achieved by preparing a self-assembled monolayer (SAM) from initiator-terminated adsorbates. These adsorbates are often synthesized to contain thiol[4,5,35] or disulfide[36,37] head groups to enable chemisorption at gold and other coinage metals or chlorosilane[4,7,18,38] head groups for modification of oxide surfaces of silicon. In some cases, the simplest route is to chemically couple the initiator to an existing SAM, for example, by exposing a hydroxyl-terminated monolayer to a functionalized initiator.[39,40] In addition, initiator groups can often be anchored to polymers and other materials that present or are modified to present carboxylic acid-[11,41] or alcohol-rich[42] surfaces.

There are many different classes of surface-initiated polymerizations as defined by the chemical mechanism for propagation, including anionic, cationic, ring-opening (ROP), radical, the more specific atom transfer radical (ATRP), and ring-opening

metathesis (ROMP). The general types of initiators and monomers used for each method and some key advantages and disadvantages of each approach are summarized in Table 2.1. Living anionic routes[4,43-45] are highly controlled polymerizations that enable the preparation of chains with low polydispersity and films with complex polymer architectures. However, the growth rates for anionic polymerizations are rather slow such that long exposure times (a few days) are commonly required to produce films with thicknesses of 10 – 20 nm at room temperature.[4] These polymerizations are also extremely sensitive to moisture and impurities.[4] Cationic polymerizations[1,46,47] exhibit many of the same advantages and disadvantages as anionic polymerizations but tend to propagate a bit faster and are generally not as controlled due to higher termination rates. Traditional radical polymerizations generally exhibit more rapid kinetics, often with significant loss of control, and are compatible with a wide variety of monomers, including those that contain polar or unprotected functional groups.[21,39] Unlike most other methods, traditional radical polymerizations do not allow the reactivation of chain ends to prepare block copolymer films. A specific class of controlled radical polymerizations, ATRP,[2,7] has become the most popular approach for preparing thin films due in part to the wide variety of vinyl monomers that can be polymerized and the ability to prepare films with different blocks by reactivating chain ends.[8,9,27] ATRP also tolerates moisture; in fact, for polar monomers, the kinetics of polymerization is greatly accelerated when water is used as solvent.[6,37] PDIs for ATRP chains are generally below 1.5,[2] lower than those for traditional radical polymerizations. ROP proceeds by either cationic[16] or anionic[44] mechanisms and is used to produce linear polymers from cyclic monomers. ROMP exhibits rapid kinetics under mild conditions but is somewhat limited

Table 2.1. Commonly studied monomers and initiators for some different surface-initiated polymerization (SIP) techniques and key advantages and disadvantages of each technique.

SIP Type	Initiators	Monomers	Advantages	Disadvantages	References
Anionic	Diphenyl-ethylene (activated by BuLi)	Vinyl	Low PDI, living (dienes and styrenes only)	Affected by moisture and impurities, slow kinetics	[4, 43]
Cationic	Triflate, $-OCH_3$	Vinyl, propylene glycol	Larger propagation rate constants than anionic	Affected by moisture and impurities	[46,47]
Radical	Azo compounds	Vinyl	Allows monomers having polar functional groups	Cannot form block or graft copolymers	[21,39]
ATRP	Haloesters, halides	Vinyl	Rapid kinetics in water, can form multiple blocks, chemical diversity	Higher PDI than ionic, difficult with acidic monomers	[6,7,36]
ROP	Triflate, tin(II) octoate	Cyclic esters, oxazolines, glycidol	Preparation of biologically important polymers	Limited chemical diversity	[16,44]
ROMP	Ruthenium carbenes	Norbornenes	Mild reaction conditions, thick films	Limited chemical diversity	[5,13,49]

compositionally.[5,19,48-50] The predominate ROMP monomer studied in surface-initiated cases has been norbornene and its functional derivatives. Surface-initiated polymerizations may be used in a variety of contexts, including the modification of planar surfaces, in microfabrication or nanofabrication, and in the modification of nonplanar surfaces and particles. Typically, surface properties are altered using these methods, yielding changes in surface-environment interactions.

The ability to modify and control the surface properties of materials has become increasingly important due in part to the recent emergence of nanostructured materials where surface area to volume ratios are high. Successful control over surface properties, such as wettability, adhesion, and adsorption, relies on engineering the composition and structure at the outer few angstroms of a material. Within the past 20 years, SAMs have been utilized widely to modify surface properties due to their ability to present a two-dimensional sheet of dense, homogeneous chemical functionality at a surface. Limitations of SAMs have included the difficulty in producing films thicker than a few nanometers[51] and the finite stability of these molecular films.[52,53] Since the stability of tethered organic films generally improves with molecular weight (and thickness) due to increased interchain interactions,[54] surface-initiated polymerizations provide a controlled method to greatly amplify the thickness and stability of molecular films. In addition, surface-initiated films can be synthesized and engineered to exhibit interesting dynamic behavior, such as stimuli-driven conformational changes that affect wettability or biological adhesion. To date, surface-initiated films have been used widely to alter surface wettability,[25,55-58] reduce protein adsorption,[34] and affect adhesion at a surface.[29,59]

Literature Examples of Surface-Initiated Polymerizations on Planar Surfaces

Stimuli-Responsive Films

Another attractive feature of surface-initiated polymer films, particularly in very thin (<30 nm) films, is the ability to prepare loosely packed, stimuli-responsive brushes that alter their conformation upon changes in the environment. This reversibility of conformation enables "switchable" surface properties, which could lead to applications in sensors as well as "smart" membranes and fabrics. ATRP enables the preparation of di- and triblock copolymer films from a wide range of monomers where each block has a different interaction with a solvent to provide the framework for a solvent-sensitive film. Brittain and coworkers[8] have used ATRP to develop solvent-responsive films from ABA type triblock copolymer brushes where the middle block has different physicochemical properties than the end blocks. The film adopted an extended brush configuration when exposed to a good solvent for all the blocks but adopted a folded brush conformation when exposed to a good solvent for the middle block. Using a ~15 nm poly(methyl acrylate) (PMA)-*block*-polystyrene (PS)-*block*-PMA film grown from silicon and initially exposed to dichloromethane (good solvent for all the blocks), the advancing water contact angle changed by ~20° upon exposure to cyclohexane (good solvent for PS). Brittain and coworkers have shown that this difference in wettability upon solvent exposure can be amplified to ~40° using diblock films with PMA as the lower block and poly(pentafluorostyrene) as the upper block on Si/SiO_2.[27]

Barrier Coatings

Due to the ability to produce dense, conformal layers of controlled thickness and composition over any surface topology, surface-initiated polymer films have potential impact as dielectric layers in the preparation of low-cost, light-weight organic thin film transistors. Rutenberg et al.[5] have used ROMP to prepare polynorbornene dielectric layers atop a gold strip gate electrode on silicon. The use of ROMP enables mild conditions and rapid access to sufficiently thick films (1.2 μm) that exhibit low capacitances (3 nF/cm^2) and are essentially pinhole free. The polynorbornene film provided a conformal coating over the electrode and was subsequently used to support a thin, vapor-deposited film of pentacene (semiconductor) before the entire structure was pressed against a PDMS substrate that contained two gold strips as drain and source electrodes. The resulting FET exhibited mobility ranges of 0.1–0.3 cm^2/V s and on/off ratios of 10–100. While polynorbornene films function well here, the future investigation of other film compositions with even lower dielectric constants could lead to further improvements in dielectric properties at reduced film thicknesses. This work nicely illustrates a case where the characteristics of surface-initiated polymerizations well match the needs of an emerging technology.

Effective barrier films for applications in etch resistance and membrane separations may also be created using surface-initiated approaches. As a case in point, Bruening and coworkers[26] have used fluorocarbon-modified polyhydroxyethyl methacrylate (PHEMA) as an ultrathin (~50 nm) dense outer skin grown atop a gold-coated porous alumina membrane for separation of gases. While unmodified PHEMA provides little or no selectivity, fluorinated PHEMA exhibits selectivities of 8–9 for

CO_2/N_2 and CO_2/CH_4. Bruening and coworkers[26] also showed that cross-linked poly(ethylene glycol dimethacrylate) (PEGDMA) skins grown atop polyelectrolyte-coated alumina membranes exhibited an enhanced selectivity of ~20 for CO_2/N_2. The high level of control over thickness and composition of these surface-initiated films and the ability to initiate their growth from different surfaces—in this latter case, a polyelectrolyte layer atop porous alumina—is highly advantageous in the preparation of dense membrane skins. They have more recently extended the fluorinated PHEMA films to pervaporation membranes and demonstrated extremely high fluxes and VOC/water selectivities as high as 500 with film thickness <200 nm.[60]

Patterning Polymer Films

The ability to pattern surface-initiated polymer films can lead to advances in surface-directed events and in microfabrication. The patterning of surface-initiated polymer films has been achieved by various methods that each succeed in localizing initiator-terminated groups on the surface. The most common method is to microcontact print an inert alkanethiol and subsequently backfill the pattern with an active thiol or disulfide to initiate polymerization locally.[31,36] Another method uses ultraviolet light through a mask to irradiate and activate an initiator layer for subsequent polymerization in selective regions.[61] These methods generally enable rapid patterning of fairly large surface areas (up to a few cm^2) but have not yet been reliably used to achieve submicron polymeric features. Irradiation with an electron beam (instead of uv light) has produced features as small as 70 nm with good throughput.[62] Methods based on the use of AFM tips can either remove and backfill (nanoshaving)[30] or deposit (dip pen

nanolithography)[50] molecular components and offer the capability to produce submicron features and to control feature composition in a site-specific manner. Nonetheless, throughput is an issue with scanning probe methods, and to be successful, these methods require the user to develop a significant expertise.

Hawker and coworkers[31,36] reported the first patterning of surface-initiated polymer films based on microcontact printing. They prepared patterned ultrathin films of poly(caprolactone) by ROP or poly(methyl methacrylate) (PMMA), PHEMA, and others by ATRP. More hydrophobic polymers were observed to greatly resist the penetration of aqueous-phase etchants and reduced the rate of etching by two orders of magnitude over that of the initiator SAM. In this manner, the polymer greatly amplifies the etch resistance of the SAM.

To achieve a similar goal, Zhou et al.[32] exposed PMMA and PHEMA films prepared by surface-initiated ATRP to ultraviolet irradiation through a TEM grid to completely remove the polymer brush and initiator in the irradiated regions. They then electrodeposited conducting polypyrrole microstructures in the bare regions of the surface or exposed the patterned films to etchants to create polymer-capped gold microstructures. While hydrophobic PMMA films exhibited good etch resistance, hydrophilic PHEMA films did not. Nonetheless, capping the hydroxyl groups of PHEMA by reaction with trimethylchlorosilane greatly improved the etch resistance of the films.

Literature Examples of Surface-Initiated Polymerizations on Nonplanar Surfaces

As compared with traditional methods of applying polymer films, surface-initiated approaches provide a key advantage in their ability to uniformly coat nonplanar

surfaces. A variety of nonplanar surfaces have been used as supports for polymerization, including gold,[13,16] silica,[15,18,19,21,22,24,63] clay,[64] latex,[14] dextran,[42] polystyrene,[65,66] and magnetite[67] particles, and carbon nanotubes.[10,11,68-71] This list is only a sampling of possible surfaces from which polymerization can be performed,[72] as any surface may be suitable if it can be functionalized with an initiator species. Furthermore, many surface-initiated polymerization techniques have been used to accomplish these modifications, including ROP,[16] ROMP,[13,19] free radical,[21,63,64,67,68] ATRP,[10,11,14,18,24,42,65,66,70-72] and anionic[69] routes.

With a focus on the ability to tailor properties at the molecular level, surface-initiated techniques are increasingly finding use in modification of nonplanar substrates. The most common reason for modification of particles, nanotubes, and supports is to alter interactions of these materials with the surrounding environment, and thin polymer layers offer a straightforward way to accomplish this. Modification of a particle, for instance, with an initiator allows subsequent controlled polymerization to occur equally from the entire surface area, allowing tremendous control over film growth and properties. Surface-initiated techniques enhance the dispersion or solvation of particles and nanotubes and alter composition for materials in separations processes.

A large volume of work has been devoted to nonplanar surfaces in a few key research areas: chromatographic supports, nanoparticles, and nanotubes. Work in separations has focused on functionalization of materials to improve selectivity while nanotube and particle work has been concerned mainly with increasing the dispersion of these materials in solvents, constructing a polymer layer around a particle to protect from chemical or mechanical attack, or preparing well-defined nanoscale structures.

Separation Media

Modification of surfaces for use in separations processes has been widely used in recent years to improve selectivity.[19,20,26] The tremendous control over uniformity, thickness, and composition offered by surface-initiated polymerization techniques is again the reason they have found use in these applications. Of particular interest in this area, work by Buchmeiser and coworkers has centered on the use of ROMP to grow functionalized norbornenes from silica surfaces.[20,73,74] For the chromatographic separation of phenols, anilines, lutidines, and hydroxyquinolines, they have demonstrated the ability to grow poly(norborn-2-ene), poly(7-oxanorborn-2-ene-5,6 dicarboxylic acid), or copolymers of these two compounds on silica supports.[20] As compared to supports created by coating solution polymers onto silica, which tends to clog pores and reduce surface area, the surface-initiated supports provided much improved separations.

Micro- and Nanoparticles

A significant amount of interest has been shown in the surface-initiated modification of particles, both on the nanometer and micron size scales. For the most part, research on particles has focused on increasing their solubility or dispersibility in solutions by augmenting their interactions with solvents while some work has focused on materials synthesis. Of the considerable work in this latter area, Mandal et al.[75] and more recently Blomberg et al.[63] have utilized nanoscale particles as scaffolds to prepare hollow, polymeric capsules. Blomberg et al.[63] grafted poly(styrene-co-vinylbenzocyclobutene) or poly(styrene-co-maleic anhydride) onto silica nanoparticles (600 nm) via a free radical polymerization to create core-shell nanoparticles. Similar

polymer modifications have been used on numerous particles to impart desirable surface interactions, such as to increase solubility or to protect the inner core material while maintaining its properties. However, since the desired application in these cases was not to improve particle-solvent interactions but to create hollow nanospheres, the choice of monomers was driven by one simple factor, the ability to exhibit crosslinking. To facilitate crosslinking in the polymer films surrounding the core, the benzocyclobutene group exhibits intermolecular coupling at elevated temperatures or maleic anhydride may be reacted with a diamine compound. After polymerization and crosslinking, the inner silica core was chemically etched away with HF to reveal a nanocapsule. Only with the maleic anhydride polymer was the crosslinking sufficiently robust to withstand the conditions of core removal, enabling the nanocapsules to remain intact after processing. Control over the structural integrity of a system such as this allows for applications in drug and dye encapsulation upon infusion and other areas where protection or gradual release of an inner substance is desirable.

Carbon Nanotubes

Due to their extraordinary mechanical and electrical properties, carbon nanotubes have the potential to be used in a variety of applications (molecular wires, sensors, and in composite materials) but are limited by poor solubility in most solvents that dramatically hinders their processibility.[11,71] Covalent modifications of the nanotube surfaces tend to destroy the structure or properties of the nanotubes because a large number of sidewall carbons (at least 1 in 10) must be modified to achieve desirable solubility.[10] However, surface initiated techniques can achieve good solubility while minimally altering

nanotube structure by growing polymer from 1 in ~250 sidewall carbons.[10] Only a handful of examples of surface-initiated polymerization from carbon nanotubes exist in the literature.[10,11,68-71] Qin et al.[11] grew PS from carbon nanotubes using ATRP and found, as have other groups that perform surface-initiated polymerization from carbon nanotubes, that the starting carbon nanotube bundles tend to separate into smaller bundles or even individual tubes during modification. Furthermore, the PS exterior resulted in good dissolution of the nanotubes into common organic solvents.[11] Kong et al.[70] took this general approach (but using PMMA instead of PS) one step further. As has often been achieved on planar surfaces using ATRP (since chain ends may be reactivated by addition of a transition metal species), they grew a second polymer layer atop the PMMA layer. They chose a functional polymer (PHEMA) for this second layer, thus yielding a nanotube surrounded by a nonpolar PMMA layer which itself was surrounded by a more polar PHEMA layer. The resulting solubility of the block copolymer-grafted nanotube was dependent on solvent, with good solvents for PHEMA providing effective solvation. This methodology, adapted from work on simpler planar surfaces, may find use in creating novel devices and materials from functionalized carbon nanotubes and further demonstrates the wide applicability of surface-initiated polymerization techniques.

Overview of Dissertation

The work contained herein is focused on surface-initiated ATRP, a controlled free radical polymerization technique that allows a high level of control over film growth,[6,7,37,40,76] and post-polymerization modifications to films. ATRP has become one of the most popular controlled polymerization methods due to the wide array of available

monomers and a propagation that is not highly sensitive to many impurities. The mechanism for ATRP polymer chain growth has been discussed extensively by Matyjaszewski and others.[1,2,77] As shown in Figure 2.1, a halide-terminated alkyl initiator is converted to a radical by a Cu^{I} species, which in turn is oxidized to Cu^{II}. The active radical can then add to a monomer with a double bond, creating a new species with the radical now transferred to the end of the polymerized chain. Propagation may continue by adding more monomers or the process may be deactivated at any time by recombining with Cu^{II}. To minimize termination reactions, a relatively low concentration of radical species should be maintained. This is accomplished, as evident from Figure 2.1, by simply adding deactivating Cu^{II} species to the solution initially. Adding a greater amount of Cu^{II} to the reaction slows the polymerization but also improves the polydispersity of the resulting polymer.[7]

ATRP in solution has been performed extensively on numerous vinyl monomers with recently increasing focus on growing films from a surface. When ATRP was originally applied to the surface-initiated case, polymerization kinetics was slowed tremendously due to an increase in termination reactions.[7,76] Growth of thick polymer films using traditional ATRP is, therefore, somewhat problematic. Accordingly, ATRP and other controlled polymerization techniques have difficulty growing thick surface-initiated partially fluorinated films. In fact, relatively few surface-initiated polymerizations involving direct growth of partially fluorinated polymer films from fluorinated monomers have even been conducted. Park, Rühe, and coworkers[25] prepared ultrahydrophobic surfaces by polymerizing perfluoroalkylethyl acrylates via a radical mechanism onto the surface of porous silicon (up to ~70 nm thick films). Andruzzi et

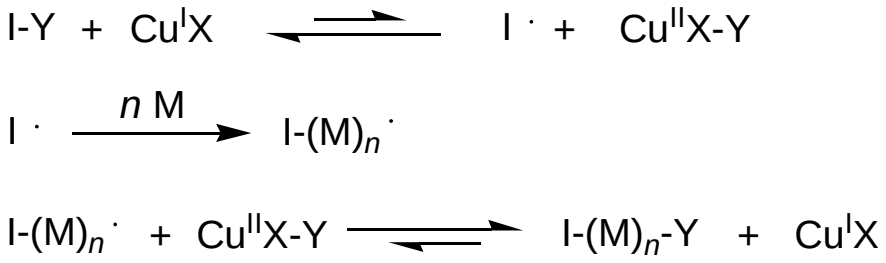

Figure 2.1. General ATRP polymerization scheme, including activation, propagation, and deactivation steps. X and Y are halogens, and M is a monomer having vinyl functionality.

al.[78] utilized surface-initiated nitroxide-mediated radical polymerization on silica to grow diblock copolymer films having an outer polystyrene block (up to 11 nm thick) with semifluorinated alkyl side chains. Brittain and coworkers[27] used surface-initiated ATRP on silica to grow diblock copolymer films having either perfluorinated polystyrene or perfluorinated acrylate outer blocks of thickness <5 nm. In each of these examples, inclusion of the semifluorinated groups was primarily to induce hydrophobicity, but film thickness was typically low.

Recent efforts to increase surface-initiated growth rates have relied on innovations in solution-phase ATRP. Researchers have shown that water and other polar solvents increase polymerization kinetics while still maintaining good kinetic control.[79-82] Bruening, Baker, and coworkers[6] have remarkably and successfully extended this water-accelerated ATRP strategy to prepare surface-initiated films of PHEMA with controlled thickness of up to 700 nm. Furthermore, the ability to derivatize the reactive hydroxyl side chains of PHEMA after film growth has been demonstrated. Bruening, Baker, and coworkers used low-molecular-weight hydrocarbon acid chlorides in an acylation reaction.[6] Other recent work has exploited the hydroxyl groups of PHEMA by reaction with trimethylchlorosilane to make the film more hydrophobic and improve its etch resistance.[32] Kraft and Moore have investigated the effects of reacting PHEMA microgels with hydrocarbon acid chlorides (ranging from m = 1 to 15) to form fatty acid layers that delay microgel expansion.[83] They found that acetyl-modified and unmodified microgels expand readily, that rather short (m = 4) alkyl chains offer maximum resistance to microgel expansion, and that as the chain length is further increased, the resistance decreases. These methods provide insight toward an alternative strategy for preparation

of derivatized (i.e. partially fluorinated) polymer films. Use of water-accelerated surface-initiated ATRP followed by various chemical modifications of the polymer allows us to use a base film as a test stage for creation of numerous polymer films with varying chemical composition and film properties.

Specific Focus of Dissertation

The primary objectives of this research, which will be addressed in subsequent chapters, are the following:

1. Grow surface-initiated polymer films on gold, with side chains that can be reacted to introduce fluorocarbon functionality. Characterize surface, structural, and barrier properties upon modification with different fluorocarbon groups.
2. Modify polymer side chains with hydrocarbons. Evaluate dependence of film properties on alkyl chain length. Compare properties of hydrocarbon films with those of fluorocarbon films.
3. Combine film modifications to create copolymer films. Surface and bulk properties can be tailored by reaction with different species.
4. Pattern polymer films onto a surface via microcontact printing. Demonstrate the ability to grow and derivatize well-defined polymer patterns on a surface, and explore the modification of fluorocarbon-modified films using a reactive printing technique.

References

1. Matyjaszewski, K. "Macromolecular Engineering by Controlled/Living Ionic and Radical Polymerizations," *Macromolecular Symposia* **2001**, *174*, 51-67.

2. Wang, J. S.; Matyjaszewski, K. "Controlled Living Radical Polymerization - Atom-Transfer Radical Polymerization in the Presence of Transition-Metal Complexes," *Journal of the American Chemical Society* **1995**, *117*, 5614-5615.

3. Shea, K. J.; Walker, J. W.; Zhu, H.; Paz, M.; Greaves, J. "Polyhomologation. A Living Polymethylene Synthesis," *Journal of the American Chemical Society* **1997**, *119*, 9049-9050.

4. Advincula, R.; Zhou, Q. G.; Park, M.; Wang, S. G.; Mays, J.; Sakellariou, G.; Pispas, S.; Hadjichristidis, N. "Polymer Brushes by Living Anionic Surface Initiated Polymerization on Flat Silicon (SiOx) and Gold Surfaces: Homopolymers and Block Copolymers," *Langmuir* **2002**, *18*, 8672-8684.

5. Rutenberg, I. M.; Scherman, O. A.; Grubbs, R. H.; Jiang, W. R.; Garfunkel, E.; Bao, Z. "Synthesis of Polymer Dielectric Layers for Organic Thin Film Transistors Via Surface-Initiated Ring-Opening Metathesis Polymerization," *Journal of the American Chemical Society* **2004**, *126*, 4062-4063.

6. Huang, W. X.; Kim, J. B.; Bruening, M. L.; Baker, G. L. "Functionalization of Surfaces by Water-Accelerated Atom-Transfer Radical Polymerization of Hydroxyethyl Methacrylate and Subsequent Derivatization," *Macromolecules* **2002**, *35*, 1175-1179.

7. Matyjaszewski, K.; Miller, P. J.; Shukla, N.; Immaraporn, B.; Gelman, A.; Luokala, B. B.; Siclovan, T. M.; Kickelbick, G.; Vallant, T.; Hoffmann, H.; Pakula, T. "Polymers at Interfaces: Using Atom Transfer Radical Polymerization in the Controlled Growth of Homopolymers and Block Copolymers from Silicon Surfaces in the Absence of Untethered Sacrificial Initiator," *Macromolecules* **1999**, *32*, 8716-8724.

8. Boyes, S. G.; Brittain, W. J.; Weng, X.; Cheng, S. Z. D. "Synthesis, Characterization, and Properties of Aba Type Triblock Copolymer Brushes of Styrene and Methyl Acrylate Prepared by Atom Transfer Radical Polymerization," *Macromolecules* **2002**, *35*, 4960-4967.

9. Kim, J.-B.; Huang, W.; Bruening, M. L.; Baker, G. L. "Synthesis of Triblock Copolymer Brushes by Surface-Initiated Atom Transfer Radical Polymerization," *Macromolecules* **2002**, *35*, 5410-5416.

10. Qin, S. H.; Oin, D. Q.; Ford, W. T.; Resasco, D. E.; Herrera, J. E. "Polymer Brushes on Single-Walled Carbon Nanotubes by Atom Transfer Radical Polymerization of N-Butyl Methacrylate," *Journal of the American Chemical Society* **2004**, *126*, 170-176.

11. Qin, S. H.; Qin, D. Q.; Ford, W. T.; Resasco, D. E.; Herrera, J. E. "Functionalization of Single-Walled Carbon Nanotubes with Polystyrene Via Grafting to and Grafting from Methods," *Macromolecules* **2004**, *37*, 752-757.

12. Advincula, R. C. "Surface Initiated Polymerization from Nanoparticle Surfaces," *Journal of Dispersion Science and Technology* **2003**, *24*, 343-361.

13. Watson, K. J.; Zhu, J.; Nguyen, S. T.; Mirkin, C. A. "Hybrid Nanoparticles with Block Copolymer Shell Structures," *Journal of the American Chemical Society* **1999**, *121*, 462-463.

14. Guerrini, M. M.; Charleux, B.; Vairon, J. P. "Functionalized Latexes as Substrates for Atom Transfer Radical Polymerization," *Macromolecular Rapid Communications* **2000**, *21*, 669-674.

15. Chen, X. Y.; Armes, S. P.; Greaves, S. J.; Watts, J. F. "Synthesis of Hydrophilic Polymer-Grafted Ultrafine Inorganic Oxide Particles in Protic Media at Ambient Temperature Via Atom Transfer Radical Polymerization: Use of an Electrostatically Adsorbed Polyelectrolytic Macroinitiator," *Langmuir* **2004**, *20*, 587-595.

16. Jordan, R.; West, N.; Ulman, A.; Chou, Y. M.; Nuyken, O. "Nanocomposites by Surface-Initiated Living Cationic Polymerization of 2-Oxazolines on Functionalized Gold Nanoparticles," *Macromolecules* **2001**, *34*, 1606-1611.

17. Tsujii, Y.; Ejaz, M.; Sato, K.; Goto, A.; Fukuda, T. "Mechanism and Kinetics of Raft-Mediated Graft Polymerization of Styrene on a Solid Surface. 1. Experimental Evidence of Surface Radical Migration," *Macromolecules* **2001**, *34*, 8872-8878.

18. Huang, X. Y.; Wirth, M. J. "Surface-Initiated Radical Polymerization on Porous Silica," *Analytical Chemistry* **1997**, *69*, 4577-4580.

19. Buchmeiser, M. R.; Sinner, F.; Mupa, M.; Wurst, K. "Ring-Opening Metathesis Polymerization for the Preparation of Surface-Grafted Polymer Supports," *Macromolecules* **2000**, *33*, 32-39.

20. Mayr, B.; Buchmeiser, M. R. "Influences of Surface Chemistry on the Separation Behavior of Stationary Phases for Reversed-Phase and Ion-Exchange Chromatography: A Comparison of Coated and Grafted Supports Prepared by Ring-Opening Metathesis Polymerization," *Journal of Chromatography A* **2001**, *907*, 73-80.

21. Prucker, O.; Rühe, J. "Synthesis of Poly(Styrene) Monolayers Attached to High Surface Area Silica Gels through Self-Assembled Monolayers of Azo Initiators," *Macromolecules* **1998**, *31*, 592-601.

22. Quaglia, M.; De Lorenzi, E.; Sulitzky, C.; Massolini, G.; Sellergren, B. "Surface Initiated Molecularly Imprinted Polymer Films: A New Approach in Chiral Capillary Electrochromatography," *Analyst* **2001**, *126*, 1495-1498.

23. Chen, X.; Armes, S. P. "Surface Polymerization of Hydrophilic Methacrylates from Ultrafine Silica Sols in Protic Media at Ambient Temperature: A Novel Approach to Surface Functionalization Using a Polyelectrolyte Macroinitiator," *Advanced Materials* **2003**, *15*, 1558-1562.

24. Fu, Q.; Rao, G. V. R.; Ista, L. K.; Wu, Y.; Andrzejewski, B. P.; Sklar, L. A.; Ward, T. L.; Lopez, G. P. "Control of Molecular Transport through Stimuli-Responsive Ordered Mesoporous Materials," *Advanced Materials* **2003**, *15*, 1262-1266.

25. Jung, D. H.; Park, I. J.; Choi, Y. K.; Lee, S. B.; Park, H. S.; Rühe, J. "Perfluorinated Polymer Monolayers on Porous Silica for Materials with Super Liquid Repellent Properties," *Langmuir* **2002**, *18*, 6133-6139.

26. Balachandra, A. M.; Baker, G. L.; Bruening, M. L. "Preparation of Composite Membranes by Atom Transfer Radical Polymerization Initiated from a Porous Support," *Journal of Membrane Science* **2003**, *227*, 1-14.

27. Granville, A. M.; Boyes, S. G.; Akgun, B.; Foster, M. D.; Brittain, W. J. "Synthesis and Characterization of Stimuli-Responsive Semifluorinated Polymer Brushes Prepared by Atom Transfer Radical Polymerization," *Macromolecules* **2004**, *37*, 2790-2796.

28. Kizhakkedathu, J. N.; Norris-Jones, R.; Brooks, D. E. "Synthesis of Well-Defined Environmentally Responsive Polymer Brushes by Aqueous ATRP," *Macromolecules* **2004**, *37*, 734-743.

29. Jones, D. M.; Smith, J. R.; Huck, W. T. S.; Alexander, C. "Variable Adhesion of Micropatterned Thermoresponsive Polymer Brushes: AFM Investigations of Poly(N-Isopropylacrylamide) Brushes Prepared by Surface-Initiated Polymerizations," *Advanced Materials* **2002**, *14*, 1130-1134.

30. Kaholek, M.; Lee, W.-K.; LaMattina, B.; Caster, K. C.; Zauscher, S. "Fabrication of Stimulus-Responsive Nanopatterned Polymer Brushes by Scanning Probe Lithography," *Nano Letters* **2004**, *4*, 373-376.

31. Husemann, M.; Mecerreyes, D.; Hawker, C. J.; Hedrick, J. L.; Shah, R.; Abbott, N. L. "Surface-Initiated Polymerization for Amplification of Self-Assembled Monolayers Patterned by Microcontact Printing," *Angewandte Chemie-International Edition* **1999**, *38*, 647-649.

32. Zhou, F.; Liu, W. M.; Hao, J. C.; Xu, T.; Chen, M.; Xue, Q. J. "Fabrication of Conducting Polymer and Complementary Gold Microstructures Using Polymer Brushes as Templates," *Advanced Functional Materials* **2003**, *13*, 938-942.

33. Ista, L. K.; Mendez, S.; Perez-Luna, V. H.; Lopez, G. P. "Synthesis of Poly(N-Isopropylacrylamide) on Initiator-Modified Self-Assembled Monolayers," *Langmuir* **2001**, *17*, 2552-2555.

34. Ma, H.; Hyun, J.; Stiller, P.; Chilkoti, A. "Non-Fouling Oligo(Ethylene Glycol)-Functionalized Polymer Brushes Synthesized by Surface-Initiated Atom Transfer Radical Polymerization," *Advanced Materials* **2004**, *16*, 338-341.

35. Paul, R.; Schmidt, R.; Dyer, D. J. "Synthesis of Ultrathin Films of Polyacrylonitrile by Photoinitiated Polymerization from Self-Assembled Monolayers on Gold," *Langmuir* **2002**, *18*, 8719-8723.

36. Shah, R. R.; Merreceyes, D.; Husemann, M.; Rees, I.; Abbott, N. L.; Hawker, C. J.; Hedrick, J. L. "Using Atom Transfer Radical Polymerization to Amplify Monolayers of Initiators Patterned by Microcontact Printing into Polymer Brushes for Pattern Transfer," *Macromolecules* **2000**, *33*, 597-605.

37. Jones, D. M.; Huck, W. T. S. "Controlled Surface-Initiated Polymerizations in Aqueous Media," *Advanced Materials* **2001**, *13*, 1256-1259.

38. Zhao, B.; Brittain, W. J. "Synthesis of Tethered Polystyrene-Block-Poly(Methyl Methacrylate) Monolayer on a Silicate Substrate by Sequential Carbocationic Polymerization and Atom Transfer Radical Polymerization," *Journal of the American Chemical Society* **1999**, *121*, 3557-3558.

39. Huang, W. X.; Skanth, G.; Baker, G. L.; Bruening, M. L. "Surface-Initiated Thermal Radical Polymerization on Gold," *Langmuir* **2001**, *17*, 1731-1736.

40. Gopireddy, D.; Husson, S. M. "Room Temperature Growth of Surface-Confined Poly(Acrylamide) from Self-Assembled Monolayers Using Atom Transfer Radical Polymerization," *Macromolecules* **2002**, *35*, 4218-4221.

41. Roux, S.; Duwez, A. S.; Demoustier-Champagne, S. "Surface-Initiated Polymerization of Styrene from a Carboxylic Acid Functionalized Polypyrrole Coated Electrode," *Langmuir* **2003**, *19*, 306-313.

42. Kim, D. J.; Heo, J. Y.; Kim, K. S.; Choi, I. S. "Formation of Thermoresponsive Poly(Nisopropylacrylamide)/Dextran Particles by Atom Transfer Radical Polymerization," *Macromolecular Rapid Communications* **2003**, *24*, 517-521.

43. Jordan, R.; Ulman, A.; Kang, J. F.; Rafailovich, M. H.; Sokolov, J. "Surface-Initiated Anionic Polymerization of Styrene by Means of Self-Assembled Monolayers," *Journal of the American Chemical Society* **1999**, *121*, 1016-1022.

44. Khan, M.; Huck, W. T. S. "Hyperbranched Polyglycidol on Si/Sio2 Surfaces Via Surface-Initiated Polymerization," *Macromolecules* **2003**, *36*, 5088-5093.

45. Quirk, R. P.; Mathers, R. T. "Surface-Initiated Living Anionic Polymerization of Isoprene Using a 1,1-Diphenylethylene Derivative and Functionalization with Ethylene Oxide," *Polymer Bulletin* **2001**, *45*, 471-477.

46. Ingall, M. D. K.; Honeyman, C. H.; Mercure, J. V.; Bianconi, P. A.; Kunz, R. R. "Surface Functionalization and Imaging Using Monolayers and Surface-Grafted Polymer Layers," *Journal of the American Chemical Society* **1999**, *121*, 3607-3613.

47. Zhao, B.; Brittain, W. J. "Synthesis of Polystyrene Brushes on Silicate Substrates Via Carbocationic Polymerization from Self-Assembled Monolayers," *Macromolecules* **2000**, *33*, 342-348.

48. Weck, M.; Jackiw, J. J.; Rossi, R. R.; Weiss, P. S.; Grubbs, R. H. "Ring-Opening Metathesis Polymerization from Surfaces," *Journal of the American Chemical Society* **1999**, *121*, 4088-4089.

49. Kim, N. Y.; Jeon, N. L.; Choi, I. S.; Takami, S.; Harada, Y.; Finnie, K. R.; Girolami, G. S.; Nuzzo, R. G.; Whitesides, G. M.; Laibinis, P. E. "Surface-Initiated Ring-Opening Metathesis Polymerization on Si/Sio2," *Macromolecules* **2000**, *33*, 2793-2795.

50. Liu, X. G.; Guo, S. W.; Mirkin, C. A. "Surface and Site-Specific Ring-Opening Metathesis Polymerization Initiated by Dip-Pen Nanolithography," *Angewandte Chemie-International Edition* **2003**, *42*, 4785-4789.

51. Jennings, G. K.; Yong, T.-H.; Munro, J. C.; Laibinis, P. E. "Structural Effects on the Barrier Properties of Self-Assembled Monolayers Formed from Long-Chain W-Alkoxy-*N*-Alkanethiols on Copper," *Journal of the American Chemical Society* **2003**, *125*, 2950-2957.

52. Jennings, G. K.; Laibinis, P. E. "Enhanced Stability of Self-Assembled Monolayers on Underpotentially Deposited Metal Layers," *Langmuir* **1996**, *12*, 6173-6175.

53. Yan, D.; Saunders, J. A.; Jennings, G. K. "Formation and Stability of Hexadecanethiolate Sams Prepared in Aqueous Micellar Solutions of C12e6," *Langmuir* **2003**, *19*, 9290-9296.

54. Bain, C. D.; Troughton, E. B.; Tao, Y. T.; Evall, J.; Whitesides, G. M.; Nuzzo, R. G. "Formation of Monolayer Films by the Spontaneous Assembly of Organic Thiols from Solution onto Gold," *Journal of the American Chemical Society* **1989**, *111*, 321-335.

55. Sun, T.; Wang, G.; Feng, L.; Liu, B.; Ma, Y.; Jiang, L.; Zhu, D. "Reversible Switching between Superhydrophilicity and Superhydrophobicity," *Angew. Chem. Int. Edit.* **2004**, *43*, 357-360.

56. Brantley, E. L.; Jennings, G. K. "Fluorinated Polymer Films from Acylation of ATRP Surface-Initiated Poly(Hydroxyethyl Methacrylate)," *Macromolecules* **2004**, *37*, 1476-1483.

57. Bantz, M. R.; Brantley, E. L.; Weinstein, R. D.; Moriarty, J.; Jennings, G. K. "Effect of Fractional Fluorination on the Properties of ATRP Surface-Initiated Poly(Hydroxyethyl Methacrylate) Films," *Journal of Physical Chemistry B* **2004**, *108*, 9787-9794.

58. Brantley, E. L.; Holmes, T. C.; Jennings, G. K. "Modification of ATRP Surface-Initiated Poly(Hydroxyethyl Methacrylate) Films with Hydrocarbon Side Chains," *Journal of Physical Chemistry B* **2004**, *108*, 16077-16084.

59. Gutowski, W. S. "Interface/Interphase Engineering of Polymers for Adhesion Enhancement: Part I. Review of Micromechanical Aspects of Polymer Interface Reinforcement through Surface Grafted Molecular Brushes," *Journal of Adhesion* **2003**, *79*, 445-482.

60. Sun, L.; Baker, G. L.; Bruening, M. L. "Polymer Brush Membranes for Pervaporation of Organic Solvents from Water," *Macromolecules* **2005**, *38*, 2307-2314.

61. Dyer, D. J. "Patterning of Gold Substrates by Surface-Initiated Polymerization," *Advanced Functional Materials* **2003**, *13*, 667-670.

62. Schmelmer, S.; Jordan, R.; Geyer, W.; Eck, W.; Golzhauser, A.; Grunze, M.; Ulman, A. "Surface-Initiated Polymerization on Self-Assembled Monolayers: Amplification of Patterns at the Micrometer and Nanometer Scale," *Angew. Chem. Int. Edit.* **2003**, *42*, 559-563.

63. Blomberg, S.; Ostberg, S.; Harth, E.; Bosman, A. W.; Van Horn, B.; Hawker, C. J. "Production of Crosslinked, Hollow Nanoparticles by Surface-Initiated Living Free-Radical Polymerization," *Journal of Polymer Science Part a-Polymer Chemistry* **2002**, *40*, 1309-1320.

64. Fan, X. W.; Xia, C. J.; Fulghum, T.; Park, M. K.; Locklin, J.; Advincula, R. C. "Polymer Brushes Grafted from Clay Nanoparticles Adsorbed on a Planar Substrate by Free Radical Surface-Initiated Polymerization," *Langmuir* **2003**, *19*, 916-923.

65. Bontempo, D.; Tirelli, N.; Feldman, K.; Masci, G.; Crescenzi, V.; Hubbell, J. A. "Atom Transfer Radical Polymerization as a Tool for Surface Functionalization," *Advanced Materials* **2002**, *14*, 1239-1241.

66. Bontempo, D.; Tirelli, N.; Masci, G.; Crescenzi, V.; Hubbell, J. A. "Thick Coating and Functionalization of Organic Surfaces Via ATRP in Water," *Macromolecular Rapid Communications* **2002**, *23*, 418-422.

67. Matsuno, R.; Yamamoto, K.; Otsuka, H.; Takahara, A. "Polystyrene- and Poly(3-Vinylpyridine)-Grafted Magnetite Nanoparticles Prepared through Surface-Initiated Nitroxide-Mediated Radical Polymerization," *Macromolecules* **2004**, *37*, 2203-2209.

68. Shaffer, M. S. P.; Koziol, K. "Polystyrene Grafted Multi-Walled Carbon Nanotubes," *Chemical Communications* **2002**, 2074-2075.

69. Viswanathan, G.; Chakrapani, N.; Yang, H. C.; Wei, B. Q.; Chung, H. S.; Cho, K. W.; Ryu, C. Y.; Ajayan, P. M. "Single-Step in Situ Synthesis of Polymer-Grafted Single-Wall Nanotube Composites," *Journal of the American Chemical Society* **2003**, *125*, 9258-9259.

70. Kong, H.; Gao, C.; Yan, D. Y. "Controlled Functionalization of Multiwalled Carbon Nanotubes by in Situ Atom Transfer Radical Polymerization," *Journal of the American Chemical Society* **2004**, *126*, 412-413.

71. Yao, Z. L.; Braidy, N.; Botton, G. A.; Alex, A. T. "Polymerization from the Surface of Single-Walled Carbon Nanotubes - Preparation and Characterization of Nanocomposites," *Journal of the American Chemical Society* **2003**, *125*, 16015-16024.

72. Pyun, J.; Kowalewski, T.; Matyjaszewski, K. "Synthesis of Polymer Brushes Using Atom Transfer Radical Polymerization," *Macromolecular Rapid Communications* **2003**, *24*, 1043-1059.

73. Mayr, B.; Tessadri, R.; Post, E.; Buchmeiser, M. R. "Metathesis-Based Monoliths: Influence of Polymerization Conditions on the Separation of Biomolecules," *Analytical Chemistry* **2001**, *73*, 4071-4078.

74. Buchmeiser, M. R. "Metathesis-Based Monolithic Supports: Synthesis, Functionalization and Applications," *Macromolecular Rapid Communications* **2001**, *22*, 1082-1094.

75. Mandal, T. K.; Fleming, M. S.; Walt, D. R. "Production of Hollow Polymeric Microspheres by Surface-Confined Living Radical Polymerization on Silica Templates," *Chemistry of Materials* **2000**, *12*, 3481-3487.

76. Kim, J. B.; Huang, W. X.; Miller, M. D.; Baker, G. L.; Bruening, M. L. "Kinetics of Surface-Initiated Atom Transfer Radical Polymerization," *Journal of Polymer Science Part a-Polymer Chemistry* **2003**, *41*, 386-394.

77. Kato, M.; Kamigaito, M.; Sawamoto, M.; Higashimura, T. "Polymerization of Methyl-Methacrylate with the Carbon- Tetrachloride Dichlorotris(Triphenylphosphine)Ruthenium(II) Methylaluminum Bis(2,6-Di-Tert-Butylphenoxide) Initiating System - Possibility of Living Radical Polymerization," *Macromolecules* **1995**, *28*, 1721-1723.

78. Andruzzi, L.; Hexemer, A.; Li, X. F.; Ober, C. K.; Kramer, E. J.; Galli, G.; Chiellini, E.; Fischer, D. A. "Control of Surface Properties Using Fluorinated Polymer Brushes Produced by Surface-Initiated Controlled Radical Polymerization," *Langmuir* **2004**, *20*, 10498-10506.

79. Wang, X. S.; Armes, S. P. "Facile Atom Transfer Radical Polymerization of Methoxy-Capped Oligo(Ethylene Glycol) Methacrylate in Aqueous Media at Ambient Temperature," *Macromolecules* **2000**, *33*, 6640-6647.

80. Matyjaszewski, K.; Nakagawa, Y.; Jasieczek, C. B. "Polymerization of N-Butyl Acrylate by Atom Transfer Radical Polymerization. Remarkable Effect of Ethylene Carbonate and Other Solvents," *Macromolecules* **1998**, *31*, 1535-1541.

81. Robinson, K. L.; Khan, M. A.; Banez, M. V. D.; Wang, X. S.; Armes, S. P. "Controlled Polymerization of 2-Hydroxyethyl Methacrylate by ATRP at Ambient Temperature," *Macromolecules* **2001**, *34*, 3155-3158.

82. Wang, X. S.; Jackson, R. A.; Armes, S. P. "Facile Synthesis of Acidic Copolymers Via Atom Transfer Radical Polymerization in Aqueous Media at Ambient Temperature," *Macromolecules* **2000**, *33*, 255-257.

83. Kraft, M. L.; Moore, J. S. "N-Alkyl Fatty Acid-Modified Microgels: Ion Permeation as a Function of Chain Length," *Langmuir* **2003**, *19*, 910-915.

CHAPTER III

EXPERIMENTAL PROCEDURES AND CHARACTERIZATION METHODS

Experimental Procedures

Materials

CuCl (99.995+%), $CuBr_2$ (99.999%), 2,2'-bipyridine (bpy, 99+%), 2-hydroxyethyl methacrylate (HEMA, >99%), pyridine (99+%), heptafluorobutyryl chloride (C_3F_7COCl, 98%), pentadecafluorooctanoyl chloride ($C_7F_{15}COCl$, 97%), pentafluorobenzoyl chloride (C_6F_5COCl, 99%), lauroyl chloride ($C_{11}H_{23}COCl$, 98%), myristoyl chloride ($C_{13}H_{27}COCl$, 97%), palmitoyl chloride ($C_{15}H_{31}COCl$, 98%), $K_3Fe(CN)_6$ (99+%), $K_4Fe(CN)_6 \cdot 3H_2O$ (99%), KOH (85+%), and hexadecane (99%) were used as received from Aldrich. N,N-dimethylformamide (DMF, 99.9%), dichloromethane (99.9%), iso-octane (99%), trifluoroacetic anhydride ($(CF_3CO)_2O$, 99+%), acetyl chloride (CH_3COCl, 98%), octanoyl chloride ($C_7H_{15}COCl$, 99%), stearoyl chloride ($C_{17}H_{35}COCl$, >99%), KBr (99.7%), Na_2SO_4 (anhydrous), hexane (99.9%), n-octane (99%), n-decane (99+%), n-dodecane (99%), and n-tetradecane (99+%) were used as received from Fisher. Gold shot (99.99%) and chromium-coated tungsten filaments were obtained from J&J Materials and R.D. Mathis, respectively. Silicon (100) wafers (Montco Silicon) were rinsed with ethanol and deionized water and dried with nitrogen. Sylgard 184 silicone elastomer base and curing agent were purchased from Dow Corning Corporation. Ethanol (AAPER, absolute) was used as received. NaCl cover slips

(International Crystal Labs) were used as received. Deionized water (16.7 MΩ·cm) was purified with a Modu-Pure system and used as a solvent during polymerization and for rinsing. An initiator-terminated disulfide, $(BrC(CH_3)_2COO(CH_2)_{11}S)_2$, was synthesized as described in the literature.[1]

Preparation of Gold Substrates

Gold substrates were prepared by evaporating chromium (100 Å) and gold (1250 Å) in sequence onto silicon (100) wafers at rates of 1-2 Å s^{-1} in a diffusion-pumped chamber with a base pressure of 4×10^{-6} torr. After removal from the evaporation chamber, the wafers were typically cut into 1 cm × 3 cm pieces, with slightly larger 1.4 cm × 4 cm pieces used when obtaining electrochemical impedance spectra.

Polymerization of PHEMA

Procedures followed to make PHEMA films via water-accelerated ATRP are similar to those outlined in Huang et al.[2] A detailed procedure is included in Appendix A for reference. Gold substrates were first placed in a 1 mM ethanol solution of $(BrC(CH_3)_2COO(CH_2)_{11}S)_2$ for at least 24 h. The initiated samples were then rinsed with ethanol, dried with nitrogen, and placed in vials that were subsequently degassed and back-filled with nitrogen. A Cu^I/Cu^{II}/bpy (69 mM CuCl, 20 mM $CuBr_2$, 195 mM bpy) system in a 50:50 v:v water/HEMA solution[2] was used for polymerization. Since a glovebox was not available and oxygen will oxidize the activating Cu^I species and terminate polymerization, the mixture was placed in a Schlenk flask sealed with a rubber septum and was degassed by performing three freeze-pump-thaw cycles. This was

followed by transfer of the solution via cannula into vials containing up to six samples each. After polymerizing for 12 h at room temperature (Figure 3.1), the samples were thoroughly rinsed with water and DMF and then dried with nitrogen. As measured by ellipsometry, PHEMA film thicknesses were typically around 220 nm under these conditions. All of the work presented hereafter will use the 12 h, ~220 nm PHEMA film as a basis. Various modifications to the base film will be addressed as they are encountered.

As already mentioned, water-accelerated, surface-initiated ATRP allows control over film thicknesses. Using the procedure outlined in the previous paragraph but varying polymerization time is the most direct method of control. To this end, film thicknesses of PHEMA samples at polymerization times of 0.5, 1, 2, 5, 8, and 12 h were measured by ellipsometry. Figure 3.2 shows the wide range of film thicknesses that are possible with this technique. As indicated by the data, film growth is not linear with time and therefore is not consistent with a truly "living" polymerization. Our kinetics data, when compared to that of other groups, demonstrate somewhat less living character, likely because others purify the monomer before polymerization to remove inhibitors and/or perform the entire polymerization in a glovebox. Thus, while post-polymerization modification is the main aspect of control that will be highlighted by this work, Figure 3.2 demonstrates another aspect of film property control, thickness variation, which could be utilized for film engineering.

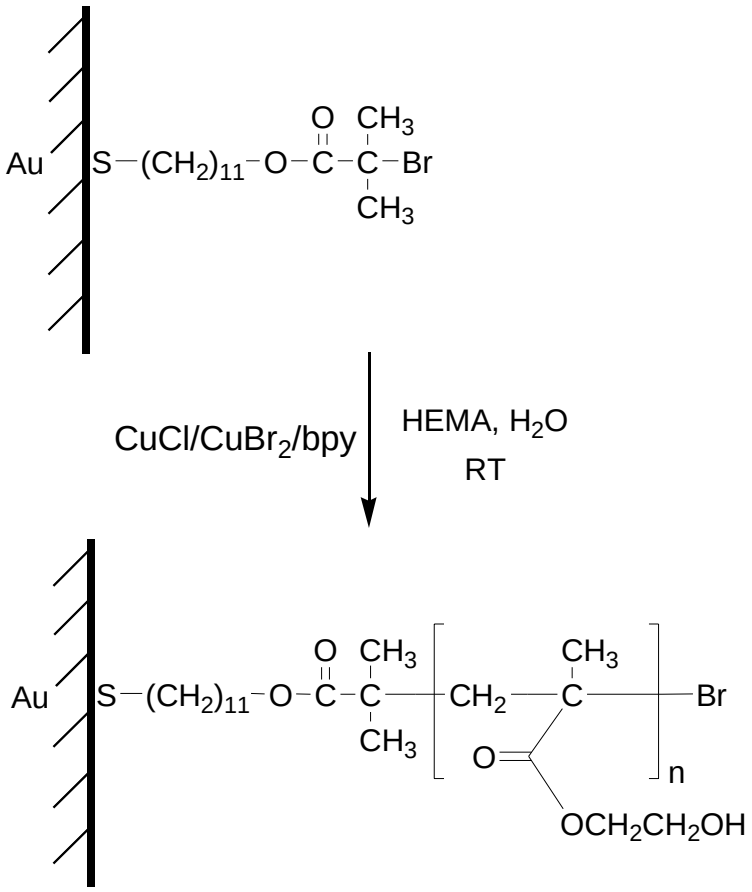

Figure 3.1. Growth of PHEMA film from initiator on gold using water-accelerated ATRP.

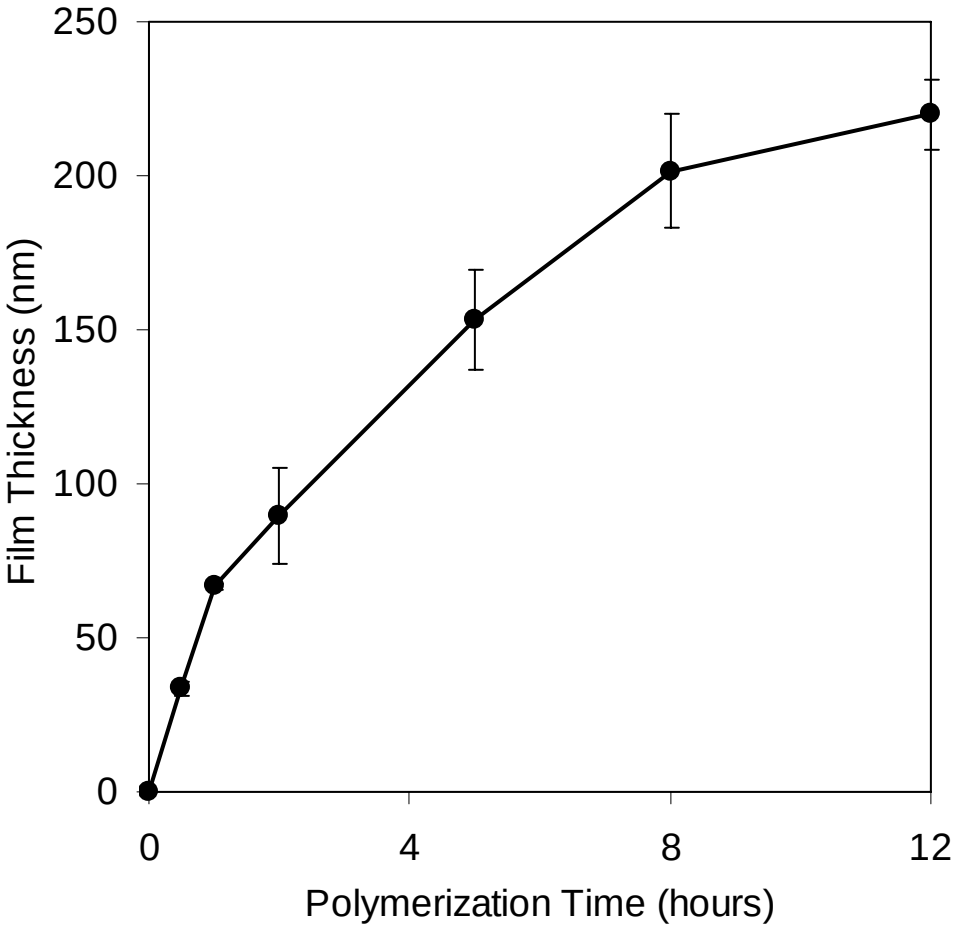

Figure 3.2. Film growth kinetics for the surface-initiated water-accelerated ATRP of PHEMA on gold. If error bars are not visible, the size of the point approximates the error.

Characterization Methods

Reflectance Absorption Infrared Spectroscopy

Reflectance absorption infrared spectroscopy (RAIRS) is used to determine film composition and to derive structural information from the polymer films. Absorbance of radiation in the IR region of the electromagnetic spectrum (400 to 4000 cm^{-1}) results in various vibrations (bending, stretching, etc.) of molecules. Molecules and functional groups absorb radiation in specific regions of the spectrum, allowing identification of species that are present by simply monitoring radiation absorbance peaks across the entire spectrum.[3]

Although several types of IR spectroscopy exist, RAIRS specifically has the ability to aid in determination of structural information of films. The observed peak intensity for a given stretching or bending mode from RAIRS is proportional to the square of the component of its dynamic dipole moment normal to the surface, as indicated by the following proportionality:[4]

$$I \propto cos^2 \theta_{mz} \tag{3-1}$$

where I represents the spectral intensity and θ_{mz} is the average angle between the transition dipole moment (m) for a particular band and the surface normal (z). This dependence arises because, for radiation polarized parallel to the plane of incidence (substrate), the resulting electric field vector is mostly perpendicular to the substrate.[5,6] Thus, during absorbance of IR radiation, band intensity will be highest when the

transition dipole moment is most closely aligned normal to the surface ($\theta_{mz} \rightarrow 0°$), and transition dipole moments that lie nearly parallel to the surface normal ($\theta_{mz} \rightarrow 90°$) will have much less spectral intensity. Table 3.1 lists the peak positions and chemical group assignments for IR peaks commonly encountered in the polymer films in this study. More detailed discussion of specific IR peaks will be addressed as necessary.

RAIRS was performed using a Bio-Rad Excalibur FTS-3000 infrared spectrometer. The p-polarized light was incident at 80° from the surface normal. The instrument was run in single reflection mode and equipped with a Universal sampling accessory. A liquid nitrogen-cooled, narrow-band MCT detector was used to detect reflected light. Spectral resolution was 2 cm^{-1} after triangular apodization. Each spectrum was accumulated over 500 or 1000 scans with a deuterated octadecanethiol-d_{37} self-assembled monolayer on gold as the background. In Chapter IV, to allow comparison between the orientation of fluorinated acid chlorides in the isotropic liquid phase and fluorinated species within the film, transmission IR spectra were obtained for the pure liquid acid chlorides confined between two NaCl cover slips. Spectra were accumulated over 1000 scans using a NaCl cover slip as background.

Electrochemical Impedance Spectroscopy

Barrier properties of polymer films may be measured with electrochemical impedance spectroscopy (EIS). In EIS, the film is part of an electrochemical cell with a solution containing redox probes and ions and connected to an alternating current source. During an EIS experiment, current is measured upon altering the potential of the working

Table 3.1. Important IR vibrational mode peak positions for characterization of PHEMA and modified PHEMA films in this study. The chemical group assignment and a brief description of the relevance of the peaks to this study are listed. Unless noted, all peaks represent stretching vibrational modes.

Absorption Range (cm^{-1})	Assignment	Comment
1000-1300	C-O	Multiple bands of varying intensity
1100-1400	C-F	Multiple strong bands, especially for long chains; ratio of certain of these peaks leads to structural information for fluorocarbon chains in bulk
1400-1500	C-H (bending)	Moderate bands, only observed in hydrocarbon-modified films
1500-1600	C⋯C	Strong bands; only observed for aryl-modified films
1700-1800	C=O	Strong bands; PHEMA film has one band with acylation modifications giving another
2800-2950	C-H	Various moderate bands; CH_2 peak positions contain crystallinity/structuring information
3000-3700	O-H	Broad, weak band; used to estimate conversion for modified PHEMA films

electrode with a sinusoidal perturbation of varying frequency. The following equation is then applicable to this situation:

$$Z = \frac{E(t)}{I(t)} = \frac{E_0 \cos(\omega t)}{I_0 \cos(\omega t - \phi)} = Z_0 \frac{\cos(\omega t)}{\cos(\omega t - \phi)} \tag{3-2}$$

where Z is the impedance in the system, $E(t)$ is the applied potential at time t, $I(t)$ is the resulting current at time t, E_0 is the amplitude of the potential, ω is the radial frequency (equals $2\pi f$ where f is the frequency in Hz), I_0 is the amplitude of the current, ϕ is the phase shift of the output signal, and Z_0 is the magnitude of the impedance. From these equations, the impedance of a system can be characterized by a magnitude and a phase shift. An impedance plot is obtained by measuring cell current while altering the frequency of the ac source. The impedance changes due to the ability of redox probes to reach the vicinity of the working electrode/metal surface underlying the film where they can be oxidized/reduced. Impedance is directly affected by the transport of ions through a film, and lower frequencies allow more time for diffusive processes to occur.[7] Since an electrochemical cell is used, the results can be modeled using equivalent electrical circuits, like those shown in Figure 3.3, consisting of resistors and capacitors that represent film properties. Resistance and capacitance values for the initiator and polymer layers in our films may be estimated using the following equations that apply to the equivalent circuits shown in Figure 3.3:

$$|Z| = \sqrt{(Z_{real})^2 + (Z_{imag})^2} \tag{3-3}$$

$$Z_{real} = R \tag{3-4}$$

$$Z_{imag} = \frac{1}{j\omega C} \tag{3-5}$$

where $|Z|$ equals Z_0 and is the magnitude of the total impedance, and Z_{real} and Z_{imag} are the real (resistance) and imaginary (capacitance) components of the impedance. As evidenced by the impedance equations for real and imaginary components, higher film resistance and lower film capacitance yield higher total impedance. Higher impedance corresponds to the inhibition of ion transport to the surface and signifies a better barrier film.[8]

EIS was performed with a Gamry Instruments CMS300 impedance system interfaced to a personal computer. A flat-cell (EG&G Instruments) was used to expose only 1 cm^2 of each sample to the aqueous solution containing electrolyte and redox probes while preventing sample edges from being exposed. The electrochemical cell consisted of an aqueous solution of 1 mM $K_4Fe(CN)_6 \cdot 3H_2O$, 1 mM $K_3Fe(CN)_6$, and 0.1 M Na_2SO_4 with a Ag/AgCl/saturated KCl reference electrode, a gold substrate counter electrode, and a gold substrate containing the film to be studied as the working electrode. Data were collected in the range from 10^{-1} to 10^4 Hz using 10 points per decade and were fit with an appropriate equivalent circuit (Figure 3.3) to determine resistance and capacitance values. Reported values and ranges for resistance and capacitance represent the averages and standard deviations of values obtained from at least four independent sample preparations. Typically, a difference of ~0.5 in log R_f or a difference of ~4 nF in C_f was found to be statistically significant based on the t-test at a 95% confidence level.

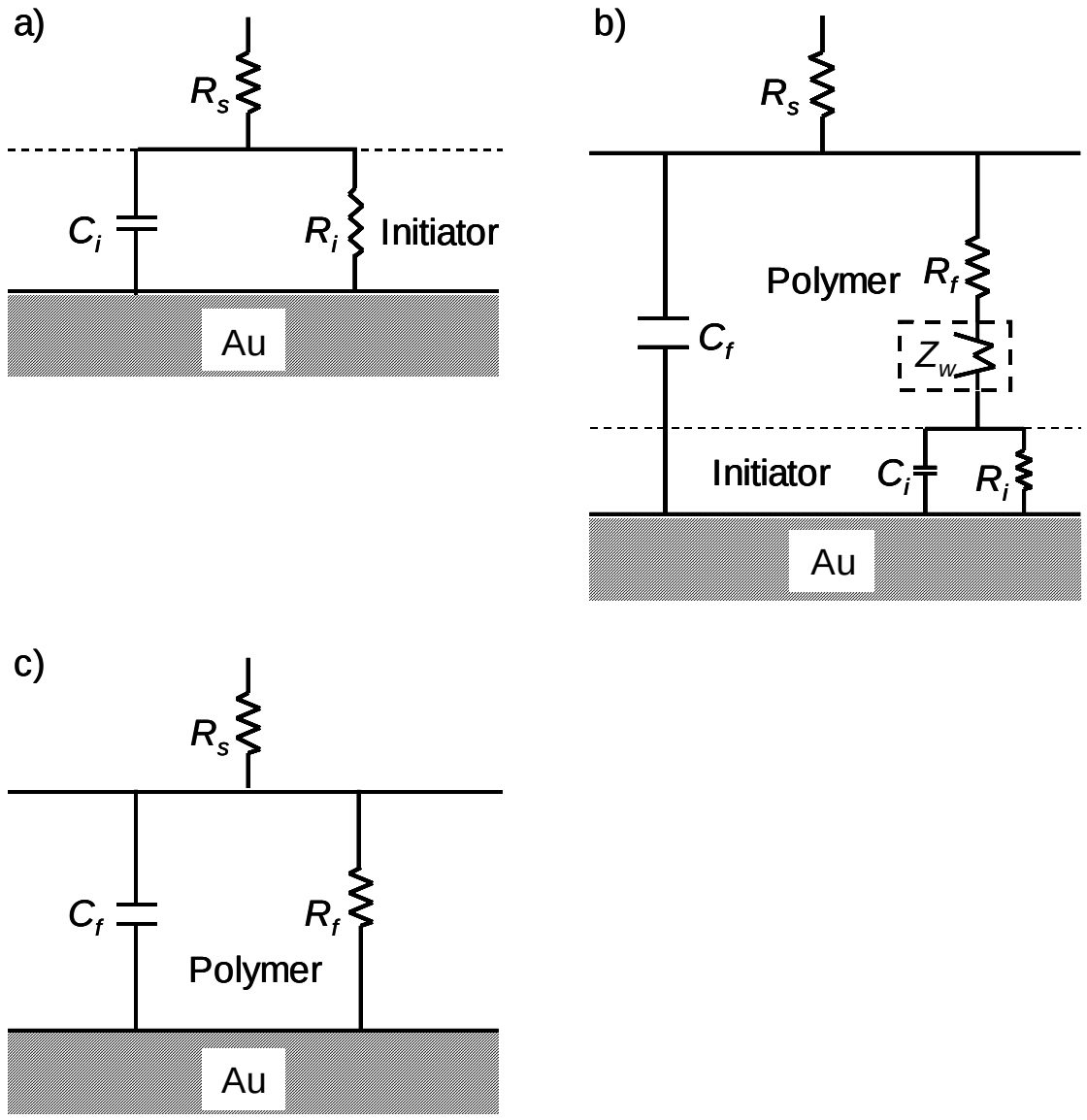

Figure 3.3. Equivalent electrical circuits to model the electrochemical impedance behavior of various films on gold. a) One time constant model for the initiator monolayer only. b) Two time constant model including the initiator layer with a polymer layer atop it. This model applies to all the polymer films encountered in this study. A Warburg impedance, Z_W, may be included in the polymer layer of this model if transport of ions through the polymer becomes diffusion-limited. c) A one time constant model containing only the polymer film. This model appropriately reflects the behavior of modified polymer films when the impedance due to R_f is much greater than the combined impedance of R_i and C_i in parallel, so the time constant due to the initiator is not observed in the impedance spectra. For these cases, the equivalent circuit in b) simplifies to this model.

Ellipsometry

Measurement of film thickness is most readily accomplished through use of ellipsometry. Linearly polarized light in a specified wavelength range is shone onto a reflective surface containing the polymer film. Upon reflection the light is elliptically polarized, and a detector collects both phase (Δ) and amplitude (Ψ) information regarding the reflected light. Model layers representing the film on the surface can be created to fit the measured data to theory. Typically for polymer films, a generic two-term Cauchy layer model is used for this purpose:

$$n = A_n + \frac{B_n}{\lambda^2} \tag{3-6}$$

where n is the film refractive index, A_n and B_n are model fit parameters, and λ is the wavelength of incident light. Since n and thickness are not usually known, the Cauchy model along with standard models for Fresnel reflection coefficients allow both of these physical film parameters to be determined by fitting the models to the experimental data for Δ and Ψ and minimizing the mean square error.[9]

A J.A. Woollam Co. M-2000DI variable angle spectroscopic ellipsometer with WVASE32 software for modeling was used for all ellipsometry experiments. Data were collected on three spots per sample at one angle (75°) and over an extensive wavelength range (usually 400–800 nm) to ensure more accurate fits of theoretical models to the data. Optical constants of bare gold samples were determined by ellipsometry and used as the baseline from which all polymer film samples were measured. The two-term Cauchy layer model worked very well for the polymer films in this study, as the index of

refraction estimated from the model decreased as lower dielectric materials (i.e. fluorocarbon or hydrocarbon) were introduced into the films. Based on the model, an unmodified PHEMA film had a value of about 1.5 for A_n, while hydrocarbon- and fluorocarbon-modified PHEMA films had A_n values of around 1.42 and 1.38, respectively, which are consistent with the expected dielectric characteristics of these films. In all cases, B_n was on the order of 10^{-3} and had a rather small effect on n.

Contact Angle Goniometry

The surface properties of films, which are dependent on the outermost ~5 Å of surface composition/structure,[10] can be evaluated by contact angle goniometry. A small drop of liquid iss placed onto the film-coated surface. Interfacial forces between the liquid drop, the film surface, and air determine the shape of the drop on the surface. The interfacial forces, or tensions, are denoted as γ_{SV} at the solid-vapor interface, γ_{SL} at the solid-liquid interface, and γ_{LV} at the liquid-vapor interface. A force balance of these tensions involved in the surface-liquid-air interface leads to Young's equation:

$$\gamma_{SV} - \gamma_{SL} = \gamma_{LV} \cos \theta \qquad (3\text{-}7)$$

where the static contact angle, θ, is the angle between the line drawn tangent to the edge of the liquid drop (at the liquid-vapor interface) and the line flush with the surface underneath the drop (the solid-liquid interface). With a given liquid, usually water or hexadecane, the values of every term except γ_{LV} change depending on surface composition. θ is readily measured with a goniometer, an optical microscope with a

protractor built into the lens, and water and hexadecane contact angles are generally reported to indicate the relative hydrophilicity/hydrophobicity and oleophilicity/oleophobicity of a surface. Larger measured angles result from more hydrophobic and oleophobic surfaces. Table 3.2 reports the expected contact angles for surfaces of varying composition that have bearing on this work.

Contact angles are useful in providing insight into surface roughness, chemical composition, and interfacial structure. By adding small liquid drops to the surface using a microliter syringe, two separate contact angle measurements, θ_A and θ_R, are generally made. θ_A, the advancing contact angle, is measured after liquid has been added to the drop, causing it to slowly advance across the surface, and θ_R, the receding contact angle, is measured after liquid has been removed from the drop, causing it to slowly recede across the surface. The contact angle hysteresis, $\theta_A - \theta_R$, gives a measure of the roughness or chemical heterogeneity of the surface. Smoother surfaces have a very low hysteresis while rough surfaces have a much larger hysteresis.[11] The chemical composition at the surface also greatly affects the measured contact angles. Depending on whether a surface is dominated by $-CH_2-$, $-CH_3$, $-CF_2-$, $-CF_3$, or higher energy (-COO-, -OH) groups, the contact angles will be altered.[12] If the measured contact angles are similar to the known values for well-structured $-CH_3$ or $-CF_3$ surfaces, the hydrocarbon or fluorocarbon chains must structure by lying normal to the air-film interface.

A Rame-Hart contact angle goniometer with a microliter syringe was used to measure advancing and receding contact angles on static drops of water and hexadecane on the polymer surfaces. The needle tip of the syringe remained inside the liquid drop

Table 3.2. Typical advancing water and hexadecane contact angles for various surface compositions. Values are based on work with self-assembled monolayers[12] with terminal group X except for $-CH_2$ and $-CF_2$, which are taken from studies of polymethylene[13] and poly(tetrafluoroethylene)[14] films, respectively.

Surface Group (X)	$\theta_A(H_2O)$	$\theta_A(HD)$
$-CH_2CH_2OH$	30	<10
-Br	83	<10
$-CH_2$	103	<10
$-CF_2$	104[a]	40[a]
$-CH_3$	115	48
$-CF_3$	118	79

[a] Equilibrium contact angles

while measurements were taken on both sides of ~5 μL drops. Reported values and ranges represent the average and standard deviation of values obtained for at least five independent sample preparations.

Atomic Force Microscopy

The surface topography of a film as well as film thickness may be investigated via atomic force microscopy (AFM). AFM is typically performed in one of two modes—contact or tapping. For soft polymeric surfaces, AFM is generally operated in tapping mode because it eliminates lateral forces (i.e. scraping) across the sample that could potentially damage the surface. In both modes of AFM, a cantilever with an attached tip is made to move vertically across a sample. A photodiode detector monitors the vertical position of the tip at each point as it rasters across the surface and uses the combined horizontal and vertical position information from every point to create an image of the surface. The difference in the two modes is the interaction of the tip with the sample. In contact mode, the tip position is adjusted vertically to maintain a constant interaction force with the surface. In tapping mode, the cantilever oscillates near its resonance frequency and, as a result, "taps" the surface during each oscillation. Setting and maintaining constant oscillation amplitude keeps interactions between the tip and the sample surface constant. The resulting AFM image is a topographical representation of the sample surface, which can give information regarding surface roughness and film thickness under the proper conditions.[15]

AFM images of patterned polymer films were obtained in a cleanroom environment with a NanoScope III scanning probe microscope equipped with a J

piezoelectric scanner (Digital Instruments, Santa Barbara, CA) having an AFM tip with a nominal radius of curvature of ~10 nm. An area of 120 μm × 120 μm was scanned in tapping mode to obtain surface topographical images. The images were plane-fitted and filtered to remove noise using the instrument software.

References

1. Shah, R. R.; Merreceyes, D.; Husemann, M.; Rees, I.; Abbott, N. L.; Hawker, C. J.; Hedrick, J. L. "Using Atom Transfer Radical Polymerization to Amplify Monolayers of Initiators Patterned by Microcontact Printing into Polymer Brushes for Pattern Transfer," *Macromolecules* **2000**, *33*, 597-605.

2. Huang, W. X.; Kim, J. B.; Bruening, M. L.; Baker, G. L. "Functionalization of Surfaces by Water-Accelerated Atom-Transfer Radical Polymerization of Hydroxyethyl Methacrylate and Subsequent Derivatization," *Macromolecules* **2002**, *35*, 1175-1179.

3. Silverstein, R. M.; Webster, F. X. *Spectrometric Identification of Organic Compounds*, 6th ed.; Wiley: New York, 1998.

4. Nuzzo, R. G.; Dubois, L. H.; Allara, D. L. "Fundamental-Studies of Microscopic Wetting on Organic-Surfaces .1. Formation and Structural Characterization of a Self-Consistent Series of Polyfunctional Organic Monolayers," *Journal of the American Chemical Society* **1990**, *112*, 558-569.

5. Greenler, R. G. "Infrared Study of Adsorbed Molecules on Metal Surfaces by Reflection Techniques," *Journal of Chemical Physics* **1966**, *44*, 310-314.

6. Parikh, A. N.; Allara, D. L. "Quantitative-Determination of Molecular-Structure in Multilayered Thin-Films of Biaxial and Lower Symmetry from Photon Spectroscopies .1. Reflection Infrared Vibrational Spectroscopy," *Journal of Chemical Physics* **1992**, *96*, 927-945.

7. Bard, A. J.; Faulkner, L. R. *Electrochemical Methods: Fundamentals and Applications*, 2nd ed.; Wiley: New York, 2001.

8. Park, S. M.; Yoo, J. S. "Electrochemical Impedance Spectroscopy for Better Electrochemical Measurements," *Analytical Chemistry* **2003**, *75*, 455A-461A.

9. Woollam, J. A.; Bungay, C.; Hilfiker, J.; Tiwald, T. "VUV and IR Spectroellipsometric Studies of Polymer Surfaces," *Nuclear Instruments & Methods in Physics Research Section B-Beam Interactions with Materials and Atoms* **2003**, *208*, 35-39.

10. Laibinis, P. E.; Bain, C. D.; Nuzzo, R. G.; Whitesides, G. M. "Structure and Wetting Properties of Omega-Alkoxy-N-Alkanethiolate Monolayers on Gold and Silver," *Journal of Physical Chemistry* **1995**, *99*, 7663-7676.

11. Zisman, W. A. *Contact Angle, Wettability, and Adhesion*; American Chemical Society: Washington, D.C., 1964; Vol. 43.

12. Laibinis, P. E.; Palmer, B. J.; Lee, S.-W.; Jennings, G. K. "The Synthesis of Organothiols and Their Assembly into Monolayers on Gold" In *Thin Films*; Ulman, A., Ed.; Academic Press: Boston, 1998; Vol. 24, pp 1-41.

13. Seshadri, K.; Atre, S. V.; Tao, Y. T.; Lee, M. T.; Allara, D. L. "Synthesis of Crystalline, Nanometer-Scale, -(CH2)(x)- Clusters and Films on Gold Surfaces," *Journal of the American Chemical Society* **1997**, *119*, 4698-4711.

14. Janczuk, B.; Bialopiotrowicz, T.; Zdziennicka, A. "Some Remarks on the Components of the Liquid Surface Free Energy," *Journal of Colloid and Interface Science* **1999**, *211*, 96-103.

15. *Scanning Probe Microscopy Training Notebook*, Digital Instruments, Inc.: Santa Barbara, CA, 1997.

CHAPTER IV

MODIFICATION OF SURFACE-INITIATED POLYMER FILMS WITH FLUOROCARBON CHAINS

Fluorinated polymer films exhibit excellent barrier properties[1] and extremely low critical surface tensions,[2] causing water and oils to bead up on exposure. Methods commonly used to deposit fluorinated polymers onto a surface include spin-coating,[3] solution casting,[4,5] and chemical adsorption.[6] These methods produce films with the properties of fluorinated polymers but often in a relatively uncontrolled fashion. While chemical adsorption produces only polymer monolayers,[6] spin-coating and solution casting exhibit poor control over film thickness in the sub-micron range and produce films that are only physically attached to the underlying substrate.[3,5] Plasma deposition[7] and chemical vapor deposition[8,9] can provide greater control over film thickness by growing the fluorinated films from an underlying surface, but these methods require low pressure and specialized equipment and may yield films with compositions that are not well defined (markedly different from the starting monomer).[7-9] In general, high cost and difficult processibility limit the use of fluorinated polymers in many applications.[3,4,10,11]

One route to fluorinated polymer films that has not been fully explored is surface-initiated polymerization. The advantages of growing a film directly from a surface include well-controlled growth, especially when the kinetics exhibit living character,[12] and stability due to covalent attachment of the polymer backbone to the surface.[13,14] Jung et al.[10] and Andruzzi et al.[15] have prepared surface-initiated films on silica from hydrophobic fluoromonomers using radical-chain polymerizations. The films exhibited

highly hydrophobic and oleophobic surfaces, but film growth was slow in both cases, with the thickest films being only 70 nm after 27 h exposures at 60 ºC.[10] The ability to prepare surface-initiated, partially fluorinated films over a much greater range of thicknesses—from ultrathin films used to modify surface properties to thicker films that are ideal as protective coatings—could greatly impact the applications of these films.

We take advantage of a controlled radical polymerization technique, water-accelerated ATRP (see Chapter II for details), to grow much thicker surface-initiated films that have reactive sites throughout. These reactive sites can then be used to introduce fluorocarbon groups, providing the ability to engineer structural, surface, and barrier properties of films while avoiding processing issues that are typically encountered with fluorinated polymers. This approach to partially fluorinated polymer films exploits the rapid kinetics, precise control, and covalent attachment of surface-initiated PHEMA growth, and fluorination is performed directly on the surface-attached film for ease of processing and separations. All work contained herein involves films that have been fluorinated as completely as possible (until reaction no longer occurs). For further information on film fluorination kinetics and film properties in various states of fluorination, the reader is referred to the Master's work of Mayker Bantz.[16,17]

Experimental Procedures

PHEMA films having reactive hydroxyl side chains were created as described in Chapter III. Derivatization of PHEMA with fluorocarbon side chains was accomplished by exposing the film to 20 mM solutions of trifluoroacetic anhydride ($(CF_3CO)_2O$), heptafluorobutyryl chloride (C_3F_7COCl), pentadecafluorooctanoyl chloride ($C_7F_{15}COCl$),

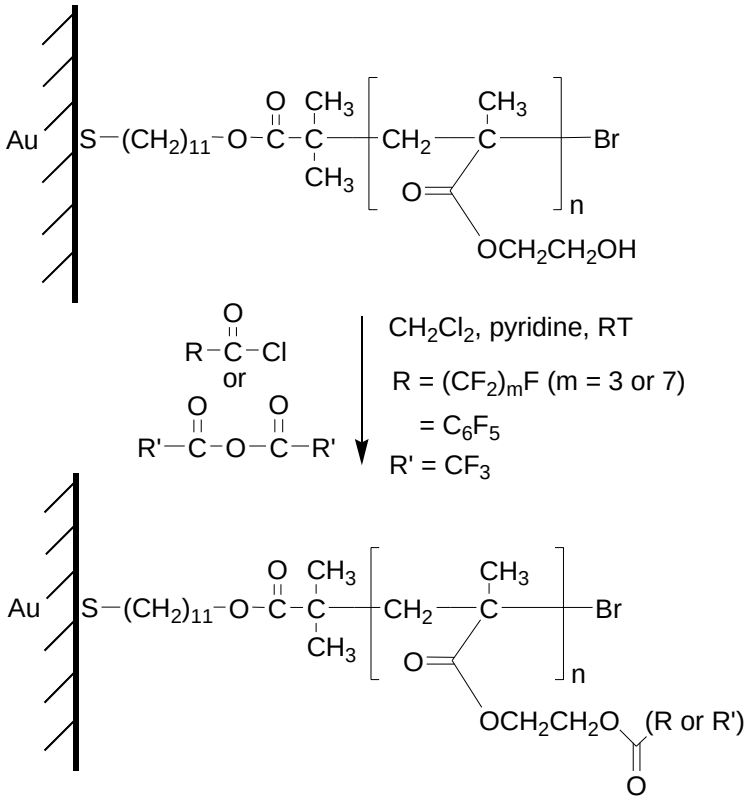

Figure 4.1. Derivatization of PHEMA hydroxyls with fluorocarbon groups via a nucleophilic acylation reaction with either acid chlorides or anhydrides.

or pentafluorobenzoyl chloride (C_6F_5COCl) with 25 mM pyridine in dichloromethane for at least 3 h to give F1, F3, F7, or FBZ films, respectively (Figure 4.1). After reaction, the films were rinsed with dichloromethane and ethanol and dried with nitrogen.

Results and Discussion

Film Composition and Structure

RAIRS was used to monitor compositional changes within the polymer films due to acylation by the various fluorinated species. Figure 4.2 shows the IR spectra of PHEMA along with all four fluorinated PHEMA films. The most readily quantifiable change in the spectra that is indicative of successful acylation is diminution of the hydroxyl peak in the region from 3100 to 3700 cm^{-1}, as the hydroxyl side chains of PHEMA are converted to fluorinated esters. We have used this diminution of integrated hydroxyl peak area (A_{OH}) to estimate conversion (χ) of the hydroxyl side chains as

$$\chi = 1 - \frac{A_{OH,\ \text{fluorinated PHEMA}}}{A_{OH,\ \text{PHEMA}}} \tag{4-1}$$

which assumes that any change in integrated hydroxyl peak area is due solely to acylation and not to orientational changes of the unreacted hydroxyl groups. Due to the distinct differences in perfluorinated chain length and type, some difference in film conversion was expected. As indicated in Table 4.1, the very short chain modification present in F1 exhibits a significantly higher conversion (~90%) than that observed in either F3 or F7

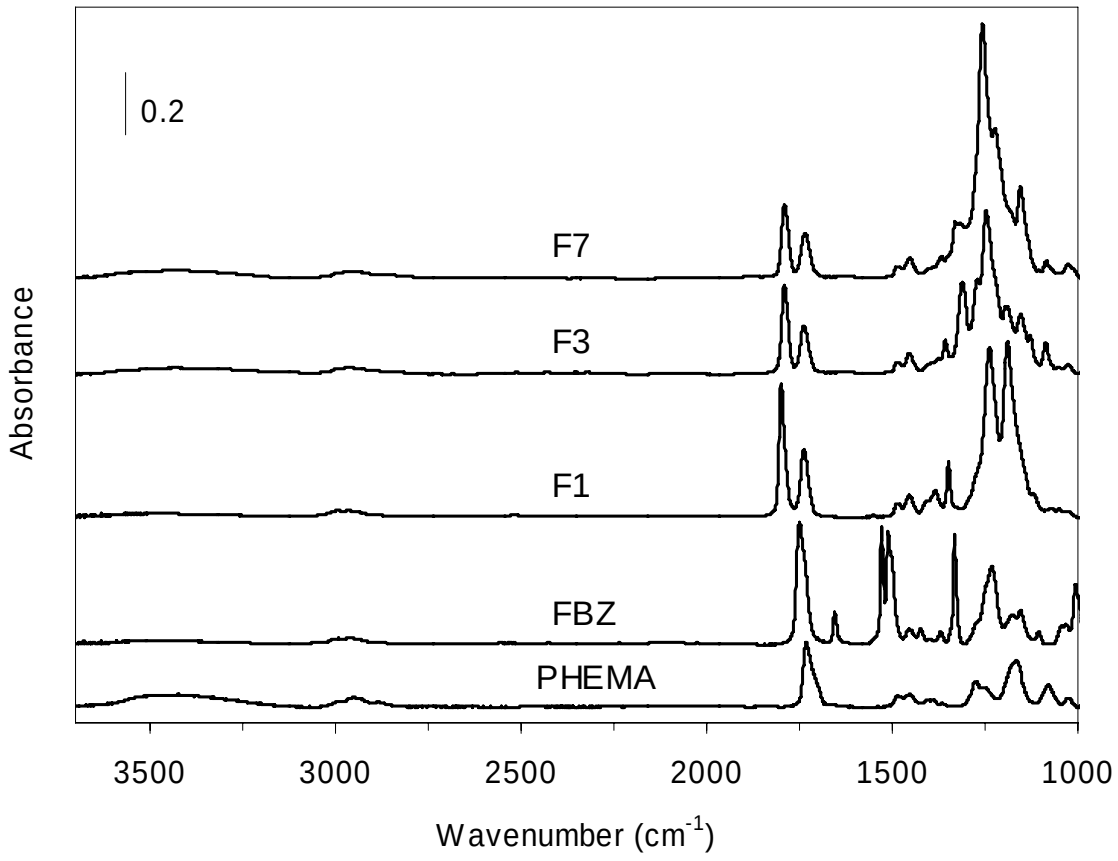

Figure 4.2. Reflectance-absorption IR of PHEMA films on gold before and after exposure to fluorinated acid chlorides or anhydrides. There are several key regions of interest when evaluating effectiveness of the acylation reaction: C-O and CF_2, 1100–1400 cm^{-1}; C⎓C, 1500–1700 cm^{-1}; C=O, 1700–1800 cm^{-1}; OH, 3100–3700 cm^{-1}.

Table 4.1. Conversion (χ) and thickness increase for fluorocarbon-modified PHEMA films as estimated from RAIR spectra and ellipsometry, respectively. Initial thickness of PHEMA films was ~220 nm.

	F1	**F3**	**F7**	**FBZ**
χ (%)	90 ± 2	79 ± 4	77 ± 5	83 ± 3
Observed Thickness Increase (%)	50	78	137	78
Predicted Increase-MW (%)	66	119	234	124
Predicted Increase-Vol (%)	41	65	121	47

films (~80%), consistent with improved transport and reduced steric hindrance for low molecular weight species. The similar conversion for F3 and F7 suggests that transport of these acid chlorides into the film does not limit the ultimate conversion but that steric effects due to the packing of adjacent fluorocarbon chains along a common backbone is the limiting factor. We attribute the high conversion in FBZ (80+%) to π-π stacking of the perfluoroaryl groups, which would result in a lower packing parameter based on the face-to-face distance between the disc-like perfluoroaryl groups[18] (3.2 Å) versus that for perfluoroalkyl chains[6] (5.6 Å) and allow greater accessibility to unreacted hydroxyl groups along a common backbone. For these and all other films presented in later chapters, a statistically significant difference in film conversion at the 95% confidence level from the t-test was ~4-5%.

Further analysis of Figure 4.2 reveals key differences between the spectra of the fluoroalkyl- and fluoroaryl-modified PHEMA and unmodified PHEMA in the region of 1100-1800 cm^{-1}. Every repeat unit of the PHEMA film has an ester immediately off the main backbone chain, and the associated carbonyl appears in the IR spectrum at 1733 cm^{-1}. Also due to the presence of hydroxyl groups throughout the PHEMA film that can hydrogen bond with this carbonyl, a shoulder appears on the carbonyl peak that causes it to broaden toward lower wavenumbers.[19,20] Acylation greatly reduces hydrogen bonding within the film, which diminishes the shoulder on the original carbonyl peak and causes an apparent shift to higher wavenumbers (1738 cm^{-1} for F1, 1737 cm^{-1} for F3, 1735 cm^{-1} for F7). Acylation also produces another ester along the side chain, which results in the appearance of a second carbonyl peak in the spectrum. For films with fluoroalkyl side chains, this new carbonyl peak appears at significantly higher

wavenumbers (1790-1800 cm^{-1}) due to α halogen substitution.[21] For FBZ, the new carbonyl peak combines with the original one to yield a broad peak at ~1749 cm^{-1}. While α halogen substitution is absent in this case (only β fluorines), the fluorine atoms on the aromatic ring are electron-withdrawing groups, and thus raise the carbonyl peak frequency. Conjugation of the carbonyl with the nearby aromatic ring likely offsets this effect and lowers the frequency[21] in comparison to the perfluoroalkyl-substituted PHEMA. The overall result of these competing effects is observed.

Careful examination of Figure 4.2 reveals that the PHEMA carbonyl peak (~1735 cm^{-1}) loses ~30% intensity upon acylation with C_3F_7COCl or $C_7F_{15}COCl$. This reduction is most likely due to film expansion, which alters the orientation of the carbonyl and thus its intensity in the RAIR spectrum as discussed in Chapter III. This explanation is supported by the fact that hydrolysis of the fluorinated esters (vide infra) returns the PHEMA carbonyl to its original, prefluorinated intensity. As fluorocarbon groups are added to the side chain, the surface-attached polymer chain (backbone plus side chains) requires additional space and likely expands to orient more normal to the surface, thus altering the orientation of the original carbonyl groups.

Introduction of fluorinated side chains to the polymer film is also evidenced by the appearance of large peaks throughout the region from 1100 to 1400 cm^{-1}, indicative of CF (in FBZ), CF_2 (in F3 and F7), or CF_3 (in F1) stretching. While the presence of peaks in this region verifies the presence of fluorinated moieties, some structural information can also be gathered, particularly for F3 and F7 films. Since fluoroalkyl chains exhibit a helical structure, there are two types of CF_2 stretching peaks expected in the IR for F3 and F7: those lying along the helical axis ($\nu_{ax}^{CF_2}$, 1300-1400 cm^{-1}) and those

perpendicular to the helical axis ($\nu_{pd}^{CF_2}$, 1100-1300 cm^{-1}).[6,22] The ratio of $\nu_{pd}^{CF_2}$ to $\nu_{ax}^{CF_2}$ absorbance for the film, relative to the same ratio for an isotropic orientation of the acid chlorides in the liquid state, provides information on the orientation of the fluorocarbon side chains in the polymer film relative to the surface normal. Given the surface selection rules for RAIRS,[23,24] the intensity for a given mode in the IR spectrum is proportional to the square of the component of its dynamic dipole moment oriented along the surface normal (Chapter III). Hence, when the ratio of $\nu_{pd}^{CF_2}$ to $\nu_{ax}^{CF_2}$ is greater in the film than in the isotropic liquid, the fluorocarbon helical axis generally lies more along the parallel to the substrate surface, but when this ratio is less in the film than in the isotropic liquid, the fluorocarbon helical axis is more normal to the surface.[6]

Transmission IR spectra of the randomly oriented liquid fluoroalkyl acid chlorides (Figure 4.3) yields a $\nu_{pd}^{CF_2}$:$\nu_{ax}^{CF_2}$ absorbance ratio of ~1.8. For the bulk liquid, $\nu_{pd}^{CF_2}$ are more readily observed than $\nu_{ax}^{CF_2}$ even when chains are randomly oriented. For the F3 film (Figure 4.2), the $\nu_{pd}^{CF_2}$:$\nu_{ax}^{CF_2}$ absorbance ratio is also ~1.8, which suggests that these chains are randomly oriented within the film in similar fashion to the pure acid chloride. F7, however, exhibits a much higher $\nu_{pd}^{CF_2}$:$\nu_{ax}^{CF_2}$ absorbance ratio (~4.5) indicating that the C_7F_{15} side chains in the polymer film are generally aligned more parallel to the metal surface such that the axial CF_2 peaks are nearly undetected. Most likely, the C_7F_{15} side chains align within the film to maximize interchain van der Waals interactions, whereas C_3F_7 side chains are too short to promote such structuring and thereby assume more random orientations. The fluorobenzoyl and trifluoromethyl side chains also show activity in the C-F region but cannot form a helical structure and have no CF_2 stretching.

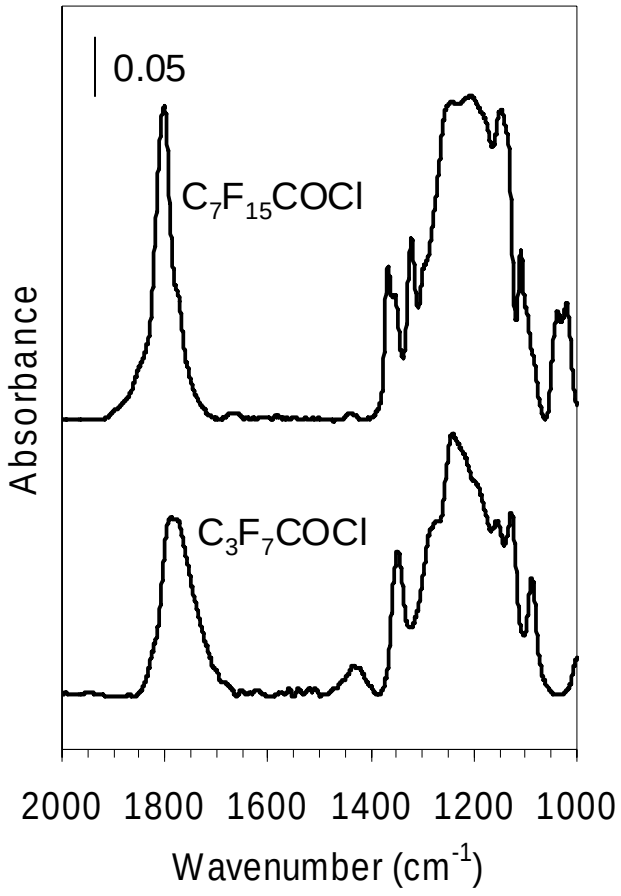

Figure 4.3. Transmission IR spectra of perfluoroalkyl acid chlorides in the liquid state. The relative intensity of $\nu_{pd}^{CF_2}$ (1100–1300 cm^{-1}) and $\nu_{ax}^{CF_2}$ (1300-1400 cm^{-1}) peaks (1.8:1 ratio) for the pure liquids provides a reference to assess orientation of fluorinated side chains in the polymer films.

The aromatic C-F stretch shows two peaks between 1200 and 1350 cm^{-1}, but there is no good indicator from IR of how these aromatic side chains are oriented within the film. Other evidence for the addition of the fluorobenzoyl group to the side chain is the presence of peaks for fluorinated C⎓C aromatic ring stretching from 1500 to 1700 cm^{-1}.[7,25] The trifluoromethyl group of F1 exhibits three stretching peaks between 1190 and 1350 cm^{-1}.[7]

Film Thickness

Table 4.1 shows fluorinated film thickness increases obtained by taking ellipsometry measurements both before and after acylation of PHEMA. The water-accelerated ATRP of PHEMA resulted in 220 ± 11 nm thick films after 12 h. PHEMA is envisioned as being loosely packed, but the addition of fluorocarbon side chains would still cause an expansion of the film to minimize constraints. After fluorination, the greatest thickness increase over that of PHEMA was observed for F7, followed by FBZ and F3, and then F1. As expected, a longer side chain requires more space and thus increases film thickness by inducing a greater extension of the PHEMA backbone than that induced by a shorter side chain.

Expected thickness increases after addition of side chains were estimated using two separate methods while also accounting for conversion. Predictions based solely on the increase in molecular weight of the repeat unit upon acylation have been used for addition of hydrocarbon chains to films.[26] Based on this model, the trend in thickness for the fluorinated groups is correct but the actual thickness increases are not nearly as high as predicted (Table 4.1; up to 100% overprediction). We developed another model that is

based on the increase in molecular volume of the repeat unit using bond lengths[27,28] and chain packing data[6,18] from the literature. To estimate volumes of the different components in the film, we modeled the fluoroalkyl groups as cylinders with length of 1.3 Å per -CF_2- group[27] and diameter of 5.6 Å based on chain packing data.[6] The fluoroaryl group was modeled as a disk with diameter of 5.0 Å (estimated from the benzene carbon-carbon cross-ring length of 2.8 Å[28] in addition to two C-F lengths of 1.1 Å[27] each) and a thickness of 3.2 Å based on crystal interplanar face-to-face packing distance.[18] The remainder of the side chain along with the main polymer backbone (-$CH_2C(CH_3)CO_2(CH_2)_2CO_2$-) was approximated as cylinders behaving as normal hydrocarbon chains (lengths of 1.25 Å per -CH_2- group[27] and diameter of 4.2 Å from chain packing data).[6] Carbonyl and ether bonds were approximated as -CH_3 or -CH_2- groups, respectively, due to lack of exact data for these groups in similar compounds. As with the molecular weight prediction, all samples were referenced to the basic PHEMA repeat unit to estimate relative increases in the molecular volume. With the volume-based predictor, the predicted changes are much closer to the experimental values at the expense of the overall trend; FBZ is predicted to give a smaller increase in film thickness than F3, which is not observed experimentally. The volume-based model does provide much closer agreement with experimental values, as all fluoroalkyl modifications are underpredicted by 15% or less and FBZ is underpredicted by only ~30%.

Surface Wettability and Structuring

Advancing and receding contact angles (θ_A and θ_R) of water were measured for all polymer films to determine the relative hydrophobicity of the surface. Table 4.2 gives

average contact angles for the fluorinated films along with the values for PHEMA and the bromine-terminated initiator monolayer for comparison. The advancing contact angle of water on the initiator is 80°, which is identical to that reported for a bromine-terminated monolayer film.[29] The extremely low contact angle hysteresis ($\theta_A - \theta_R = 6°$) for the initiator is indicative of a smooth monolayer film as well. Once PHEMA is grown from the initiator, the advancing contact angle does not change significantly, but the hysteresis becomes quite high, suggesting that the surface of the film becomes rough and/or chemically heterogeneous. Upon acylation with the fluorinated acid chlorides, the advancing contact angles of water increase dramatically, consistent with hydrophobic groups at the outermost surface, with the largest effect being observed for the addition of C_7F_{15} side chains. The contact angle hysteresis remains high for all fluorocarbon-modified films, so there seems to be no or minimal smoothing of the film due to acylation. The advancing contact angle for FBZ, while much lower than the fluoroalkyl-modified films, is similar to that for a film prepared from the plasma deposition of perfluorobenzene.[7]

Contact angles of hexadecane were also measured on all polymer films. Compared to water, hexadecane is a more sensitive probe of fluorocarbon groups over hydrocarbon groups.[30] F1, F3, and F7 exhibit advancing hexadecane contact angles of 48°, 67°, and 79°, respectively. Monolayers exhibiting well-structured CF_3 surfaces are known to exhibit hexadecane contact angles from 80° down to 70°, depending on the length of the fluorinated chain.[29] The fact that the fluoroalkyl-modified PHEMA films exhibit contact angles that fall in or near this range while hexadecane wets unmodified PHEMA reveals that fluorocarbon groups dominate the surface of these polymers.

Table 4.2. Advancing and receding contact angles (°) of water and hexadecane and critical surface energy (γ_C) of films on gold.

	Water		Hexadecane		γ_C
Film	θ_A	θ_R	θ_A	θ_R	**(mN/m)**
Disulfide Initiator	80 ± 2	74 ± 2	<10	<10	
PHEMA	75 ± 3	23 ± 2	<10	<10	
FBZ	90 ± 2	69 ± 3	<10	<10	
F1	89 ± 1	65 ± 1	48 ± 2	43 ± 2	21
F3	110 ± 2	70 ± 9	67 ± 2	54 ± 3	15
F7	128 ± 2	71 ± 5	79 ± 2	64 ± 3	9

Hexadecane completely wets FBZ, but this result is not unexpected for the aromatic side group. Fluoroaromatics, as also evidenced by lower water contact angles, do not generally yield surfaces as hydrophobic or oleophobic as their straight chain counterparts.[31]

Since F1, F3, and F7 are both hydrophobic and oleophobic, these films should have low critical surface energies, γ_C, in which the value will suggest whether $-CF_3$ groups indeed dominate the outermost surface. A surface consisting entirely of $-CF_3$ groups[2] has a γ_C as low as 6 mN/m whereas one consisting entirely of $-CF_2-$ groups, as with polytetrafluoroethylene,[32] exhibits a γ_C of ~18 mN/m. To estimate the critical surface energies of the films, we used the Zisman method[32,33] and selected a series of alkanes having even numbers of carbons, from hexane to hexadecane, as contacting liquids. θ_A for each of the liquids was measured and $\cos \theta_A$ was plotted against γ_L, the surface tension of the liquid (Figure 4.4). A straight line fit of the data and extrapolation of the line to $\cos \theta_A = 1$ gives γ_C of the film such that a liquid with $\gamma_L < \gamma_C$ will completely wet the surface. From Figure 4.4, F7 exhibits a γ_C of 9 mN/m, indicating that the interface consists of $-CF_3$ groups and that the fluorocarbon chains are oriented near the surface normal there. F3 exhibits a γ_C of 15 mN/m, which is consistent with a mixture of $-CF_3$ groups and other slightly higher energy groups, most likely $-CF_2-$ or $-CH_2-$, at the outer surface. F1 exhibits a γ_C of 21 mN/m, indicative of the presence of $-CF_3$ groups but also other higher energy groups.

A proposed structure of these fluorinated PHEMA films is surmised based on results from wetting measurements and RAIRS. The γ_C value indicates that the F7 surface consists primarily of $-CF_3$ groups, so the fluorocarbon chains at the surface are

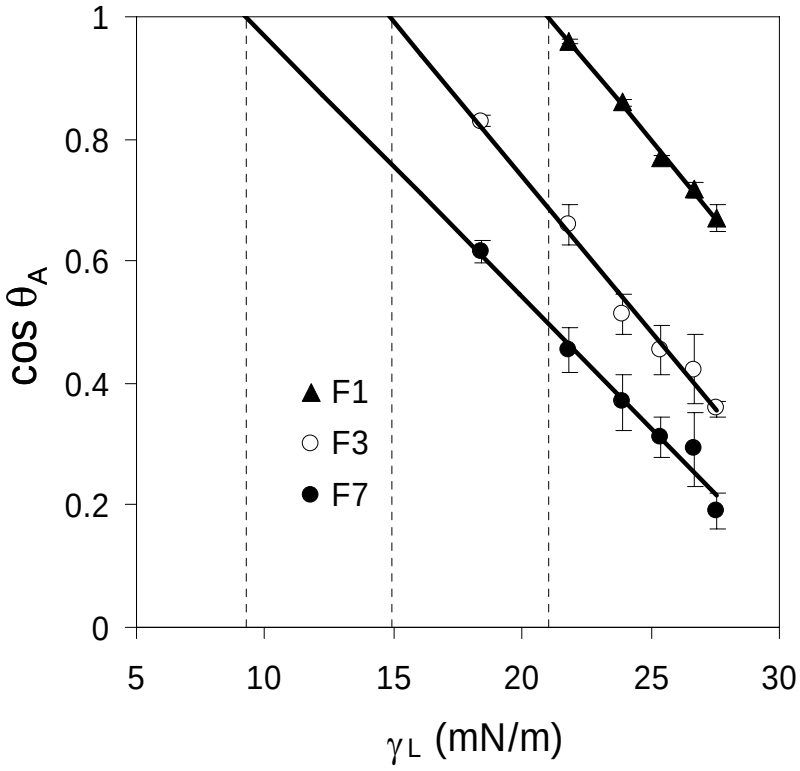

Figure 4.4. Zisman plot to determine critical surface energy, γ_C, of F1, F3, and F7. A series of even-numbered *n*-alkanes from hexane to hexadecane was used as contacting liquids. γ_C is 9 mN/m for F7, 15 mN/m for F3, and 21 mN/m for F1. When an error bar is not observed, the size of the symbol provides an estimate of the error.

mostly normal to the substrate. The dominance of $\nu_{pd}^{CF_2}$ absorbance in the IR, on the other hand, points to the C_7F_{15} chains being oriented more parallel to the substrate in the bulk film. This follows closely with the findings of Genzer and coworkers[34] for spun-cast isoprene polymers with semifluorinated ether side chains. They observed that the fluorinated groups oriented parallel to the surface in the bulk but more normal to the surface at the outer layers. From wettability data, the shorter CF_3 and C_3F_7 chains are unable to orient at the surface like C_7F_{15}, and other groups besides -CF_3 are present at the outer film layer. The presence of stronger $\nu_{ax}^{CF_2}$ bands in the IR for F3 suggests these fluorocarbon groups in the bulk are not parallel to the substrate but randomly oriented. Overall, the short side chains present in F3 and F1 are unable to induce structuring within the bulk film or at the air-film interface. The critical chain length for fluorocarbon structuring is around seven; fluorinated chain lengths even of length three provide no structuring in the bulk or at the interface.

Barrier Properties

We evaluated the effect of fluorination on the barrier properties of the PHEMA films using EIS upon exposure to 1 mM $K_3Fe(CN)_6$ and 1 mM $K_4Fe(CN)_6$ in 0.1 M Na_2SO_4(aq). Figure 4.5 contains the EIS spectra, in the form of Bode plots, for bare gold, the initiator-terminated monolayer, PHEMA, and the four fluorinated polymer films, all on gold. The solid curves in the plot represent best fits of the data with appropriate equivalent circuit models (Figure 3.3) to provide quantitative information on the effect of film composition on the resistance and capacitance of the films. For uncoated gold, the spectrum is fit with a model containing a solution resistance (R_s) in series with the

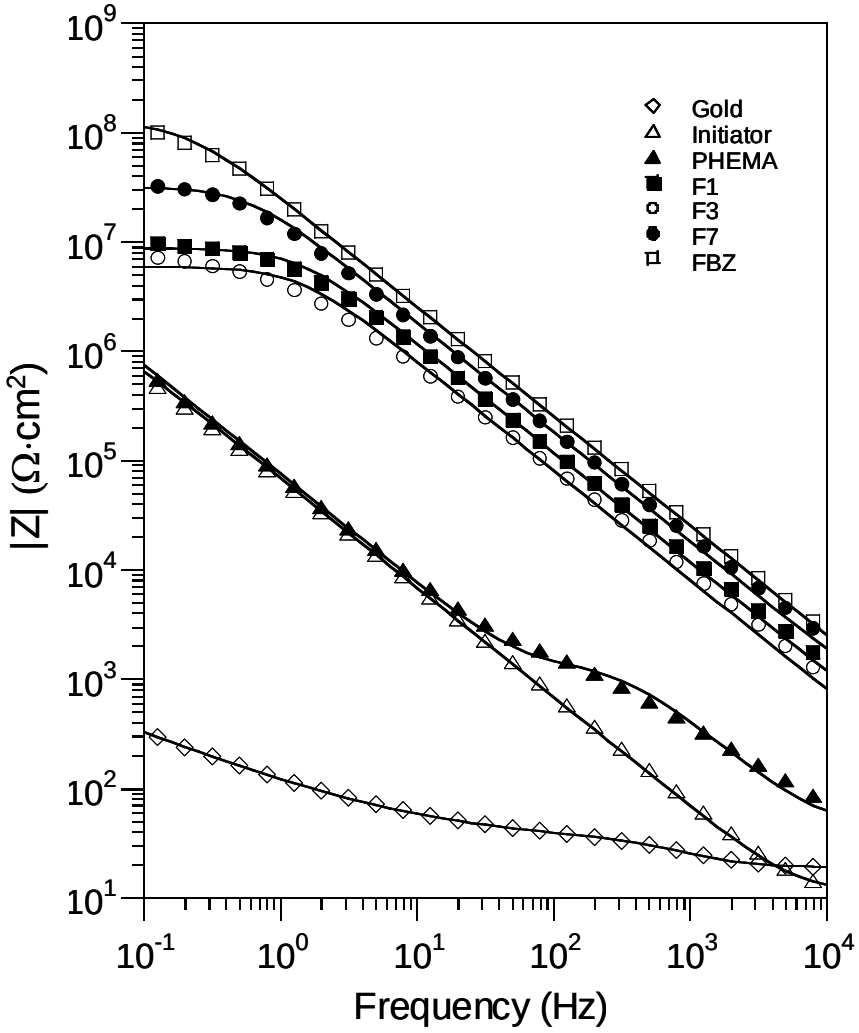

Figure 4.5. Electrochemical impedance spectra obtained in 1 mM $K_3Fe(CN)_6$ and 1 mM $K_4Fe(CN)_6$ in 0.1 M Na_2SO_4(aq) for films on gold. Spectra are shown for PHEMA before and after various fluorocarbon modifications with bare gold and initiator-modified gold for reference. Solid curves represent a fit of the data to an equivalent circuit.

following combination: Warburg impedance (Z_W) and charge transfer resistance (R_{ct}) in series with one another but in parallel with a double layer capacitance (C_{dl}).[35] The Warburg impedance that dominates this spectrum at low frequencies is consistent with rapid charge transfer between the redox probes and the uncoated surface. The mere presence of the initiator monolayer on the gold surface dramatically increases the impedance and produces a spectrum that is fit with a parallel combination of initiator resistance (R_i) and capacitance (C_i) in series with R_s, identical in form to a Randles model equivalent circuit used previously to describe self-assembled monolayers (Figure 3.3a).[36,37] Similar to the behavior of other types of monolayers on metal surfaces, this film blocks gold surface sites and greatly reduces charge transfer.

When a 220-nm-thick film of PHEMA is grown atop the monolayer, the impedance spectrum in Figure 4.5 shows two time constants and is appropriately fitted with a more complex model (Figure 3.3b) containing a polymer film resistance (R_f) and a total film (polymer plus initiator) capacitance (C_f). The time constant at low frequencies is caused by the initiator layer ($\tau_i = R_iC_i$) and is larger than that caused by PHEMA ($\tau_f = R_fC_f$). One surprising observation from Figure 4.5 is that growth of a ~220 nm film of PHEMA from the surface did not affect the impedance properties at low frequency as compared with those of the monolayer. This observation confirms that the contribution of PHEMA to the impedance spectrum is limited to the time constant at high frequencies. Table 4.3 enables comparison of the average capacitances and resistances for the initiator-terminated monolayer and PHEMA. Addition of the PHEMA layer reduces the total film capacitance (C_f) due to its enhanced thickness but exhibits a very low resistance (R_f) in comparison to that of the initiator (R_i). On a per unit thickness basis, SAMs

Table 4.3. Values for film capacitance (C_f) and resistance (R_f) of fluorocarbon-modified PHEMA films.

Film	C_f (nF/cm^2)	Log R_f (Ω·cm^2)
Initiator[a]	2400 ± 300	6.0 ± 0.4
PHEMA	640 ± 200	3.0 ± 0.3
FBZ	6.2 ± 0.7	7.8 ± 0.3
F1	12 ± 1	6.9 ± 0.1
F3	12 ± 7	6.7 ± 0.5
F7	9.2 ± 1.7	7.4 ± 0.4

[a] C_i and R_i values are given for the initiator.

generally provide much greater resistances than thin polymer films due to the minimization of defects during the monolayer assembly process.[38] The very low resistance of PHEMA indicates that it is loosely packed and a poor barrier film. This characteristic allows a larger molecule, namely a fluorinated acid chloride in our case, to effectively diffuse into the film and react with side chains throughout. If the PHEMA film were well-packed, acylation and film expansion would be unfavorable.

In contrast to the impedance behavior of PHEMA, fluorinated PHEMA films exhibit only one time constant. The key difference for the fluorinated films is that the time constant due to the initiator does not appear in the spectrum because R_f due to the fluorinated polymer is much greater than the combined impedance corresponding to R_i and C_i. Therefore, the equivalent circuit in Figure 3.3b simplifies to a Randles model in which R_s is in series with a parallel combination of R_f and C_f (Figure 3.3c). Both R_i and C_i should remain relatively constant throughout all polymer films although they could not be measured for the fluorinated films. Thus, for comparison purposes, only R_f and C_f values are compared between the different polymer films in Table 4.3.

In general, the best barrier films are those having the highest resistance and the lowest capacitance (Equations 3-3 through 3-5). Relating this idea to the impedance spectra in Figure 4.5, the films become progressively better barriers in going from the lowest curve (bare gold) to the highest curve (FBZ). Comparison of R_f for either F1 or F3 with that for PHEMA shows ~4 orders of magnitude improvement upon fluorination. Also, the film capacitance was lowered by a factor of ~50 in both cases due to the capping of hydrophilic hydroxyl groups and the enhanced hydrophobicity of the partially fluorinated film that more effectively excludes water and yields a lower effective

dielectric constant. The fact that even the short chain modification present in F1 gives much improved barrier properties over PHEMA suggests that conversion of hydroxyl groups plays a significant role in boosting film resistance and capacitance, as F1 is unable to structure the film but does have a very high side chain conversion. F1 and F3 likely show similar impedance behavior because even though F1 has a higher film conversion, F3 includes more hydrophobic material in the film. For F7, the resistance was increased by a factor of 5 above F3 with capacitance ~25% lower. The improved barrier performance of F7 over F3 is attributed to the higher fluorocarbon content and the ability of the longer fluoroalkyl chains to structure the film and minimize defects. As already stated, hydroxyl conversion plays a role in this process, but for these two films conversion is almost identical (~80%) but the drastically improved structuring of F7 gives a much smaller yet still significant improvement in R_f. The most surprising result from Figure 4.5 and Table 4.3 was that FBZ, even though the perfluorobenzoyl group was a short addition to the side chain, was actually the best barrier film studied, with the highest resistance and lowest capacitance. This film provided an improvement over PHEMA by nearly five orders of magnitude for resistance and two full orders of magnitude for capacitance. Even compared to the thicker F7 film, FBZ exhibited a higher resistance (by a factor of 2.5) and a 30% lower capacitance. We attribute the superior protection of FBZ to its high conversion (~85%) and the ability of the perfluoroaryl groups to exhibit dominant π-π interactions, effectively stacking atop one another to structure the film and eliminate ion-conducting pathways. Fluoroaromatics like perfluorobenzene have been shown[18,39] to exhibit such strong π-π interactions, even packing closer together than typical aromatic rings.

Fluorinated side chains greatly improve barrier properties over PHEMA, most likely due to the capping of hydrophilic hydroxyl groups throughout the film. Structuring of the chains within the film, enhanced for longer perfluoroalkyl groups and for perfluoroaryl groups, and the water-repellent nature of the fluorocarbons that minimize water penetration also play key roles in the creation of these barrier coatings. Merely taking up available space in the film does not account for the observed results, particularly when considering the resistance and capacitance of FBZ as compared with the other fluorinated films.

Film Stability

In this work, the acylation reaction results in a fluorinated ester linkage on the polymer side chains. Esters having fluorocarbon constituency α or β to the carbonyl moiety are known to be susceptible to degradation upon exposure to heat[40,41] or base.[42] If so desired, the fluorocarbon side chains could be strengthened in regard to hydrolysis by addition of a hydrocarbon (CH_2) spacer next to the carbonyl. While gaining the surface properties of fluorinated polymers is directly advantageous for our method of surface-initiated polymerization and modification, the ability to simply and effectively cleave the fluorocarbon side chains could have a broad impact on the preparation of temporary resists or patterned films and surfaces.[40]

The stability of PHEMA–based polymer films against hydrolysis was evaluated by placing samples of PHEMA, F1, F3, F7, and FBZ in deionized water or a 0.5 M KOH solution in ethanol for various amounts of time, rinsing with deionized water, drying with nitrogen, and then reexamining their IR spectra. IR spectra for the samples exposed to

water showed no detrimental effects even after 5 days of exposure. The PHEMA sample in KOH also showed no change in the IR spectrum. The IR spectra of the fluorinated polymers in KOH, on the other hand, showed conversion of the film back to PHEMA almost instantaneously (within 1-2 s) for the fluoroalkyl side chains (Figure 4.6) and within 20 min for the fluoroaryl side chain (not shown). Reversion to PHEMA was evidenced by the complete loss of the carbonyl peak at ~1790 cm^{-1} (for the fluoroalkyl films) and CF stretching peaks from 1100 to 1400 cm^{-1}, the regained peak in the hydroxyl region from 3100 to 3500 cm^{-1}, and the regained intensity of the carbonyl at 1733 cm^{-1} (Figure 4.6). As previously mentioned, this last point provides confirmation that the original reduction in the carbonyl at 1733 cm^{-1} upon acylation was not due to chain loss but rather to orientational effects. Even the perfluorobenzoyl side chain, having no α fluorine but only β fluorine, reverted back to PHEMA within 20 min as the ester was gradually hydrolyzed. These attributes are consistent with rapid hydrolysis of the fluorinated ester but an inability to hydrolyze the hydrocarbon PHEMA ester, which is much more stable.[42] The remarkable ability to convert these partially fluorinated polymer films back to PHEMA by simple immersion in base may provide a new strategy to control the depth-dependent composition within polymer films and holds promise for the efficient patterning of polymer films and structures. This particular attribute will be explored more fully in subsequent chapters to create novel polymeric architectures.

Conclusions

Addition of fluorinated side chains to surface-initiated PHEMA through an acylation reaction results in a partially fluorinated polymer film and imparts desirable

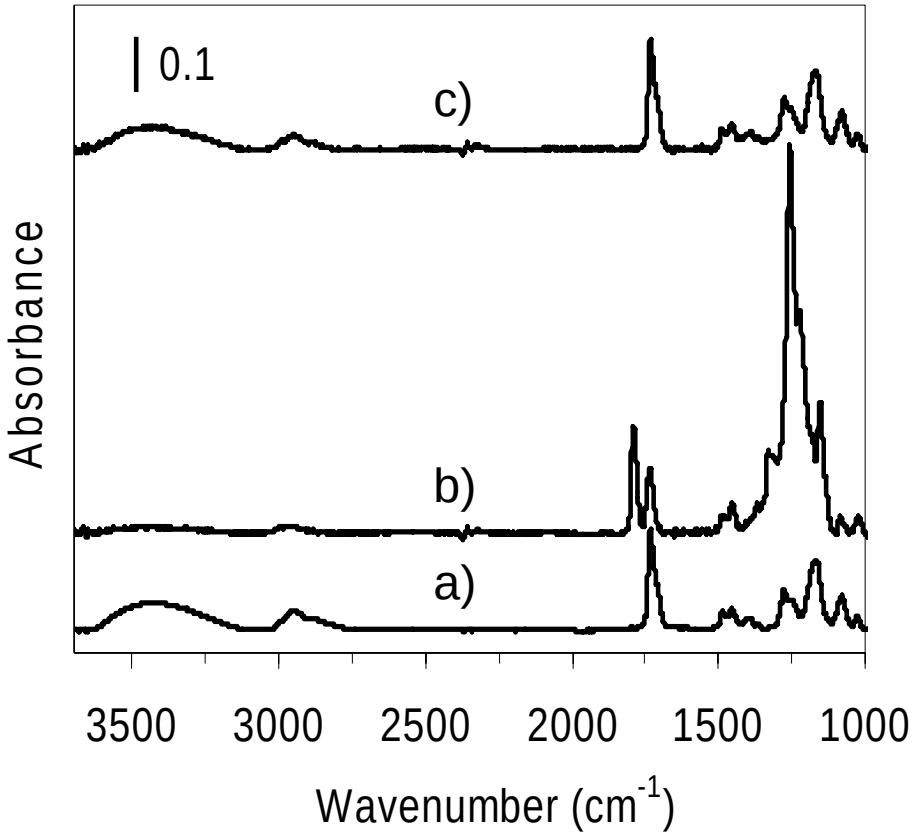

Figure 4.6. RAIR spectrum of a single PHEMA sample: a) before fluorination; b) after fluorination with $C_7F_{15}COCl$ to form F7; and c) after hydrolysis with 0.5 M KOH in ethanol for ~1 s.

attributes such as surface hydrophobicity and oleophobicity, bulk and interfacial film structuring, and dramatically improved barrier properties. A longer fluoroalkyl side group (C_7F_{15}) on PHEMA greatly improves the film properties in all areas—higher resistance, lower capacitance and critical surface tension, and a more well-defined structure—as compared with shorter fluoroalkyl chains (CF_3 or C_3F_7), due to enhanced interchain interactions. A perfluoroaryl side group (C_6F_5) provides the greatest resistance and lowest capacitance of all the films, due to its high conversion and strong intermolecular stacking interactions of the fluoroaryl groups to greatly reduce ion-conducting paths. The production of fluorinated PHEMA in the manner described avoids many problems encountered with traditional fluorinated polymer films, such as solubility and adhesional issues, and enables rapid assessment of the role of side chain length and composition on film properties while maintaining a common reference film (PHEMA). Furthermore, the critical surface energies of the fluoroalkyl-modified films are at least comparable to and, with long side chain modifications, even much lower than those of PTFE and many other fluorinated polymers.

References

1. Delucchi, M.; Turri, S.; Barbucci, A.; Bassi, M.; Novelli, S.; Cerisola, G. "Fluoropolyether Coatings: Relationships of Electrochemical Impedance Spectroscopy Measurements, Barrier Properties, and Polymer Structure," *Journal of Polymer Science Part B-Polymer Physics* **2002**, *40*, 52-64.

2. Wang, J. G.; Mao, G. P.; Ober, C. K.; Kramer, E. J. "Liquid Crystalline, Semifluorinated Side Group Block Copolymers with Stable Low Energy Surfaces: Synthesis, Liquid Crystalline Structure, and Critical Surface Tension," *Macromolecules* **1997**, *30*, 1906-1914.

3. Tirelli, N.; Ahumada, O.; Suter, U. W.; Menzel, H.; Castelvetro, V. "Investigation on the Wettability Properties of Thin Films of Methacrylic Polymers with Partially Fluorinated Side Chains," *Macromolecular Chemistry and Physics* **1998**, *199*, 2425-2431.

4. Li, K.; Wu, P. P.; Han, Z. W. "Preparation and Surface Properties of Fluorine-Containing Diblock Copolymers," *Polymer* **2002**, *43*, 4079-4086.

5. Sivakumar, C.; Wen, T. C.; Gopalan, A.; Teng, H. "Electroactive Conducting Blends of Poly(O-Toluidine) and Poly(Vinylidene Fluoride) and Characterisation," *Synthetic Metals* **2003**, *132*, 219-226.

6. Fukushima, H.; Seki, S.; Nishikawa, T.; Takiguchi, H.; Tamada, K.; Abe, K.; Colorado, R.; Graupe, M.; Shmakova, O. E.; Lee, T. R. "Microstructure, Wettability, and Thermal Stability of Semifluorinated Self-Assembled Monolayers (SAMs) on Gold," *Journal of Physical Chemistry B* **2000**, *104*, 7417-7423.

7. Mackie, N. M.; Castner, D. G.; Fisher, E. R. "Characterization of Pulsed-Plasma-Polymerized Aromatic Films," *Langmuir* **1998**, *14*, 1227-1235.

8. Lau, K. K. S.; Murthy, S. K.; Lewis, H. G. P.; Caulfield, J. A.; Gleason, K. K. "Fluorocarbon Dielectrics Via Hot Filament Chemical Vapor Deposition," *Journal of Fluorine Chemistry* **2003**, *122*, 93-96.

9. Lau, K. K. S.; Bico, J.; Teo, K. B. K.; Chhowalla, M.; Amaratunga, G. A. J.; Milne, W. I.; McKinley, G. H.; Gleason, K. K. "Superhydrophobic Carbon Nanotube Forests," *Nano Letters* **2003**, *3*, 1701-1705.

10. Jung, D. H.; Park, I. J.; Choi, Y. K.; Lee, S. B.; Park, H. S.; Rühe, J. "Perfluorinated Polymer Monolayers on Porous Silica for Materials with Super Liquid Repellent Properties," *Langmuir* **2002**, *18*, 6133-6139.

11. Lovinger, A. J. "If Nothing Sticks to Teflon, How Does It Stick to Pans?," *Scientific American* **2002**, *286*, 100.

12. Matyjaszewski, K. "Macromolecular Engineering by Controlled/Living Ionic and Radical Polymerizations," *Macromolecular Symposia* **2001**, *174*, 51-67.

13. Boyes, S. G.; Brittain, W. J.; Weng, X.; Cheng, S. Z. D. "Synthesis, Characterization, and Properties of ABA Type Triblock Copolymer Brushes of Styrene and Methyl Acrylate Prepared by Atom Transfer Radical Polymerization," *Macromolecules* **2002**, *35*, 4960-4967.

14. Prucker, O.; Rühe, J. "Synthesis of Poly(Styrene) Monolayers Attached to High Surface Area Silica Gels through Self-Assembled Monolayers of Azo Initiators," *Macromolecules* **1998**, *31*, 592-601.

15. Andruzzi, L.; Hexemer, A.; Li, X. F.; Ober, C. K.; Kramer, E. J.; Galli, G.; Chiellini, E.; Fischer, D. A. "Control of Surface Properties Using Fluorinated Polymer Brushes Produced by Surface-Initiated Controlled Radical Polymerization," *Langmuir* **2004**, *20*, 10498-10506.

16. Bantz, M. R. *Effect of Fractional Fluorination on the Properties of Surface-Initiated Poly(Hydroxyethyl Methacrylate) Films*. Master's Thesis, Chemical Engineering, Vanderbilt University, 2004.

17. Bantz, M. R.; Brantley, E. L.; Weinstein, R. D.; Moriarty, J.; Jennings, G. K. "Effect of Fractional Fluorination on the Properties of ATRP Surface-Initiated Poly(Hydroxyethyl Methacrylate) Films," *Journal of Physical Chemistry B* **2004**, *108*, 9787-9794.

18. Adams, N.; Cowley, A. R.; Dubberley, S. R.; Sealey, A. J.; Skinner, M. E. G.; Mountford, P. "Evaluation of the Relative Importance of Ti-Cl Center Dot Center Dot Center Dot H-N Hydrogen Bonds and Supramolecular Interactions between Perfluorophenyl Rings in the Crystal Structures of Ti(Nr)Cl-2(NHMe2)(2) (R = Pr-I, C6H5 or C6F5)," *Chemical Communications* **2001**, 2738-2739.

19. Nuzzo, R. G.; Dubois, L. H.; Allara, D. L. "Fundamental-Studies of Microscopic Wetting on Organic-Surfaces .1. Formation and Structural Characterization of a Self-Consistent Series of Polyfunctional Organic Monolayers," *Journal of the American Chemical Society* **1990**, *112*, 558-569.

20. Coleman, M. M.; Lee, K. H.; Skrovanek, D. J.; Painter, P. C. "Hydrogen-Bonding in Polymers .4. Infrared Temperature Studies of a Simple Polyurethane," *Macromolecules* **1986**, *19*, 2149-2157.

21. Silverstein, R. M.; Webster, F. X. *Spectrometric Identification of Organic Compounds*, 6th ed.; Wiley: New York, 1998.

22. Tsao, M. W.; Hoffmann, C. L.; Rabolt, J. F.; Johnson, H. E.; Castner, D. G.; Erdelen, C.; Ringsdorf, H. "Studies of Molecular Orientation and Order in Self-Assembled Semifluorinated N-Alkanethiols: Single and Dual Component Mixtures," *Langmuir* **1997**, *13*, 4317-4322.

23. Greenler, R. G. "Infrared Study of Adsorbed Molecules on Metal Surfaces by Reflection Techniques," *Journal of Chemical Physics* **1966**, *44*, 310-314.

24. Parikh, A. N.; Allara, D. L. "Quantitative-Determination of Molecular-Structure in Multilayered Thin-Films of Biaxial and Lower Symmetry from Photon Spectroscopies .1. Reflection Infrared Vibrational Spectroscopy," *Journal of Chemical Physics* **1992**, *96*, 927-945.

25. Han, L. C. M.; Timmons, R. B.; Lee, W. W.; Chen, Y. Y.; Hu, Z. B. "Pulsed Plasma Polymerization of Pentafluorostyrene: Synthesis of Low Dielectric Constant Films," *Journal of Applied Physics* **1998**, *84*, 439-444.

26. Huang, W. X.; Kim, J. B.; Bruening, M. L.; Baker, G. L. "Functionalization of Surfaces by Water-Accelerated Atom-Transfer Radical Polymerization of Hydroxyethyl Methacrylate and Subsequent Derivatization," *Macromolecules* **2002**, *35*, 1175-1179.

27. Naud, C.; Calas, P.; Commeyras, A. "Critical Influence of the Fluorinated Chain Length in the Self- Assembly of Terminally Perfluorinated Alkanethiol Monolayers on Gold Surfaces. An Electrochemical Study," *Langmuir* **2001**, *17*, 4851-4857.

28. Levitt, M.; Perutz, M. F. "Aromatic Rings Act as Hydrogen-Bond Acceptors," *Journal of Molecular Biology* **1988**, *201*, 751-754.

29. Laibinis, P. E.; Palmer, B. J.; Lee, S.-W.; Jennings, G. K. "Self-Assembled Monolayers of Thiols" In *Thin Films*; Ulman, A.; Powell, R.; Francombe, M. H., Eds.; Academic Press, 1998; Vol. 24, pp 1-41.

30. Weinstein, R. D.; Moriarty, J.; Cushnie, E.; Colorado, R.; Lee, T. R.; Patel, M.; Alesi, W. R.; Jennings, G. K. "Structure, Wettability, and Electrochemical Barrier Properties of Self-Assembled Monolayers Prepared from Partially Fluorinated Hexadecanethiols," *Journal of Physical Chemistry B* **2003**, *107*, 11626-11632.

31. de Boer, B.; Meng, H.; Perepichka, D. F.; Zheng, J.; Frank, M. M.; Chabal, Y. J.; Bao, Z. N. "Synthesis and Characterization of Conjugated Mono- and Dithiol Oligomers and Characterization of Their Self-Assembled Monolayers," *Langmuir* **2003**, *19*, 4272-4284.

32. Zisman, W. A. *Contact Angle, Wettability, and Adhesion*; American Chemical Society: Washington, D.C., 1964; Vol. 43.

33. Bin Zhang, Z.; Ying, S. K.; Hu, Q. H.; Xu, X. D. "Semifluorinated ABA Triblock Copolymers: Synthesis, Characterization, and Amphiphilic Properties," *Journal of Applied Polymer Science* **2002**, *83*, 2625-2633.

34. Genzer, J.; Sivaniah, E.; Kramer, E. J.; Wang, J. G.; Korner, H.; Xiang, M. L.; Char, K.; Ober, C. K.; DeKoven, B. M.; Bubeck, R. A.; Chaudhury, M. K.; Sambasivan, S.; Fischer, D. A. "The Orientation of Semifluorinated Alkanes Attached to Polymers at the Surface of Polymer Films," *Macromolecules* **2000**, *33*, 1882-1887.

35. Janek, R. P.; Fawcett, W. R.; Ulman, A. "Impedance Spectroscopy of Self-Assembled Monolayers on Au(111): Sodium Ferrocyanide Charge Transfer at Modified Electrodes," *Langmuir* **1998**, *14*, 3011-3018.

36. Jennings, G. K.; Munro, J. C.; Yong, T. H.; Laibinis, P. E. "Effect of Chain Length on the Protection of Copper by N-Alkanethiols," *Langmuir* **1998**, *14*, 6130-6139.

37. Yan, D.; Saunders, J. A.; Jennings, G. K. "Enhanced Chain Densities of N-Alkanethiolate Self-Assembled Monolayers on Gold from Aqueous Micellar Solutions," *Langmuir* **2000**, *16*, 7562-7565.

38. Jennings, G. K.; Munro, J. C.; Laibinis, P. E. "Effects of Film Crystallinity on the Protective Properties of Self-Assembled Monolayers of Alkanethiols on Copper," *Advanced Materials* **1999**, *11*, 1000-1003.

39. Lorenzo, S.; Lewis, G. R.; Dance, I. "Supramolecular Potentials and Embraces for Fluorous Aromatic Molecules," *New Journal of Chemistry* **2000**, *24*, 295-304.

40. Boker, A.; Reihs, K.; Wang, J. G.; Stadler, R.; Ober, C. K. "Selectively Thermally Cleavable Fluorinated Side Chain Block Copolymers: Surface Chemistry and Surface Properties," *Macromolecules* **2000**, *33*, 1310-1320.

41. Boker, A.; Herweg, T.; Reihs, K. "Selective Alteration of Polymer Surfaces by Thermal Cleavage of Fluorinated Side Chains," *Macromolecules* **2002**, *35*, 4929-4937.

42. Tonelli, C.; Di Meo, A.; Barchiesi, E. "Perfluoropolyether Alkyl Diesters: Structure Effects of the Alkyl Group on the Kinetics of the Hydrolysis Reactions," *Journal of Polymer Science Part a-Polymer Chemistry* **2002**, *40*, 4266-4280.

CHAPTER V

MODIFICATION OF SURFACE-INITIATED POLYMER FILMS WITH HYDROCARBON CHAINS

Hydrocarbon polymers are potentially useful in thin films applications because they are inert, available at low cost, and resistant to penetration by moisture.[1-5] However, many hydrocarbon polymers, such as polyethylene, are extremely difficult to process into ultrathin films due to solubility issues.[6] In similar fashion to well-controlled preparation of polymer films having fluorocarbon side chains, films exhibiting hydrocarbon side chains may also be created using the same growth and similar post-polymerization reaction scheme (Figure 5.1). This methodology again utilizes a base film as a test stage for creation of numerous polymer films with varying chemical composition and enables a fundamental understanding of how hydrocarbon side chain length affects film properties. Comparisons with fluorocarbon chains can be made regarding bulk and interfacial structuring, wettability, and barrier properties. Uncovering these molecular-level details will be advantageous in the molecular-level design of polymer films.

Other groups have performed work on the modification of polymer hydroxyl groups with hydrocarbon chains or on the effect of hydrocarbon chain length on the properties of thin films. One recent work has exploited the hydroxyl groups of PHEMA by reaction with trimethylchlorosilane to make the film more hydrophobic and improve its etch resistance.[7] Additionally, modification of hydroxyl groups with $C_{15}H_{31}COCl$ has been shown to dramatically improve surface hydrophobicity of thin ($\leq$ 40 nm) surface-initiated polyglycidol brushes grown via anionic ring-opening polymerization on silicon.[8]

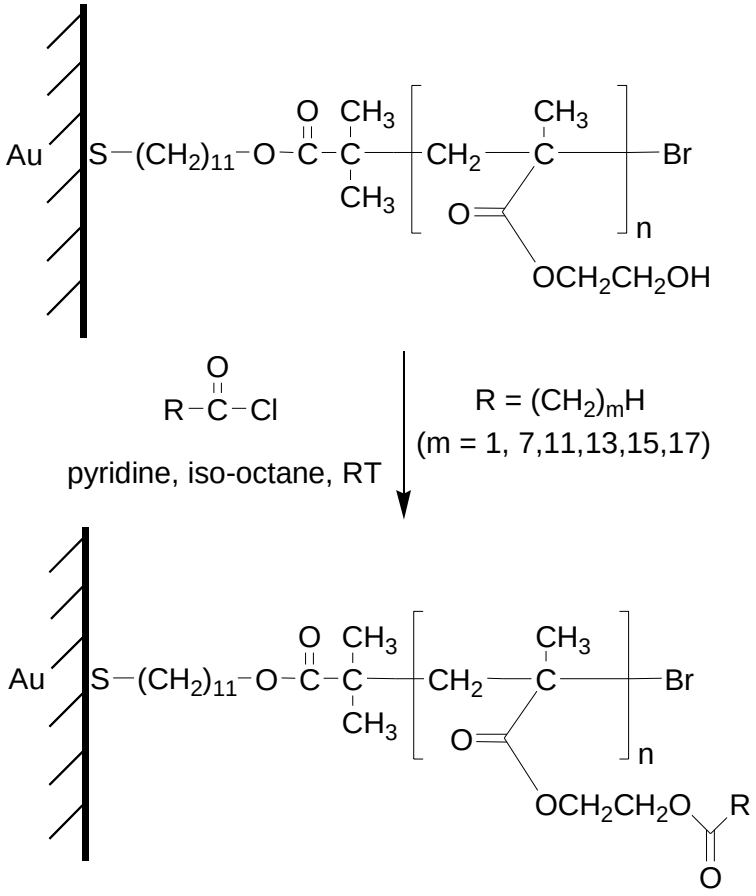

Figure 5.1. Derivatization of PHEMA hydroxyl groups with hydrocarbon chains via a nucleophilic acylation reaction with alkanoyl chlorides.

Kraft and Moore have investigated the effects of reacting PHEMA microgels with hydrocarbon acid chlorides (ranging from m = 1 to 15) to form fatty acid surface layers that delay microgel expansion.[9] They found that acetyl-modified and unmodified microgels expand readily, that rather short (m = 4) alkyl chains offer maximum resistance to microgel expansion, and that as the chain length is further increased, the resistance decreases. Varying alkyl side chain length has also been tested on Langmuir-Blodgett films, specifically to investigate the role of chain length on the structure and order of film packing. Of particular relevance, acylethylenimines having short hydrocarbon side chains were found to exist in an easily compressible, liquid-like state.[10] As the side chain length was increased, the monolayers became more condensed until at chain lengths greater than 13, the resulting monolayers became crystallized, rigid structures. Similarly, a hydrocarbon side chain length of 18 in polyimide Langmuir-Blodgett films resulted in crystallized structures, as verified by IR peak positions for methylene stretching modes.[11] As for surface-initiated polymers, Stöhr and Rühe grew various n-alkyl methacrylates from physisorbed poly(caprolactone) macroinitiators on silicon oxide.[12] They found that the surface became increasingly hydrophobic as the length of the polymer side chain was increased from a methyl to a stearyl group. However, to our knowledge, the combined structural, surface, and barrier properties of polymer films with varying alkyl side chain length has not been investigated. Our general film preparation methods allow us to make these film property comparisons among various hydrocarbon-modified films along with comparisons to the fluorocarbon-modified PHEMA films.

Experimental Procedures

PHEMA films having reactive hydroxyl side chains were created as described in Chapter III. Derivatization of PHEMA with hydrocarbon side chains was accomplished by exposing the film to 20 mM solutions of acetyl chloride (CH_3COCl), octanoyl chloride ($C_7H_{15}COCl$), lauroyl chloride ($C_{11}H_{23}COCl$), myristoyl chloride ($C_{13}H_{27}COCl$), palmitoyl chloride ($C_{15}H_{31}COCl$), or stearoyl chloride ($C_{17}H_{35}COCl$) with 25 mM pyridine in iso-octane for at least 3 h to give H1, H7, H11, H13, H15, or H17 films, respectively (Figure 5.1). After reaction, the films were rinsed with iso-octane and ethanol and dried with nitrogen. To facilitate discussion and comparison of the multiple chain lengths employed in this work, *m* will be used to denote the chain length of the hydrocarbon modification: C_mH_{2m+1}; m = 1, 7, 11, 13, 15, 17.

Results and Discussion

Film Composition and Structure

We used RAIRS to monitor compositional changes within the polymer films due to acylation by the various hydrocarbon acid chlorides. Figure 5.2 shows a survey IR spectrum for a representative hydrocarbon-modified PHEMA film, H7, along with the spectrum for PHEMA. All other hydrocarbon-modified films exhibit the same peaks in the IR spectrum as H7 but at slightly different positions and intensities. Differences between the films, particularly in the C=O and CH_2 stretching regions, are accentuated in Figures 5.3 and 5.4, respectively. In similar fashion to the fluorocarbon-modified PHEMA films, diminution of the hydroxyl peak in the region from 3100 to 3700 cm^{-1}

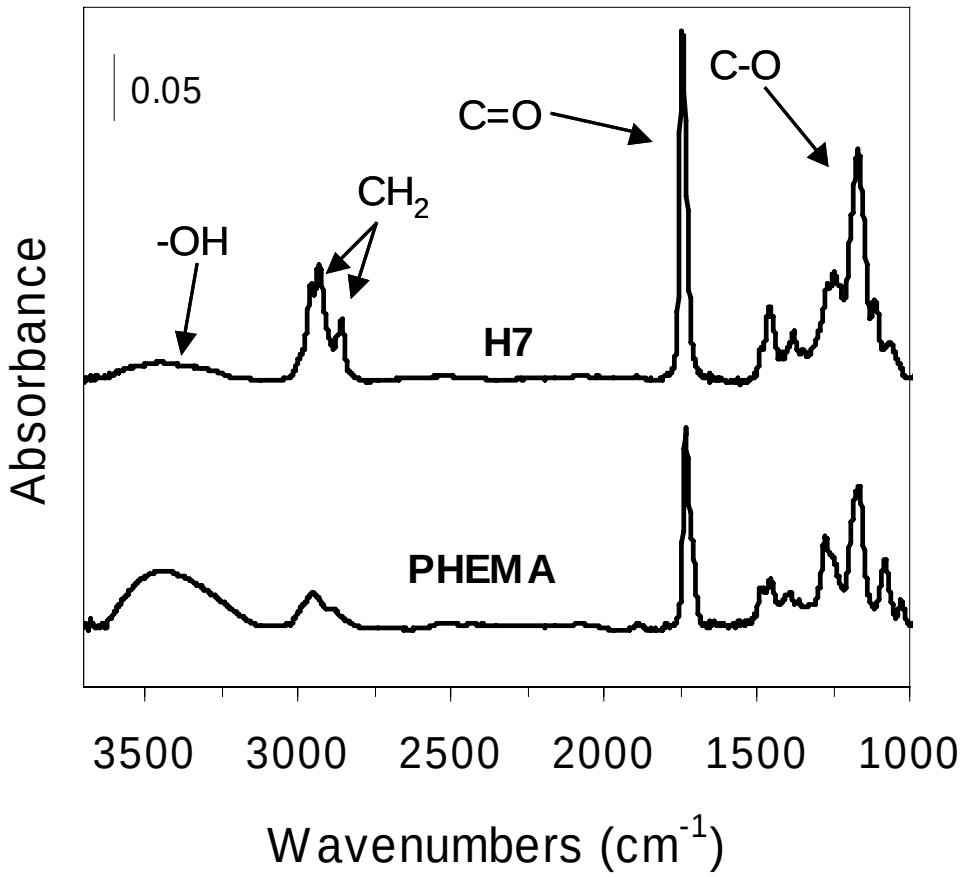

Figure 5.2. Reflectance-absorption IR spectra of PHEMA and a representative hydrocarbon-modified PHEMA film, H7. Regions of interest are labeled on the plot.

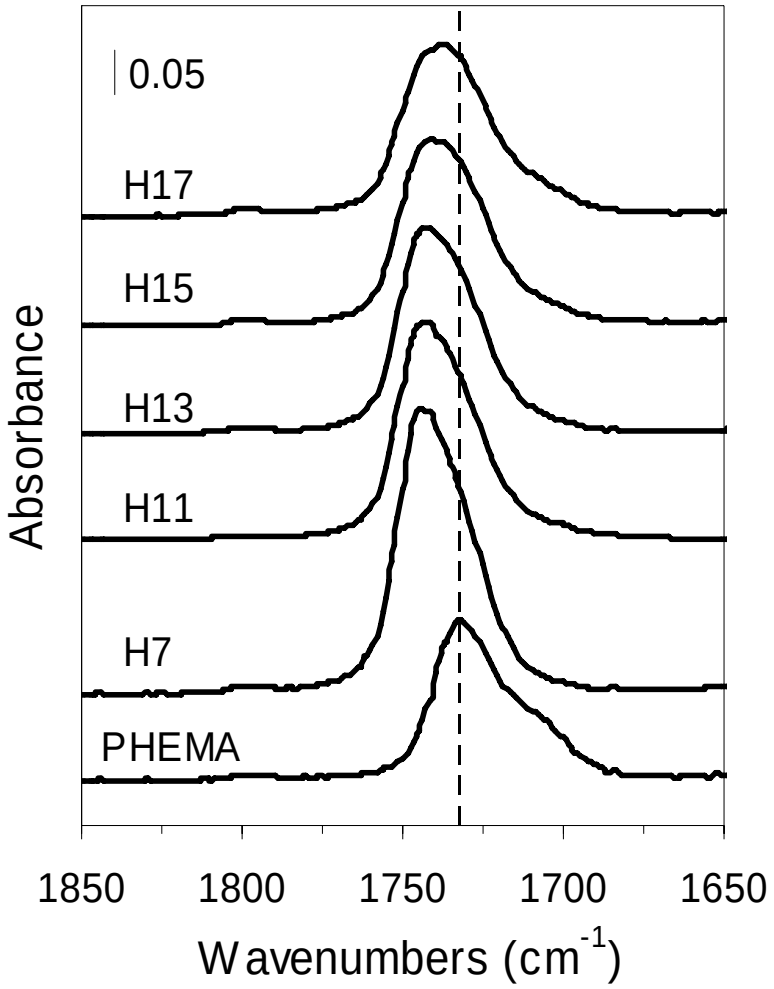

Figure 5.3. Carbonyl (C=O) stretching region of IR spectra for PHEMA and hydrocarbon-modified PHEMA films. The dashed line at 1733 cm^{-1} indicates the position of the carbonyl peak for PHEMA.

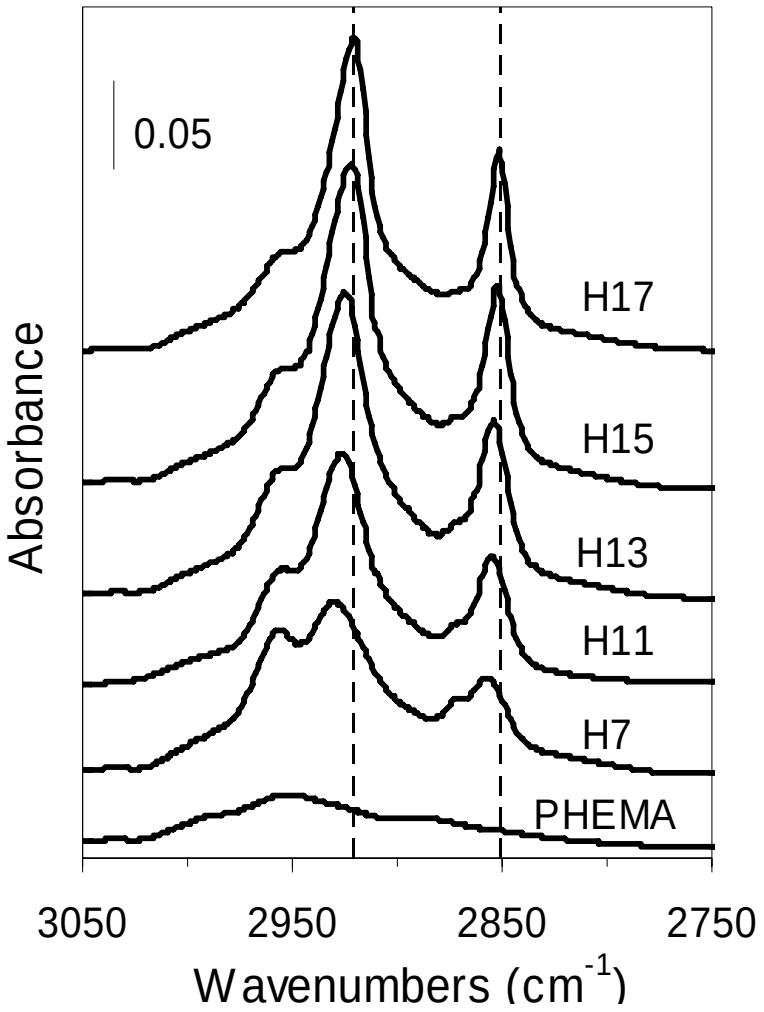

Figure 5.4. C-H stretching region of IR spectra for PHEMA and hydrocarbon-modified PHEMA films. The dashed lines are positioned at 2852 and 2921 cm^{-1}, corresponding to the lowest peak positions observed for $\nu_s(CH_2)$ and $\nu_a(CH_2)$ in these films.

may be used to estimate conversion of hydroxyl side chains of PHEMA to esters. Table 5.1 lists conversions, calculated using Eq 4-1, from at least five independent preparations for each acid chloride. As the length of the hydrocarbon side chain is increased, conversion drops substantially, suggesting molecular size limits penetration and subsequent reaction of acid chlorides within the film. H1 exhibits extremely high conversion since, as a small molecule, it can easily diffuse into the film and provides little steric hindrance after reaction. For the modification with the longest side chain group ($C_{17}H_{35}$), conversion was significantly lower than that for the other hydrocarbon films. Several attempts were made, without success, to increase conversion for H17 by using different solvents and raising temperature.

The acylation reaction studied here causes two other differences in the IR spectra of modified PHEMA films as compared to PHEMA: introduction of an additional ester linkage and the presence of hydrocarbon chains of varying length on each modified side chain. The hydrocarbon ester from acylation of the side chain results in a second carbonyl peak in the spectrum around 1750 cm^{-1} and enhanced C-O stretching peaks from 1100 to 1300 cm^{-1}. The introduction of long hydrocarbon chains into the polymer film results in a significant increase in the intensity of C-H bending (1400 to 1500 cm^{-1}) and C-H stretching (2800 to 3000 cm^{-1}) modes in the IR spectrum.

The carbonyl peak resulting from acylation is not easily distinguished from the original PHEMA ester carbonyl peak (Figure 5.3) due to similar chemical environment and therefore similar peak positions. The peak for the carbonyl associated with the PHEMA ester appears at 1733 cm^{-1}, whereas the carbonyl peak due to acylation appears at somewhat higher wavenumbers (~1750 cm^{-1}, as evidenced by this peak position in H1)

Table 5.1. Conversion, IR peak positions, and film thickness information for hydrocarbon-modified PHEMA films.

		IR Peak Positions			Film Thickness		
Film	**χ (%)**	**ν (C=O)[a]**	**ν_s (CH_2)**	**ν_a (CH_2)**	**Observed Increase (%)**	**Repeat Unit MW (g mol^{-1})**	**Predicted Increase (%)**
H1	93 ± 3	1750	—	—	29	172	30
H7	82 ± 5	1744	2858	2930	110	256	81
H11	77 ± 6	1744	2855	2926	127	312	116
H13	68 ± 5	1742	2855	2925	124	341	121
H15	64 ± 4	1742	2852	2922	111	369	119
H17	37 ± 6	1737	2852	2921	40	397	75
H17/H1	82 ± 4	1750	2852	2920	53	—	87[b]

[a] The C=O peak positions are typical for each film but can shift slightly as conversion deviates from the average values.
[b] Based on 35% conversion for H17 and 47% for H1.

but still relatively close to the PHEMA carbonyl peak. Upon acylation, one broader peak appears in the region, representing the combined intensities of the PHEMA carbonyl and the carbonyl from the acylation reaction. From Figure 5.3 and Table 5.1, the resultant carbonyl peak position shifts with increasing hydrocarbon chain length. This shift is due to lower conversion within the film as *m* increases, meaning that less IR peak intensity is introduced at higher wavenumbers by the new carbonyl. Furthermore, the overall intensity of the combined carbonyl peak is also reduced as *m* is increased because of diminishing conversion.

Addition of alkyl groups to the PHEMA side chains also results in a significant increase in C-H bending and stretching bands in the IR spectrum, and the position of these peaks gives an indication of chain packing and crystallinity. As compared to the spectrum for PHEMA, those for modified PHEMA show a sharper CH_2 bending peak at ~1470 cm^{-1} (Figure 5.2). However, there is no peak splitting as observed in crystalline polymethylene lattices with orthorhombic chain packing.[6] Symmetric and asymmetric methylene stretching modes, $\nu_s(CH_2)$ and $\nu_a(CH_2)$ respectively, become much more prominent and sharper after addition of alkyl side chains (Figure 5.4). From previous IR studies of polymethylene chains,[6,13] a $\nu_s(CH_2)$ mode positioned at ~2850 cm^{-1} and a $\nu_a(CH_2)$ mode positioned at ~2918 cm^{-1} are indicative of highly crystalline chain packing while shifts to higher wavenumbers indicate less dense, more liquid-like packing.[14] Figure 5.4 shows that increasing the hydrocarbon chain length results in more crystalline chain packing (fewer gauche conformers) within the film as the $\nu_a(CH_2)$ position decreases from 2930 (m = 7) to 2921 (m = 17) cm^{-1}. The improved crystallinity observed for longer alkyl side groups is consistent with greater van der Waals interactions among

hydrocarbon chains, which increase proportionally with chain length and facilitate chain structuring within the film.[15] Additionally, in copolymer systems having one component that packs efficiently and one that packs poorly (i.e. ethylene-butene copolymers[16]), the more efficient-packing chains tend to order while the poorer-packing chains do not. Similarly in our system, increasing hydrocarbon chain length results in more crystalline packing because the van der Waals interactions between the alkyl chains become increasingly important as compared with the interactions between other groups within the polymer film.

Film Thickness

Table 5.1 also shows film thickness increases obtained by ellipsometry for acylation of PHEMA with the various hydrocarbon acid chlorides. Starting with a PHEMA film, the polymer layer expands upon acylation with hydrocarbon acid chlorides to accommodate the additional side chain volume. The observed trends roughly agree (within ~30%) with theoretical estimates based on conversion and molecular weight considerations, which have been used previously[17] to model the addition of short hydrocarbon groups to PHEMA. Unlike for the fluorocarbon modifications, there is no need to model the thickness changes with a volumetric model since the entire polymer composition remains hydrocarbon; the volumetric and molecular weight models give the same expected thickness increases. H1 results in only ~30% increased film thickness since minimal side chain volume was introduced even at very high conversion. With the exception of H17, which exhibits exceptionally low conversion, the addition of long hydrocarbon groups (m = 7 to 15) resulted in slightly more than a doubling of polymer

film thickness. Since the hydrocarbon chains exhibit lower conversions from H7 to H15, the film thickness change remains relatively constant for this series.

Surface Wettability

Advancing and receding contact angles (θ_A and θ_R) of water were measured for all polymer films to provide a measure of surface hydrophobicity. Table 5.2 gives average contact angles for the modified films along with the values for PHEMA and the bromine-terminated initiator monolayer for comparison. Evaluation of water contact angles for the initiator monolayer and the PHEMA film have already been discussed in Chapter IV. The advancing and receding contact angles for water on H1 were consistent with a moderately hydrophilic surface and a smoothing of the film as compared with PHEMA (Table 5.2). Longer chain hydrocarbon-modified PHEMA films (m = 7 to 17) show much higher advancing water contact angles, ranging from 104° to 117°. Within this series, H7 gives a lower contact angle than the other films, indicating that the shorter chain is unable to fully affect surface properties likely due to insufficient chain length. All other alkyl-modified films (H11 to H17) provide fairly high water contact angles, consistent with those reported for methyl-terminated surfaces.[18] Within this group, the lowest contact angle hysteresis is observed for H17 with the highest observed for H11, suggesting that longer alkyl side chains result in smoother or more homogeneous surfaces.

Contact angles of hexadecane were also measured on all polymer films. Hexadecane is a sensitive probe of hydrocarbon surface composition, indicating whether a surface consists primarily of $-CH_2-$ or $-CH_3$ groups. Well-structured methyl surfaces

Table 5.2. Water and hexadecane advancing and receding contact angles (º) for hydrocarbon-modified PHEMA films on gold.

	Water		Hexadecane	
Film	θ_A	θ_R	θ_A	θ_R
Initiator	80 ± 2	74 ± 2	<10	<10
PHEMA	75 ± 3	23 ± 2	<10	<10
H1	70 ± 2	52 ± 3	<10	<10
H7	104 ± 2	60 ± 4	<10	<10
H11	113 ± 1	59 ± 4	16 ± 3	<10
H13	117 ± 1	70 ± 4	21 ± 2	<10
H15	117 ± 2	65 ± 5	44 ± 1	26 ± 3
H17	115 ± 3	77 ± 7	47 ± 2	34 ± 4

exhibit advancing hexadecane contact angles of ~50°, whereas hexadecane completely wets methylene surfaces.[19] Table 5.2 shows that the advancing hexadecane contact angle increases with increasing hydrocarbon side chain length. For H7, hexadecane completely wets the surface, indicating that $-CH_3$ groups are not at the surface of this film and remaining consistent with the lower advancing water contact angle. As the side chain is lengthened from m = 11 to 17, the hexadecane contact angle increases and approaches that for a purely methyl surface. For H11 and H13, the hexadecane contact angle is low, indicating that these surfaces contain a large proportion of methylene or ester groups with some methyl functionality as well. For H15 and H17, however, the higher hexadecane contact angles suggest that the surface consists almost entirely of $-CH_3$ groups. Dense methyl surfaces are only possible with modified PHEMA films if the added hydrocarbon side chains orient nearly normal to the air-film interface at the outer few angstroms.[a] These results are consistent with those from RAIRS, which indicate films with improved crystallinity as the hydrocarbon chain length is increased. Furthermore, other researchers[10] have noted an improvement in the crystallinity of acylethylenimine Langmuir-Blodgett films containing alkyl side chains having more than 13 carbons. We observe similar results here, particularly on the basis of RAIRS and hexadecane wetting

[a] Bartell et. al have shown that hexadecane may insert itself into a film that has defects at the surface, thus artificially raising the hexadecane contact angle and yielding a surface that appears to have densely packed methyl groups. Bicyclohexyl is often used to more clearly verify a methyl surface since it is unable to insert into a film due to its bulkiness but has only a slightly higher surface tension than hexadecane (32.8 vs. 27.6). The advancing contact angle of bicyclohexyl on H15 and H17 was found to approach 53°, confirming the methyl functionality of these surfaces. See Bartell and Ruch. *J. Phys. Chem.* **1959**, *63*, 1045-1049 or Bain et. al. *J. Am. Chem. Soc.* **1989**, *111*, 321-335 for further information on this phenomenon.

results, with both H15 and H17 exhibiting superior crystalline packing and surface structuring as compared to films modified with shorter hydrocarbon groups.

For PHEMA modified with hydrocarbon as well as fluorocarbon chains, a critical chain length must first be utilized to induce well-structured surfaces. From previous work with fluorocarbon chains (Chapter IV), we found that F3 is not a well-structured film at the interface but that F7 results in a densely packed, oriented fluorocarbon layer at the interface, exhibiting an extremely low critical surface energy (9 mN/m). For the hydrocarbon films, alkyl chain lengths below 15 do not structure the surface to any great extent. However, modification with chain lengths of either 15 or 17 yield densely packed, oriented hydrocarbon surface layers analogous to dense fluorocarbon layers observed for F7. This offset in critical chain length was expected since, for Langmuir-Blodgett acylethylenimine films having either hydrocarbon or fluorocarbon side chains, longer hydrocarbon chains were required to achieve similar structure and air-film interfacial behavior as much shorter fluorocarbon chains.[10] The authors were unable to form LB films once a critical chain length was reached ($m > 13$ for hydrocarbons and $m > 7$ for fluorocarbons), as these polymers tended to form crystallized structures that were difficult to transfer to a substrate. They attributed the shorter critical chain length to the increased rigidity and hydrophobicity for fluorocarbon chains. For modified PHEMA films, the much larger area occupied by fluorocarbon chains as compared to hydrocarbon chains (diameter of 5.6 Å compared to 4.2 Å, or 80% greater area)[20] and the enhanced fluorocarbon rigidity likely result in a shorter critical chain length. In either case, these outermost groups orient normal to yield a mostly (perfluoro)methyl surface only when

the chains are sufficiently long to achieve interchain van der Waals interactions and prevent chain collapse at the surface that would expose (perfluoro)methylene groups.

Barrier Properties

We investigated the barrier properties of modified PHEMA films having various hydrocarbon side chains using EIS upon exposure to 1 mM $K_3Fe(CN)_6$ and 1 mM $K_4Fe(CN)_6$ in 0.1 M Na_2SO_4(aq). Figure 5.5 shows EIS spectra in the form of Bode plots for the initiator, PHEMA, and the hydrocarbon-modified polymer films on gold. Solid curves in the plot represent best fits of the data with appropriate equivalent circuit models (Figure 3.3) to provide quantitative information (Table 5.3) on the effect of composition on film resistance and capacitance. The following terms are used to denote various film and solution characteristics: solution resistance, R_s; initiator capacitance, C_i; initiator resistance, R_i; total film (polymer plus initiator) capacitance, C_f; and polymer film resistance, R_f. Chapter IV includes extensive discussion of the impedance spectra for both bare gold and the initiator monolayer on gold, so this will not be reiterated here.

While the more complex two time constant equivalent circuit (Figure 3.3b) rigorously applies to the hydrocarbon-modified PHEMA films, only one time constant typically appears in their impedance spectra. For the hydrocarbon films other than H17, R_f is greater than the combined impedance of R_i and C_i in parallel, so only a single time constant due to the hydrocarbon-modified film is observed in the spectra. In the same manner as for the fluorocarbon-modified PHEMA films, the impedance spectra for these films may be modeled using the one time constant circuit shown in Figure 3.3c. The impedance behavior of H17 (Figure 5.5), due to a poor fit with the basic two time

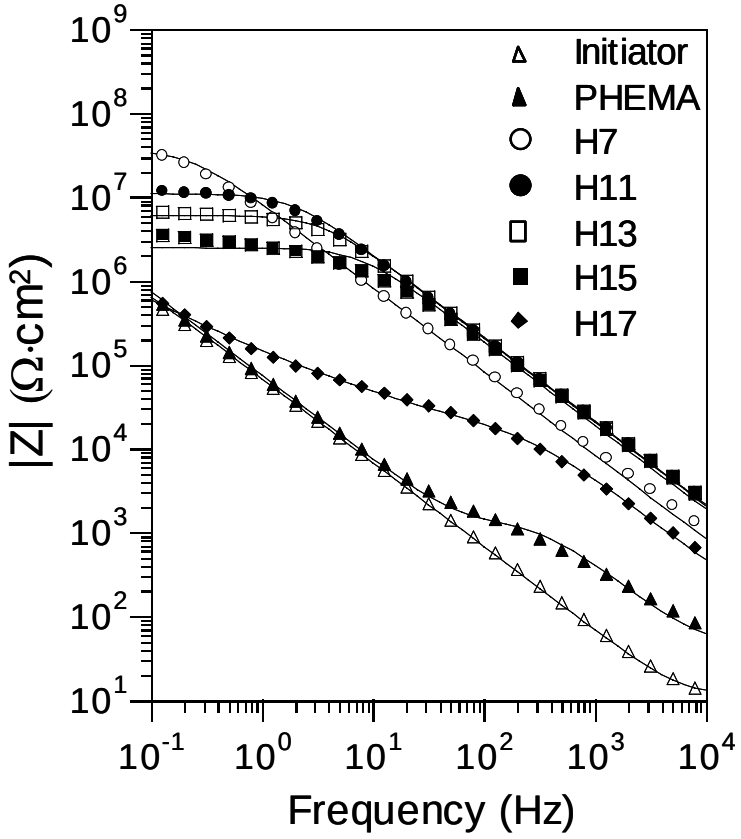

Figure 5.5. Electrochemical impedance spectra for films on gold obtained in 1 mM $K_3Fe(CN)_6$ and 1 mM $K_4Fe(CN)_6$ in 0.1 M Na_2SO_4(aq). Spectra are shown for PHEMA before and after various hydrocarbon modifications with initiator-modified gold as a reference. Solid curves represent a fit of the data to an equivalent circuit.

Table 5.3. Film capacitance (C_f) and resistance (R_f) values for PHEMA and hydrocarbon-modified PHEMA films.

Film	C_f (nF/cm^2)	log R_f (Ω ·cm^2)
Initiator[a]	2400 ± 300	6.0 ± 0.4
PHEMA	640 ± 200	3.0 ± 0.3
H1	20 ± 3	6.7 ± 0.8
H7	13.3 ± 4.8	7.0 ± 0.7
H11	9.2 ± 2.3	6.9 ± 0.3
H13	8.6 ± 2.1	6.7 ± 0.3
H15	9.1 ± 2.4	6.5 ± 0.3
H17[b]	25 ± 19	4.2 ± 0.4
H17/H1	11 ± 2	7.7 ± 0.2

[a] C_i and R_i values given for the initiator
[b] Log Z_w (Ω ·cm^2) for H17 was determined to be 5.0 ± 0.5

constant model, requires use of a modified two time constant model created by adding a Warburg impedance (Z_w) term between R_f and the initiator circuit (indicated by the dashed box in Figure 3.3b). Z_w is used to represent a resistance to mass transfer[21] associated with the polymer film layer. The frequencies at which Z_w is observed lie between those where the initiator (low frequency, long time) and polymer (high frequency, short time) layers dominate. During these intermediate time scales, the diffusion of redox species through the polymer limits electron transfer.

Table 5.3 contains R_f and C_f values obtained for all hydrocarbon-modified films studied. As the PHEMA film is modified with hydrocarbon side chains, the impedance spectrum is observed to shift upward, due to a dramatically lower film capacitance (factor of 25 or greater) and a remarkable increase in film resistance (factor of ~10^4 except for H17) over PHEMA. Fits of the impedance data indicate minor drops in R_f as the hydrocarbon chain length is increased from 7 to 15 and a significant drop from 15 to 17 (Table 5.3). That the effect of chain length on film resistance is opposite that observed on film crystallinity and oleophobicity/hydrophobicity suggests that other film properties are influencing water and ion uptake. In terms of capacitance, C_f is 13 nF/cm^2 for H7, while for H11 through H15, C_f is about 9 nF/cm^2. These values are 50 to 70 times lower than C_f for PHEMA. This comparison is consistent with the increased film thicknesses after acylation and the lower film dielectric constant imparted by hydrocarbon chains.

As was suspected for the fluorocarbon-modified PHEMA films, the barrier properties of modified PHEMA films appear to be more closely related to side chain conversion than to surface properties or crystallinity of the film. The bulk film must have suppressed interactions with water, accomplished in our case by removal of hydrogen

bonding moieties, to improve its resistance against penetration by aqueous solutions. When unreacted, hydroxyl groups may associate through hydrogen bonding to create water and ion-diffusing pathways through the film. H1 exhibits a film resistance that is almost 4 orders of magnitude greater than that of unmodified PHEMA. Since H1 contains no long alkyl side chains and exhibits minimal structuring, the improved impedance must be due to high conversion in the capping of hydrophilic hydroxyl groups. H7, even though it is not a well-structured film and does not exhibit impressive wettability, has a higher conversion than the films with longer hydrocarbon groups and a slightly higher R_f. As the hydrocarbon chain length is increased, conversion becomes lower and R_f falls accordingly. Furthermore, H17, which yields the most structured air-film interface, exhibits a significantly reduced R_f as compared to the other hydrocarbons studied. Merely eliminating hydroxyl groups from the film is a key to developing improved barriers from modified PHEMA films while bulk and interfacial film structuring are of secondary importance. This finding is in slight contrast to results for formation of fluorocarbon-modified PHEMA films where tremendous improvements in barrier properties were observed at low conversions ($\chi \sim 20\%$) and were correlated with the surface properties of the films.[22] We attribute this phenomenon to differences in film structuring and hydrophobicity for fluorocarbon versus hydrocarbon chains.

We can utilize this capping approach to prepare films with optimal surface and barrier properties. H17 films (with $\chi \sim 35\%$) have been backfilled by exposure to a 20 mM solution of acetyl chloride in iso-octane to increase the conversion of hydroxyl groups to methyl esters (Table 5.1). When conversion for H17 was increased by backfilling with acetyl chloride to form H17/H1, no change was observed in surface

properties, consistent with the dominance of oriented heptadecyl chains at the surface and a lower H1-rich region. Thickness change for H17/H1 as compared to H17 (Table 5.1) was along the lines of that seen for a purely H1 film (13% increase due to ~45% improved conversion). Figure 5.6 shows the impedance spectra for H1, H17, and H17/H1 while Table 5.3 contains the R_f and C_f values. Of particular importance, the elimination of unreacted hydroxyl groups of H17 has a remarkable effect on resistance (over 3 orders of magnitude improvement) and capacitance (cut in half) while minimally affecting film thickness. In comparison with H7 (Table 5.3), which also has a χ of ~0.8, the H17/H1 film shows a factor of 5 higher resistance, which we attribute to the superior surface properties of H17/H1 over H7 that reduce water and ion penetration into the film. While comparison of H1 and H17 in Figure 5.6 yields the importance of conversion in elevating barrier performance, comparison of these two films with H17/H1 reveals that both high conversion within the film and the preparation of a well-structured, hydrophobic surface is required to optimize the barrier properties of a film. Our work agrees with that of Zhou et al.[7] who found that increasing the hydrophobic nature of PHEMA by reacting hydroxyl groups with trimethylchlorosilane greatly improved the resistance of the film to aqueous etching solutions.

In comparison with partially fluorinated PHEMA films generated in the same manner and exhibiting similar conversions, the hydrocarbon films exhibit comparable barrier properties (see Tables 4.3 and 5.3). The typical film resistance achieved with the hydrocarbon films is roughly 10^7 $\Omega \cdot cm^2$, with the best film (H17/H1) approaching 10^8 $\Omega \cdot cm^2$, and the best fluorinated films also approach 10^8 $\Omega \cdot cm^2$. The capacitances for both fluorocarbon and hydrocarbon films generally fall in the realm of 10 nF/cm^2.

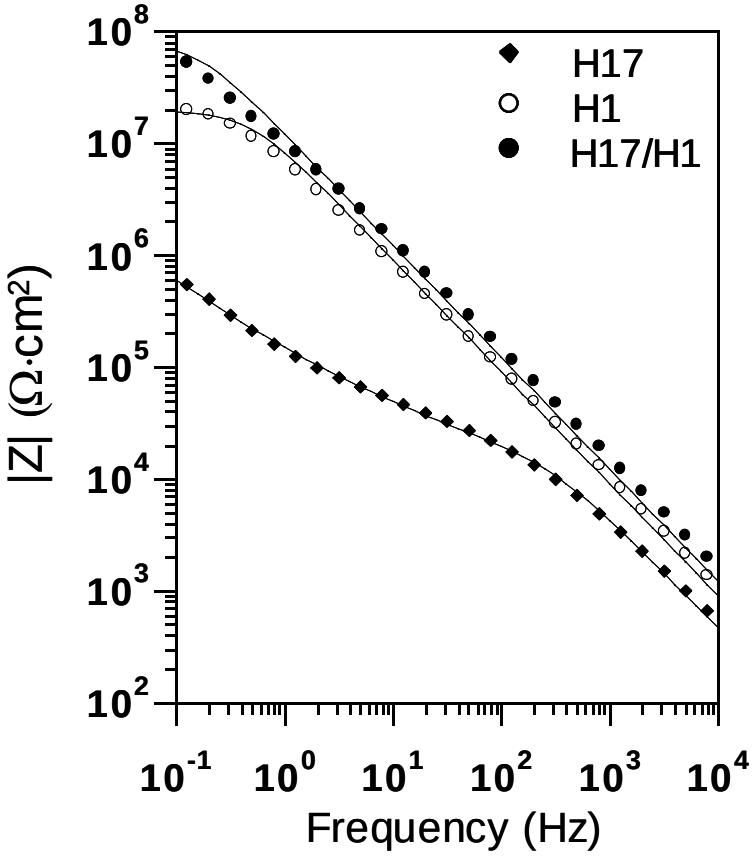

Figure 5.6. Electrochemical impedance spectra obtained in 1 mM $K_3Fe(CN)_6$ and 1 mM $K_4Fe(CN)_6$ in 0.1 M Na_2SO_4(aq) for H17, H1, and H17/H1 films on gold. Solid curves represent a fit of the data to an equivalent circuit.

Comparison between specific fluorinated films and hydrocarbon films can also be made based on side chain length and molecular weight. Based on alkyl chain length, F7 provides slightly higher R_f and lower C_f than H7, because of superior structuring at the surface and in the bulk even though H7 exhibits a bit higher χ (0.82 vs. 0.77). In comparing side groups with similar molecular weight and conversion, H11 (MW = 312.4; χ = 0.77) and F3 (MW = 326.2; χ = 0.79) exhibit similar barrier properties. We also attempted to use benzoyl chloride to modify PHEMA, but unlike a fluoroaryl-modified PHEMA film that exhibits high conversion and excellent barrier properties,[23] the benzyl-modified film exhibited poor conversion and barrier properties.

Film Stability

The hydrocarbon modifications of PHEMA made in this work result in a new ester on the polymer side chains. Unlike the fluorocarbon modifications already discussed, however, these esters cannot be hydrolyzed under mild conditions. Ethanolic KOH solutions have absolutely no effect on these films. Only when exposed to solutions containing lithium aluminum hydride ($LiAlH_4$), a strong reducing agent, were these films cleaved at the newly formed ester bond. Under these same harsh conditions, the original PHEMA ester was not cleaved, however, as it is likely more stable since it resides close to the polymeric backbone and is sterically less accessible. The chemical conditions required to damage the films are of little concern practically, and these hydrocarbon-modified PHEMA films could be used under most conditions.

Conclusions

The two-step polymerization/reaction method presented here represents a straightforward and effective way to create ultrathin films having various hydrocarbon side chains. The ability to grow PHEMA via a water-accelerated, surface-initiated scheme allows tremendous control over film thickness. Subsequent reaction of polymer side chains introduces hydrocarbon functionality into the film with diminishing conversion as the hydrocarbon chain length is increased. Increasing the hydrocarbon side chain length increases the crystallinity of the hydrocarbon groups within the polymer films due to enhanced van der Waals interactions. Films having the longest chains, H15 and H17, yield wetting properties consistent with a densely packed methyl surface, indicating that the outermost groups are oriented nearly normal to the air-film interface. Shorter chains are unable to impart this degree of structure to the film. The hydrocarbon films studied here could adequately be used in an application requiring an oleophobic/hydrophobic surface at much less cost than a fluorocarbon film. Tremendous improvement in film barrier properties was also observed upon acylation of PHEMA with hydrocarbon acid chlorides, but the improvement is linked most closely to conversion of side chains while film structure and surface properties are secondary issues. The importance of conversion is illustrated by capping the hydroxyl groups of PHEMA with acetyl chloride to achieve $\chi \sim 90\%$ and 4 orders of magnitude improvement in film resistance. Nonetheless, the best barrier film prepared in this portion of the work, H17/H1, has both high conversion of hydroxyl groups (>80%) and a densely packed hydrophobic methyl surface. Combined, the results described in this chapter demonstrate

the key roles of hydrocarbon side chain length and conversion in controlling film structure, surface properties, and barrier properties.

References

1. Dyer, D. J. "Patterning of Gold Substrates by Surface-Initiated Polymerization," *Advanced Functional Materials* **2003**, *13*, 667-670.

2. Galli, P.; Vecellio, G. "Polyolefins: The Most Promising Large-Volume Materials for the 21st Century," *Journal of Polymer Science Part a-Polymer Chemistry* **2004**, *42*, 396-415.

3. Benkoski, J. J.; Flores, P.; Kramer, E. J. "Diblock Copolymer Reinforced Interfaces between Amorphous Polystyrene and Semicrystalline Polyethylene," *Macromolecules* **2003**, *36*, 3289-3302.

4. Feldman, D. "Polymer Barrier Films," *Journal of Polymers and the Environment* **2001**, *9*, 49-55.

5. Cerofolini, G. F.; Galati, C.; Reina, S.; Renna, L. "The Addition of Functional Groups to Silicon Via Hydrosilation of 1-Alkynes at Hydrogen-Terminated, 1 x 1 Reconstructed, (100) Silicon Surfaces," *Semiconductor Science and Technology* **2003**, *18*, 423-429.

6. Seshadri, K.; Atre, S. V.; Tao, Y. T.; Lee, M. T.; Allara, D. L. "Synthesis of Crystalline, Nanometer-Scale, -(CH2)(x)- Clusters and Films on Gold Surfaces," *Journal of the American Chemical Society* **1997**, *119*, 4698-4711.

7. Zhou, F.; Liu, W. M.; Hao, J. C.; Xu, T.; Chen, M.; Xue, Q. J. "Fabrication of Conducting Polymer and Complementary Gold Microstructures Using Polymer Brushes as Templates," *Advanced Functional Materials* **2003**, *13*, 938-942.

8. Khan, M.; Huck, W. T. S. "Hyperbranched Polyglycidol on Si/SiO2 Surfaces Via Surface-Initiated Polymerization," *Macromolecules* **2003**, *36*, 5088-5093.

9. Kraft, M. L.; Moore, J. S. "N-Alkyl Fatty Acid-Modified Microgels: Ion Permeation as a Function of Chain Length," *Langmuir* **2003**, *19*, 910-915.

10. Rodriguezparada, J. M.; Kaku, M.; Sogah, D. Y. "Monolayers and Langmuir-Blodgett-Films of Poly(N-Acylethylenimines) with Hydrocarbon and Fluorocarbon Side-Chains," *Macromolecules* **1994**, *27*, 1571-1577.

11. Riou, S. A.; Chien, B. T.; Hsu, S. L.; Stidham, H. D. "A Spectroscopic Study of Polymers Containing Long Flexible Side Chains at an Air-Liquid Interface," *Journal of Polymer Science Part B-Polymer Physics* **1997**, *35*, 2843-2855.

12. Stöhr, T.; Rühe, J. "Monolayers of Amphiphilic Block Copolymers Via Physisorbed Macroinitiators," *Macromolecules* **2000**, *33*, 4501-4511.

13. Snyder, R. G.; Strauss, H. L.; Elliger, C. A. "C-H Stretching Modes and the Structure of Normal-Alkyl Chains .1. Long, Disordered Chains," *Journal of Physical Chemistry* **1982**, *86*, 5145-5150.

14. Zhang, D.; Shen, Y. R.; Somorjai, G. A. "Studies of Surface Structures and Compositions of Polyethylene and Polypropylene by IR Plus Visible Sum Frequency Vibrational Spectroscopy," *Chemical Physics Letters* **1997**, *281*, 394-400.

15. Fenter, P.; Eberhardt, A.; Liang, K. S.; Eisenberger, P. "Epitaxy and Chainlength Dependent Strain in Self-Assembled Monolayers," *Journal of Chemical Physics* **1997**, *106*, 1600-1608.

16. Neelakantan, A.; Stine, R.; Maranas, J. K. "Chain Packing in Ethylene-Butene Copolymers," *Macromolecules* **2003**, *36*, 3721-3731.

17. Huang, W. X.; Kim, J. B.; Bruening, M. L.; Baker, G. L. "Functionalization of Surfaces by Water-Accelerated Atom-Transfer Radical Polymerization of Hydroxyethyl Methacrylate and Subsequent Derivatization," *Macromolecules* **2002**, *35*, 1175-1179.

18. Laibinis, P. E.; Palmer, B. J.; Lee, S.-W.; Jennings, G. K. "Self-Assembled Monolayers of Thiols" In *Thin Films*; Ulman, A.; Powell, R.; Francombe, M. H., Eds.; Academic Press, 1998; Vol. 24, pp 1-41.

19. Bain, C. D.; Troughton, E. B.; Tao, Y. T.; Evall, J.; Whitesides, G. M.; Nuzzo, R. G. "Formation of Monolayer Films by the Spontaneous Assembly of Organic Thiols from Solution onto Gold," *Journal of the American Chemical Society* **1989**, *111*, 321-335.

20. Fukushima, H.; Seki, S.; Nishikawa, T.; Takiguchi, H.; Tamada, K.; Abe, K.; Colorado, R.; Graupe, M.; Shmakova, O. E.; Lee, T. R. "Microstructure, Wettability, and Thermal Stability of Semifluorinated Self-Assembled Monolayers (SAMs) on Gold," *Journal of Physical Chemistry B* **2000**, *104*, 7417-7423.

21. Bard, A. J.; Faulkner, L. R. *Electrochemical Methods: Fundamentals and Applications*, 2nd ed.; Wiley: New York, 2001.

22. Bantz, M. R.; Brantley, E. L.; Weinstein, R. D.; Moriarty, J.; Jennings, G. K. "Effect of Fractional Fluorination on the Properties of ATRP Surface-Initiated Poly(Hydroxyethyl Methacrylate) Films," *Journal of Physical Chemistry B* **2004**, *108*, 9787-9794.

23. Brantley, E. L.; Jennings, G. K. "Fluorinated Polymer Films from Acylation of ATRP Surface-Initiated Poly(Hydroxyethyl Methacrylate)," *Macromolecules* **2004**, *37*, 1476-1483.

CHAPTER VI

BLOCK-LIKE COPOLYMER FILMS USING CONTROLLED POST-POLYMERIZATION REACTIONS

Block copolymer thin films are often prepared by sequential polymerization of different monomers using controlled, surface-initiated polymerizations.[1-3] These films exhibit properties that are dependent on monomer choice and have applications in lithographic masks, membranes, responsive coatings, and photonic devices.[1,4-6] However, the sequential polymerization steps utilized during formation of these films are time- and labor-intensive processes and tend to result in diminished block thicknesses due to progressively lower reinitiation efficiencies.[1]

Herein, we demonstrate a method that requires only a single polymerization step but can yield copolymer films having block-like properties and controlled thickness up to several hundred nanometers (Figure 6.1). As the starting point, poly(hydroxyethyl methacrylate) (PHEMA) films are grown from gold surfaces using surface-initiated, water-accelerated atom transfer radical polymerization (ATRP).[7-11] The use of PHEMA allows, by simple post-polymerization chemical reactions, the addition of numerous side chains to tune film properties. We and others have shown that the hydroxyl side chains of the PHEMA film can be derivatized by reaction with various species, including fluorocarbon and hydrocarbon acid chlorides, an imidazole, and trimethylchlorosilane, to produce films with a wide range of wettabilities (Chapters IV and V).[10,12-18] Here, we modify PHEMA with pentafluorobenzoyl chloride (C_6F_5COCl) to generate a film denoted as FBZ that contains perfluoroaryl side groups on ~80% of the side chains. Of

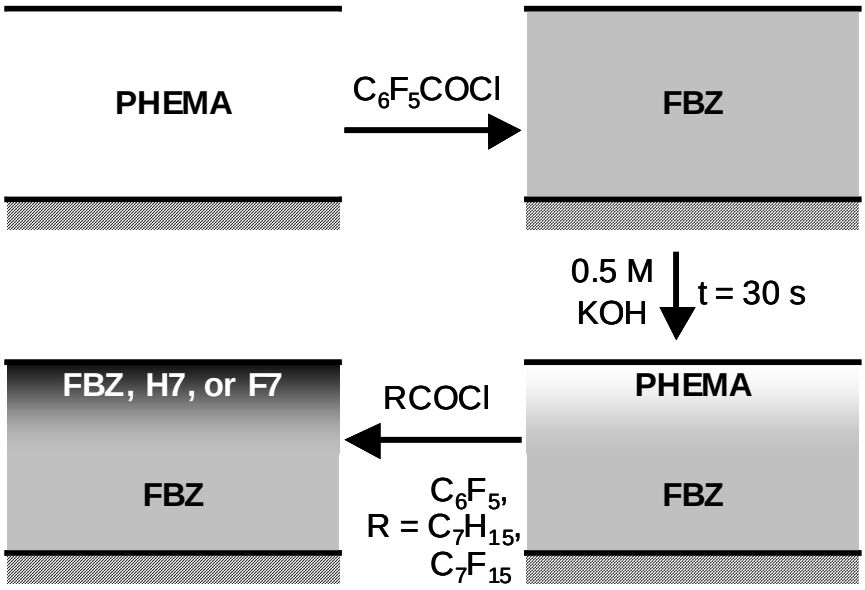

Figure 6.1. Controlled hydrolysis and acylation reactions to form block-like copolymer films from a base PHEMA film on gold.

significance here, when fluorocarbon acid chlorides such as FBZ are employed in the modification of PHEMA, the resulting fluorinated esters created via the acylation reaction are susceptible to hydrolysis in basic solutions. By controlling the base concentration and exposure time, hydrolysis of fluorinated PHEMA films can be conducted in a diffusion-limited manner, only removing fluorinated ester groups near the outer surface. Since this hydrolysis regenerates hydroxyl groups, the outer portions of the film can be subsequently rederivatized with a second moiety (i.e. another fluorocarbon or hydrocarbon) to create block-like copolymer films (Figure 6.1). The choice of modifying species allows surface as well as barrier properties to be altered to varying degrees and provides fundamental information on the effect of a dense outer block on the overall barrier properties of the film.[14,16,18] As compared to use of a single functionality within polymer films, a combination of groups to simultaneously optimize all areas of effectiveness in applications provides the ultimate ability to engineer surfaces and films at the molecular level.

In the interest of creating hydrophobic, oleophobic barriers via simple, controlled reactions, FBZ was chosen as the base film because it exhibits desirable barrier properties while presenting a surface that is oleophilic (wetted by hexadecane) and only moderately hydrophobic (undesirable for use as a non-wetting coating). Therefore, the properties of this film may be dramatically altered and improved by modification with an outer block. In addition, FBZ is readily hydrolyzed but accommodates a slower, more easily controlled hydrolysis as compared with perfluoroalkyl modifications since it is slightly more stable (β but no α fluorine atoms). The highly blocking barrier properties of FBZ

are important to achieving a controlled hydrolysis and preventing the KOH solution from penetrating into the fluorocarbon region of the film.

Baker, Bruening, and co-workers have recently demonstrated that alumina membranes coated with thin (<200 nm) hydrocarbon- and fluorocarbon-modified PHEMA films exhibit remarkable separation factors (as high as 500) in the pervaporation of volatile organic compounds (i.e. benzene or ethyl acetate) from water.[18] The ability to control both surface and barrier properties, as described herein, could ultimately be useful to affect molecular partitioning and diffusivities and perhaps, tailor separation efficiencies in a molecule-specific manner. While post-polymerization reactions within films on a surface can occasionally be found in the literature,[3,10,12,13,18,19] no analogous scheme was found for the preparation of block-like copolymer films from a homopolymer film.

Experimental Procedures

PHEMA films having reactive hydroxyl side chains were created as described in Chapter III. To create copolymer films, PHEMA was first exposed to 20 mM solutions of C_6F_5COCl with 25 mM pyridine in dichloromethane for at least 3 h to give FBZ films with high conversion (~80%) of hydroxyl groups to esters. After acylation, the films were rinsed with dichloromethane and ethanol and dried with nitrogen. Controlled hydrolysis of the films was achieved by exposing FBZ to a 0.5 M KOH ethanolic solution for 30 s, followed by rinsing with water and ethanol and drying with nitrogen. The partially hydrolyzed films (PHEMA/FBZ) were then placed in solutions containing 20 mM C_6F_5COCl, $C_7H_{15}COCl$, or $C_7F_{15}COCl$ along with 25 mM pyridine for 3 h to

form FBZ/FBZ, H7/FBZ, or F7/FBZ films, respectively. Dichloromethane was used as solvent for C_6F_5COCl and $C_7F_{15}COCl$ solutions while iso-octane was the solvent for $C_7H_{15}COCl$ solutions. In order to make the terpolymer film, F7/FBZ+F1, FBZ films were placed in a 20 mM solution of trifluoroacetic anhydride and 25 mM pyridine in dichloromethane for 3 h to form FBZ+F1. These films were then subjected to partial hydrolysis and reaction with $C_7F_{15}COCl$, as described above, to form F7/FBZ+F1.

Results and Discussion

Controlled Hydrolysis of Fluorocarbon-Modified PHEMA Films

A 220 nm PHEMA film was exposed to a 20 mM solution of pentafluorobenzoyl chloride in dichloromethane for at least 3 h to generate an FBZ film with perfluoroaryl groups on the side chains. As already shown, ~80% of the PHEMA hydroxyl groups are converted to perfluoroaryl groups, which are signified in the reflectance-absorption infrared spectra by a new carbonyl peak at ~1749 cm^{-1}, aromatic C-F stretching peaks between 1200 and 1350 cm^{-1}, and peaks for fluorinated C⎓C aromatic ring stretching from 1500 to 1700 cm^{-1} (Figure 6.2). The FBZ film was then hydrolyzed for 30 s in 0.5 M KOH ethanolic solution to form PHEMA/FBZ (outer/inner block as shown in Figure 6.1). As indicated by IR conversion estimates based on changes in the hydroxyl peak area, this brief exposure resulted in minimal overall film hydrolysis with only ~5% of fluorinated ester groups in FBZ hydrolyzed to alcohols. Accordingly, the IR spectra (Figure 6.2) for this film still indicated a predominately FBZ composition. From ellipsometric measurements (Table 6.1), film thickness dropped ~15 nm upon hydrolysis,

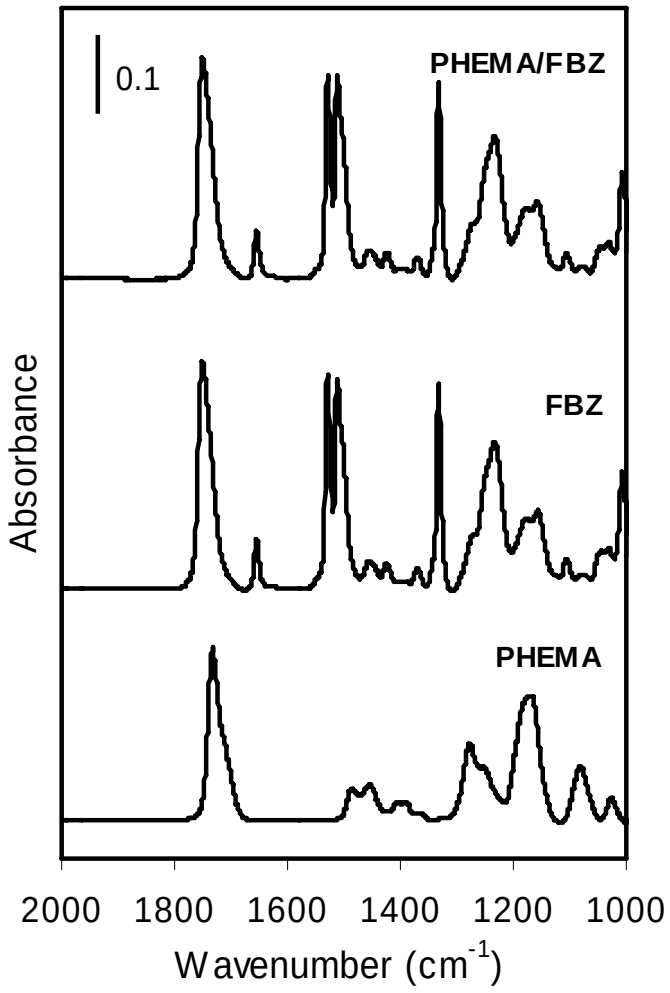

Figure 6.2. RAIR spectra for PHEMA, FBZ, and PHEMA/FBZ. Modification of PHEMA to form FBZ results in additional C-O stretching from 1100 to 1300 cm^{-1}, C-F stretching around 1350 cm^{-1}, aromatic C=C stretching between 1500 and 1700 cm^{-1}, and additional C=O stretching from the newly formed ester at 1749 cm^{-1}. Hydrolysis of FBZ to form PHEMA/FBZ results in no significant change in this low wavenumber region of the IR spectrum.

Table 6.1. Conversion, thickness, advancing water and hexadecane contact angles, and film resistance (R_f) and capacitance (C_f) of modified PHEMA block-like copolymer films.

Film	Conversion (%)	Thickness (nm)	θ_A (H_2O) (°)	θ_A (HD) (°)	Log R_f ($\Omega \cdot cm^2$)	C_f (nF/cm^2)
PHEMA		224	75 ± 3	<10	3.0 ± 0.3	640 ± 200
FBZ	81 ± 2	394	90 ± 2	<10	8.1 ± 0.6	9 ± 2
PHEMA/FBZ	76 ± 2	379	75 ± 2	<10	8.2 ± 0.5	11 ± 2
FBZ/FBZ	80 ± 2	390	92 ± 2	<10	8.2 ± 0.3	9 ± 1
H7/FBZ	82 ± 3	402	106 ± 3	<10	8.8 ± 0.4	8 ± 1
F7/FBZ	82 ± 3	444	128 ± 2	77 ± 2	9.1 ± 0.5	7 ± 1
F7/FBZ+F1	87 ± 2	448	127 ± 2	77 ± 2	10.0 ± 0.4	8 ± 1

which, based on molecular weight of the cleaved perfluoroaryl groups, is consistent with a ~20 nm layer of regenerated hydroxyl groups remaining atop the film. While the overall hydrolysis was minimal, the effect at the outer few angstroms was significant, as the advancing water contact angle indicated that surface properties reverted entirely to those of a PHEMA film. This complete conversion at the outer surface and slight change in conversion overall is consistent with a diffusion-limited hydrolysis (as suggested in Figure 6.1). As additional evidence of a diffusion-limited hydrolysis reaction, the surface properties (dependent only on the outer 5 Å of surface composition) of the films become those of PHEMA after only 1 s in 0.5 M KOH/ethanol, a condition in which ≤ 1% of the perfluorobenzoyl groups were hydrolyzed. The slight extent of this reaction combined with the rapid and complete conversion of surface properties is consistent with a fast surface reaction. A reaction-limited process would not likely cleave the entire surface layer of fluorinated esters in such a short amount of time but instead would diffuse into the bulk film, hydrolyze groups randomly, and only completely hydrolyze the surface on a longer time scale.

Two further points support the claim of a diffusion-limited hydrolysis. The first is the synthesis of F7/FBZ+F1, which is made by first forming FBZ+F1 (with F1 presumably residing in lower regions of the film) followed by hydrolysis. Our previous work has shown that in 0.5 M KOH, films having α fluorine esters (i.e. F1) hydrolyze instantaneously (~1 s), whereas films having β fluorine esters (i.e. FBZ) hydrolyze much more slowly (~20 min). Even after 30 s hydrolysis, essentially no F1 functionality was cleaved, as evidenced by the constant intensity of an IR peak at 1790 cm^{-1} due to α fluorine C=O. In a reaction-limited case, we might expect to see the base solution

diffuse into the film and rapidly cleave the F1 chains, but this is not observed. The second supporting point is evidenced by the creation of H17/FBZ, which was made by reacting PHEMA/FBZ with stearoyl chloride to rederivatize the outer film portions to H17. The RAIR spectrum for this film (not shown) indicates distinct CH_2 stretching peaks at 2920 cm^{-1} and 2851 cm^{-1}, consistent with an outer crystalline hydrocarbon region. The observed crystallinity implies that the hydrocarbon chains are well-packed and therefore exist together in the outer region of this film.

Rederivatization of Hydrolyzed FBZ Films

Diblock-like copolymer films were formed by exposing PHEMA/FBZ films to solutions of octanoyl chloride or pentadecafluorooctanoyl chloride to rederivatize the outer film surface and form H7/FBZ or F7/FBZ, respectively (see Figure 6.1). PHEMA/FBZ or films rederivatized to form FBZ/FBZ served as experimental controls. A terpolymer film, F7/FBZ+F1, was engineered by backfilling with a short chain modification (trifluoroacetic anhydride) to have elevated hydroxyl conversion before controlled hydrolysis and rederivatization with F7 at the outer film surface. After copolymerization, hydroxyl conversion estimates from the IR hydroxyl peak area (Table 6.1) returned to the same levels as before hydrolysis, indicating that essentially all regenerated hydroxyl groups had been successfully rederivatized. However, since the films still contain a predominate FBZ composition, only slight changes are observed in the low wavenumber region of the IR spectra (Figure 6.3). Spectra for F7/FBZ and F7/FBZ+F1 each show the appearance of a peak at 1790 cm^{-1} that corresponds to α fluorination of the carbonyl group to produce -$OC(O)CF_2$- linkages and an increase in

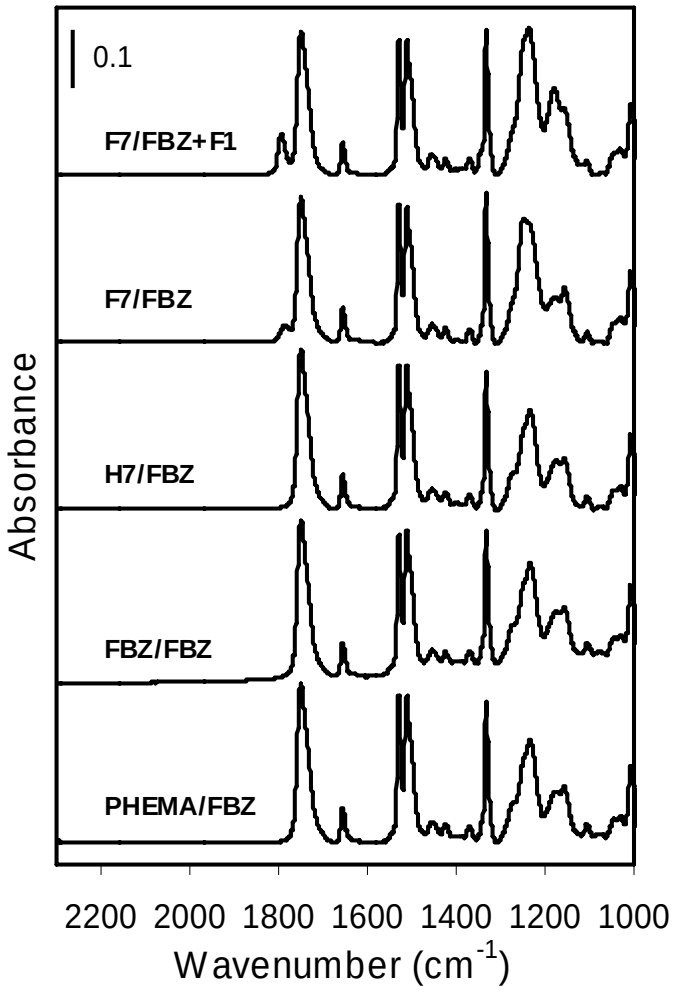

Figure 6.3. RAIR spectra for copolymer films. Rederivatization of PHEMA/FBZ to form copolymer films results in minimal changes. For F7/FBZ, a small amount of CF_2 stretching around 1350 cm^{-1} and an additional C=O peak at 1790 cm^{-1} appear. A terpolymer film, F7/FBZ+F1, exhibits even more CF_3 and C=O stretching atop those for F7/FBZ.

CF stretching at 1250 cm^{-1} over that of the FBZ/FBZ control.[15] In comparing H7/FBZ to FBZ/FBZ, the lack of spectral changes in the C-H bending region (1400-1500 cm^{-1}) or in the C-H stretching region (not shown) are attributed to the weak IR absorbance of the short hydrocarbon groups, which we have also observed in homogeneous H7 films.[16]

Copolymer film thickness (Table 6.1) increased significantly upon reacting the outer film portions with fluorocarbon or hydrocarbon groups which, as we have noted before, results from the polymer chains extending to accommodate the additional volume of long side chains.[14] In fact, increases in film thickness generally scale with the molecular volume or mass of the derivatizing species (F7 > H7 > FBZ). Upon comparison of copolymer wetting data in Table 6.1 with those for homogeneous films in Tables 4.2 and 5.2, reaction of the small portion of regenerated hydroxyl groups yielded the surface properties expected for PHEMA films modified exclusively with those acid chlorides.[14,16] The surface groups of the copolymer films were chosen to be increasingly hydrophobic (PHEMA < FBZ < H7 < F7) in order to demonstrate the ability to tune surface properties by creating copolymer films in this manner. Of the surfaces investigated here, only F7/FBZ and F7/FBZ+F1 with advancing hexadecane contact angles of 77° also exhibit oleophobic behavior, consistent with results for a homogeneous F7 film, where the fluorocarbon chains lie normal at the air-film interface and result in an extremely low critical surface energy of 9 mN/m.[14]

Engineered Barrier Properties

Work from previous chapters has shown that improving conversion of hydrophilic hydroxyl groups reduces the presence of water and ion-diffusing pathways and results in

dramatic improvement in the barrier properties (higher R_f and lower C_f) of modified PHEMA films. Controlled film hydrolysis and subsequent surface modification provide a route to hold overall conversion constant while investigating the effect of surface composition on barrier properties. To conduct this study of surface effects on barrier properties, we performed EIS on the copolymer films upon exposure to an aqueous solution of 1 mM $K_4Fe(CN)_6 \cdot 3H_2O$, 1 mM $K_3Fe(CN)_6$, and 0.1 M Na_2SO_4. The impedance spectra for all the copolymer films, as well as for PHEMA and FBZ, are presented as Nyquist plots (to demonstrate slight differences more clearly than Bode plots) in Figure 6.4. As shown in the inset, copolymer films with similar surface hydrophilicity to FBZ exhibit comparable barrier behavior, as indicated by the similar scale for Nyquist plots of FBZ, PHEMA/FBZ, and FBZ/FBZ. For comparison, the Nyquist plot of PHEMA is also presented in the inset of Figure 6.4 but exists at significantly lower Z values than can be reasonably seen on the scale of the plot. The Nyquist plots for the diblock-like films modified with more hydrophobic and structured surface compositions (H7/FBZ, F7/FBZ, and F7/FBZ+F1) exhibit distinctly higher impedances.

To extract physical film parameters, the spectra for all modified PHEMA films were fit with the simplified, one time constant Randles equivalent circuit model in Figure 3.3c. As shown quantitatively in Table 6.1 and based on equivalent circuit fits of the impedance spectra for the films, R_f for the diblock-like copolymer films increases with increasing surface hydrophobicity (F7/FBZ > H7/FBZ > FBZ/FBZ ≈ PHEMA/FBZ). Simply modifying the outer few nanometers of the film to contain hydrophobic chains produces an order of magnitude difference in R_f between F7/FBZ and PHEMA/FBZ.

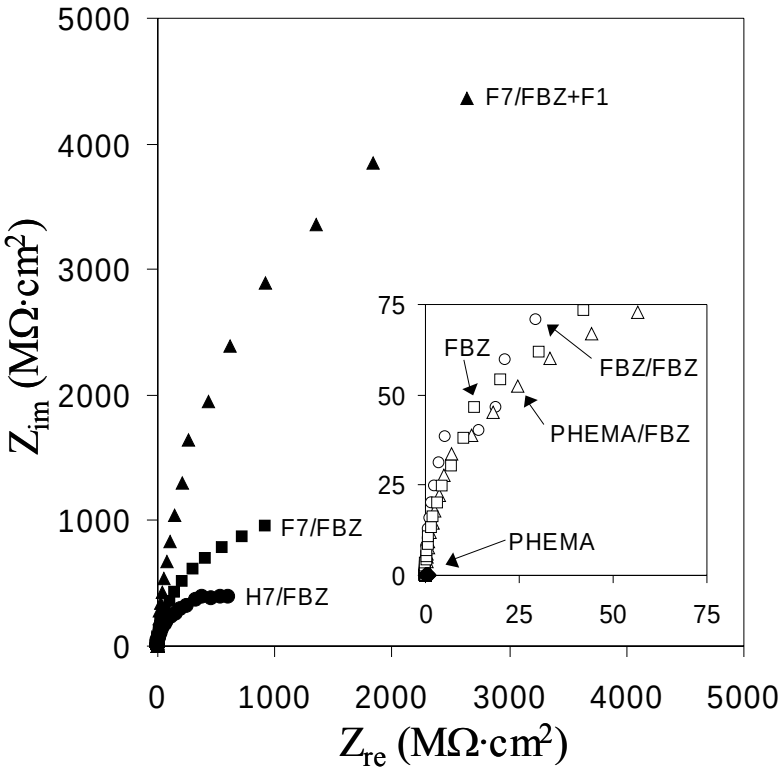

Figure 6.4. Nyquist plots for the electrochemical impedance behavior of PHEMA, FBZ, all diblock-like copolymer films, and one terpolymer film. All spectra were obtained in the frequency range from 10^{-2} to 10^4 Hz in an aqueous solution containing 1 mM $K_4Fe(CN)_6 \cdot 3H_2O$, 1 mM $K_3Fe(CN)_6$, and 0.1 M Na_2SO_4. The larger view shows only the three best barrier films created in this work: F7/FBZ+F1 followed by F7/FBZ and H7/FBZ. The inset is on a much smaller scale but shows spectra of FBZ, PHEMA/FBZ, and FBZ/FBZ, indicating that the barrier properties of these films do not vary significantly from one another. The spectrum for PHEMA, a much worse barrier than the engineered films, appears at extremely low Z values (<1 MΩ·cm^2) in the inset.

Among films with similar bulk composition and surface hydrophobicity (FBZ, PHEMA/FBZ, and FBZ/FBZ), R_f does not vary significantly, in agreement with the Nyquist plots for these films. The likely reason for barrier property enhancement with increasing hydrophobicity is the ability of low energy surfaces to resist penetration by aqueous solutions. Additionally, each of these films (R_f from 10^8 to 10^9 $\Omega \cdot cm^2$) exhibits greater than 5 orders of magnitude improvement in R_f as compared to the base PHEMA film (R_f of 10^3 $\Omega \cdot cm^2$) and up to one order of magnitude improvement in R_f as compared to the best homopolymer film, FBZ. C_f increases slightly upon regeneration of surface hydroxyl groups due to greater water penetration into the outer region of the PHEMA/FBZ film. The addition of surface groups having low dielectric constants, however, again reduces C_f, even below the starting value for FBZ. To provide additional points of reference, H7 and F7 homopolymer films exhibit log R_f of 7.0 and 7.4 $\Omega \cdot cm^2$, respectively, and C_f ranging from 9 to 13 nF/cm^2 (Chapters IV and V). The homopolymer FBZ film (used as the baseline in this study) provides a greater barrier than either of these films due to either higher hydroxyl conversion (vs. F7) or film structuring issues (vs. H7). By engineering the outer surface region of diblock-like copolymer films based on FBZ, we can achieve coatings with significantly greater resistances and lower capacitances.

Combining backfilling with controlled hydrolysis, as demonstrated with F7/FBZ+F1, enables the preparation of a film with higher overall conversion (87%) while maintaining a hydrophobic/oleophobic surface (Table 6.1). R_f and C_f derived from an equivalent circuit fit to the EIS spectrum of this film indicate that it does indeed present a greater barrier to ion transport than the other copolymer films (an order of magnitude

higher R_f than that of F7/FBZ) or any of the homogeneous films prepared previously.[14,16] The R_f values of films created in this work (up to ~10 GΩ·cm^2) are among the highest of any submicron films reported in the literature[20] and even higher than many films having thicknesses of several microns.[21] These results detail the importance of maintaining a highly hydrophobic surface and minimizing hydrophilic groups throughout to dramatically elevate the resistance of polymer films against water and ion permeation.

Conclusions

Using a single-step polymerization followed by simple chemical reactions, this approach allows creation of block-like copolymer films having partially fluorinated bulk composition with a wide range of surface chemical groups (fluorocarbon, hydrocarbon, hydroxyl-rich, etc.) to engineer film properties at the molecular level. This unique methodology for the preparation of copolymer films successfully provides a direct avenue toward the customization of thin films and coatings. Numerous potential applications of these barrier films exist. Simple modification of PHEMA films has already been demonstrated for use in membranes[12,18] and as etch resists.[13] The ability to tune film properties to a greater degree, as evidenced in this work, could provide even higher selectivity and improved performance in these and many other applications.

References

1. Boyes, S. G.; Brittain, W. J.; Weng, X.; Cheng, S. Z. D. "Synthesis, Characterization, and Properties of ABA Type Triblock Copolymer Brushes of Styrene and Methyl Acrylate Prepared by Atom Transfer Radical Polymerization," *Macromolecules* **2002**, *35*, 4960-4967.

2. Husseman, M.; Malmstrom, E. E.; McNamara, M.; Mate, M.; Mecerreyes, D.; Benoit, D. G.; Hedrick, J. L.; Mansky, P.; Huang, E.; Russell, T. P.; Hawker, C. J. "Controlled Synthesis of Polymer Brushes by "Living" Free Radical Polymerization Techniques," *Macromolecules* **1999**, *32*, 1424-1431.

3. Matyjaszewski, K.; Miller, P. J.; Shukla, N.; Immaraporn, B.; Gelman, A.; Luokala, B. B.; Siclovan, T. M.; Kickelbick, G.; Vallant, T.; Hoffmann, H.; Pakula, T. "Polymers at Interfaces: Using Atom Transfer Radical Polymerization in the Controlled Growth of Homopolymers and Block Copolymers from Silicon Surfaces in the Absence of Untethered Sacrificial Initiator," *Macromolecules* **1999**, *32*, 8716-8724.

4. Fasolka, M. J.; Mayes, A. M. "Block Copolymer Thin Films: Physics and Applications," *Annual Review of Materials Research* **2001**, *31*, 323-355.

5. Park, C.; Yoon, J.; Thomas, E. L. "Enabling Nanotechnology with Self Assembled Block Copolymer Patterns," *Polymer* **2003**, *44*, 6725-6760.

6. Green, P. F.; Limary, R. "Block Copolymer Thin Films: Pattern Formation and Phase Behavior," *Advances in Colloid and Interface Science* **2001**, *94*, 53-81.

7. Robinson, K. L.; Khan, M. A.; Banez, M. V. D.; Wang, X. S.; Armes, S. P. "Controlled Polymerization of 2-Hydroxyethyl Methacrylate by ATRP at Ambient Temperature," *Macromolecules* **2001**, *34*, 3155-3158.

8. Jones, D. M.; Huck, W. T. S. "Controlled Surface-Initiated Polymerizations in Aqueous Media," *Advanced Materials* **2001**, *13*, 1256-1259.

9. Guerrini, M. M.; Charleux, B.; Vairon, J. P. "Functionalized Latexes as Substrates for Atom Transfer Radical Polymerization," *Macromolecular Rapid Communications* **2000**, *21*, 669-674.

10. Huang, W. X.; Kim, J. B.; Bruening, M. L.; Baker, G. L. "Functionalization of Surfaces by Water-Accelerated Atom-Transfer Radical Polymerization of Hydroxyethyl Methacrylate and Subsequent Derivatization," *Macromolecules* **2002**, *35*, 1175-1179.

11. Bontempo, D.; Tirelli, N.; Masci, G.; Crescenzi, V.; Hubbell, J. A. "Thick Coating and Functionalization of Organic Surfaces Via ATRP in Water," *Macromolecular Rapid Communications* **2002**, *23*, 418-422.

12. Balachandra, A. M.; Baker, G. L.; Bruening, M. L. "Preparation of Composite Membranes by Atom Transfer Radical Polymerization Initiated from a Porous Support," *Journal of Membrane Science* **2003**, *227*, 1-14.

13. Zhou, F.; Liu, W. M.; Hao, J. C.; Xu, T.; Chen, M.; Xue, Q. J. "Fabrication of Conducting Polymer and Complementary Gold Microstructures Using Polymer Brushes as Templates," *Advanced Functional Materials* **2003**, *13*, 938-942.

14. Brantley, E. L.; Jennings, G. K. "Fluorinated Polymer Films from Acylation of ATRP Surface-Initiated Poly(Hydroxyethyl Methacrylate)," *Macromolecules* **2004**, *37*, 1476-1483.

15. Bantz, M. R.; Brantley, E. L.; Weinstein, R. D.; Moriarty, J.; Jennings, G. K. "Effect of Fractional Fluorination on the Properties of ATRP Surface-Initiated Poly(Hydroxyethyl Methacrylate) Films," *Journal of Physical Chemistry B* **2004**, *108*, 9787-9794.

16. Brantley, E. L.; Holmes, T. C.; Jennings, G. K. "Modification of ATRP Surface-Initiated Poly(Hydroxyethyl Methacrylate) Films with Hydrocarbon Side Chains," *Journal of Physical Chemistry B* **2004**, *108*, 16077-16084.

17. Jennings, G. K.; Brantley, E. L. "Physicochemical Properties of Surface-Initiated Polymer Films in the Modification and Processing of Materials," *Advanced Materials* **2004**, *16*, 1983-1994.

18. Sun, L.; Baker, G. L.; Bruening, M. L. "Polymer Brush Membranes for Pervaporation of Organic Solvents from Water," *Macromolecules* **2005**, *38*, 2307-2314.

19. Kraft, M. L.; Moore, J. S. "N-Alkyl Fatty Acid-Modified Microgels: Ion Permeation as a Function of Chain Length," *Langmuir* **2003**, *19*, 910-915.

20. Srividya, C.; Sunkara, M.; Babu, S. V. "Resistance of Plasma-Deposited a-C:H/Fluorocarbon Films to Anodic Breakdown in Aqueous Electrolytes," *Journal of Materials Research* **1997**, *12*, 2099-2103.

21. Delucchi, M.; Turri, S.; Barbucci, A.; Bassi, M.; Novelli, S.; Cerisola, G. "Fluoropolyether Coatings: Relationships of Electrochemical Impedance Spectroscopy Measurements, Barrier Properties, and Polymer Structure," *Journal of Polymer Science Part B-Polymer Physics* **2002**, *40*, 52-64.

CHAPTER VII

PATTERNED GROWTH OF PARTIALLY FLUORINATED POLYMER FILMS

Microfabrication, the creation of microstructures on surfaces, often involves the patterning of polymer films on surfaces.[1,2] Patterned films are especially useful in directing various events at surfaces, with surface energy (hydrophilicity/hydrophobicity) being one of the most common and most desirable patterned properties.[3-6] The hydrophobic nature of fluorinated surface regions has been used to direct the flow of solutions through more hydrophilic regions in microfluidic channels.[3,7] Assembly of colloidal particles in patterned hydrophilic areas has been accomplished via wetting phenomena, where suspended particles are withdrawn with a liquid into higher energy (hydrophilic) surface regions and remain after liquid evaporation.[4] In tandem on the same substrate, hydrophobic materials have been used as etch resists while hydrophilic materials have been observed to accelerate aqueous etching processes and increase etching contrast between the two areas.[8] Numerous methods exist to create micro- and nanostructures on surfaces. The most widely used technique, stemming from microelectronics fabrication, is photolithography, but various molding and printing techniques have more recently been developed to achieve patterned surfaces.[1,9]

Soft lithographic techniques have especially become popular for micropatterning surfaces. These techniques are termed “soft” because they involve “soft” organic materials (typically elastomers) as opposed to “hard” inorganic materials encountered in microelectronics. The main advantages of soft lithography over photolithography are less

expensive equipment and materials and simpler procedures. Additionally, while feature size in photolithography is limited by optical diffraction, soft lithography feature sizes are mainly limited by the properties of materials being utilized.[1,9] Microcontact printing (μCP) with polydimethylsiloxane (PDMS) stamps having micron-size relief features has become quite popular for patterning surfaces due to its simple preparation and ease of use. Simply inking a PDMS stamp with a solution containing a reactive species, drying it, and gently contacting the stamp with a surface results in transfer of the reactive species to that surface in the pattern initially present on the PDMS stamp.[1,9] A variety of chemical species have been patterned onto surfaces using μCP, including alkanethiol SAMs,[10,11] silane SAMs,[12] metal ions,[13,14] proteins,[6] and chemical reagents.[15]

Several routes to pattern surface-initiated polymer film growth are possible with μCP. The most common method is to microcontact print an inert alkanethiol and then backfill the remaining surface area with an initiator.[16-18] Since the ATRP initiator being used in this study is itself a disulfide, it is also possible to stamp the initiator directly onto the surface,[19,20] although this more direct approach has never been demonstrated for the disulfide initiator used here. ATRP will result in film growth only from initiated sites, so in either case, the surface will have clearly defined regions containing polymer film with adjacent bare gold or inert SAM-coated gold. Especially in the case where bare gold remains interspersed with PHEMA or derivatized PHEMA, further processing is possible via another polymerization step. As a demonstration of this concept, surface-catalyzed growth of polymethylene from bare gold will be conducted to create either hydrophobic/hydrophilic or fluorocarbon/hydrocarbon patterned surfaces.

Another potential patterning method that is possible exclusively with fluorinated PHEMA films is to deliver basic solution to hydrolytically pattern the surface. In the ideal hydrolytic patterning situation, the stamped regions would be converted back to PHEMA, causing a change in film thickness and surface properties where the base solution is applied (similar to controlled hydrolysis in the creation of block-like copolymer films in Chapter VI but on the microscale).

Experimental Procedures

PDMS stamps having relief features of either 10 or 20 μm wide lines and correspondingly, either 20 or 40 μm wide spacings were used to pattern surfaces. The PDMS stamps were fabricated in a clean room using lithographic masters (photoresist pattern on silicon) donated by Professor Ki-Bum Kim (Seoul National University). By volume, one part of Sylgard 184 silicone elastomer curing agent to 10 parts of Sylgard 184 silicone elastomer base were mixed thoroughly and then placed under vacuum in order to purge any entrapped air. The mixture was then poured onto the masters and cured in a 60 °C oven for 2 h. The PDMS stamps were cut into their respective sizes (~1 cm × 1 cm) using a scalpel. The stamp surfaces were inked by rubbing them with a cotton swab that had been soaked in one of the following solutions: 10 mM dodecanethiol in ethanol, 10 mM ATRP disulfide initiator ($(BrC(CH_3)_2COO(CH_2)_{11}S)_2$) in ethanol, or 0.1 M to 0.5 M KOH in either water or ethanol. After inking, the stamps were gently dried with nitrogen, and patterned surfaces were formed by pressing the inked stamps into contact with the gold or polymer-coated gold substrates. The stamp was pulled off the substrate after about 1 min of contact, and the substrate was then rinsed with ethanol.

In the case of hydrolytic patterning, the substrate was also rinsed with water to ensure complete removal of KOH. All other processing steps (polymerization and film derivatization) remained the same as described previously.

Polymethylene (PM) films were prepared on bare gold regions of patterned PHEMA films by exposure of the substrates to ether solutions containing 4 mM diazomethane (DM) at 0 °C for 16 h (overnight).[21,22] Film growth was carried out in capped 20 mL vials, and only one substrate was placed in each vial. Upon removal, the samples were rinsed with ether and dried in a stream of nitrogen.

Results and Discussion

Patterned ATRP Initiator and Subsequent Film Growth

μCP Inert Alkanethiol and Backfilling ATRP Disulfide Initiator

Hawker and coworkers[16] previously microcontact printed hexadecanethiol onto gold before exposure to the ATRP disulfide initiator, $(BrC(CH_3)_2COO(CH_2)_{11}S)_2$, to backfill the surface with sites conducive to polymer growth. We stamped dodecanethiol onto gold using the same processing sequence (except growing PHEMA and derivatizing to F7 instead of growing PMMA) and found, as they did, that polymer was reliably only found in areas backfilled with initiator. Initiator backfilling was only conducted for 15 min as compared to the usual 12+ h initiator SAM formation to minimize the possibility of the initiator disulfide displacing stamped dodecanethiol. Figure 7.1 demonstrates these results in the form of a 2D tapping mode AFM image showing 10 μm wide dodecanethiol lines and 20 μm lines of F7. The height of F7 film observed by AFM

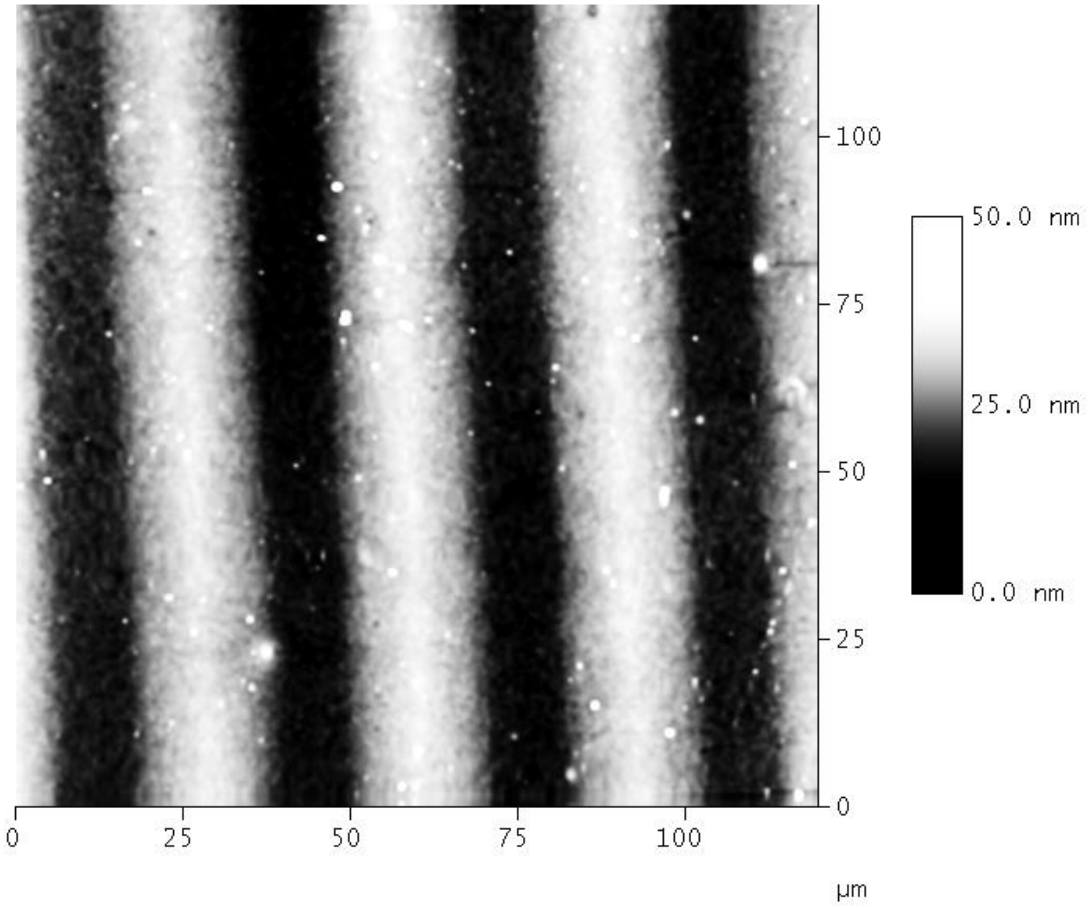

Figure 7.1. 2-D tapping mode AFM image of a sample microcontact printed with dodecanethiol, backfilled with ATRP initiator, exposed to an ATRP reaction mixture to grow PHEMA atop the initiated area, and reacted to form F7 from PHEMA. The 20 μm wide white lines denote ~25 nm thick F7 while the 10 μm wide dark areas represent dodecanethiol-coated gold.

in this case was ~25 nm. A likely cause of the thinner than expected film formation was the limited time with which the sample was backfilled with the disulfide initiator. While a longer backfill time should make available more initiator sites, pattern registration may be hindered.

μCP ATRP Disulfide Initiator

In similar fashion to μCP of an alkanethiol, the ATRP disulfide initiator may be stamped directly onto a gold surface to create a SAM. This approach of directly microcontact printing an initiator for polymerization onto a surface has been demonstrated in the literature only twice to our knowledge, once being with a trichlorosilane ATRP initiator[19] and the other an amine-terminated alkanethiol[20] for peptide polymerization. A reduction in processing steps is the main advantage of this technique over that of stamping an inert layer and then backfilling. Additionally, after polymerization, an inert layer is not present or does not have to be removed by selective etching,[16] so that further processing from the interspersed bare substrate is possible.

A PDMS stamp having 20 μm line features was inked with ATRP initiator and used to create an initiator pattern on a bare gold substrate. After exposure to the ATRP polymerization mixture for 12 h, patterned PHEMA film growth was observed on the surface. The PHEMA film was derivatized to form F7, which remained confined in initiator-patterned regions. Figure 7.2 shows the RAIR spectra of initiator-patterned gold after PHEMA film growth and after acylation to form F7. AFM images of these same patterned PHEMA and patterned F7 samples are presented in Figures 7.3 and 7.4. Based on film thickness information from Figures 7.3 and 7.4, thickness increase of PHEMA upon acylation to F7 is 100% according to AFM, comparable to an ellipsometric

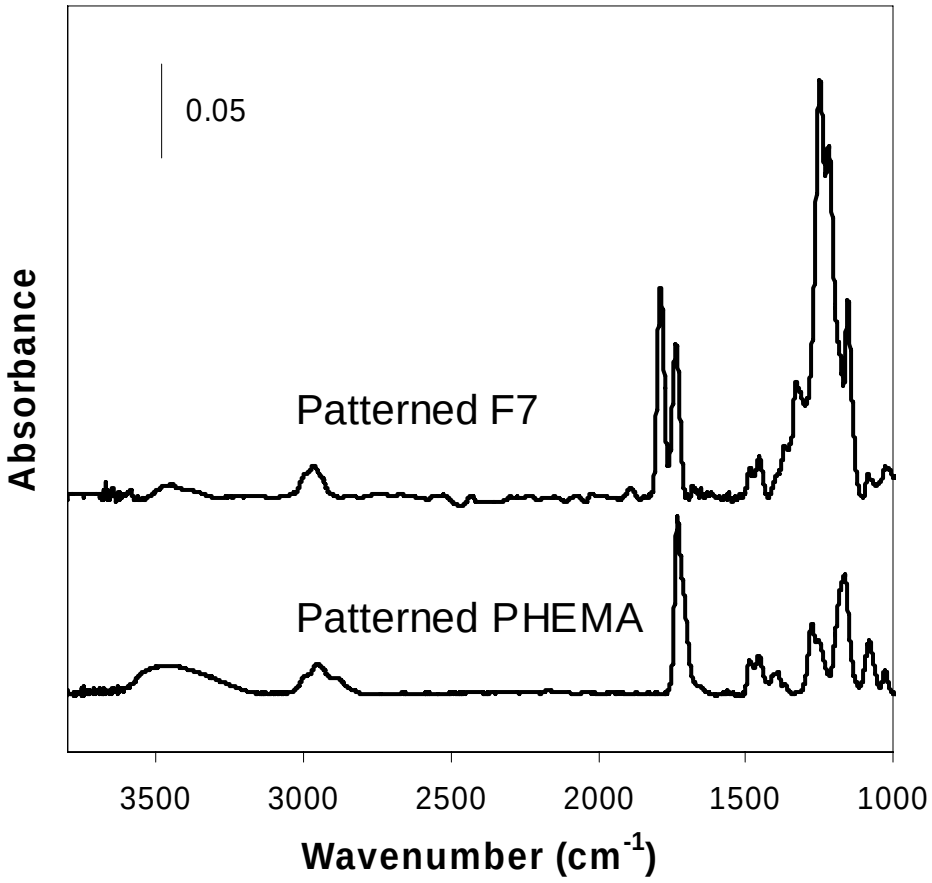

Figure 7.2. RAIR spectra for a microcontact printed PHEMA film both before and after acylation to form F7. The pattern used was 20 μm features with 40 μm spacing, resulting in one third of the surface having PHEMA growth. Peak assignments are the same as for all other PHEMA and F7 films encountered in this work, but peak intensities are diminished since the PHEMA film does not cover the entire gold substrate.

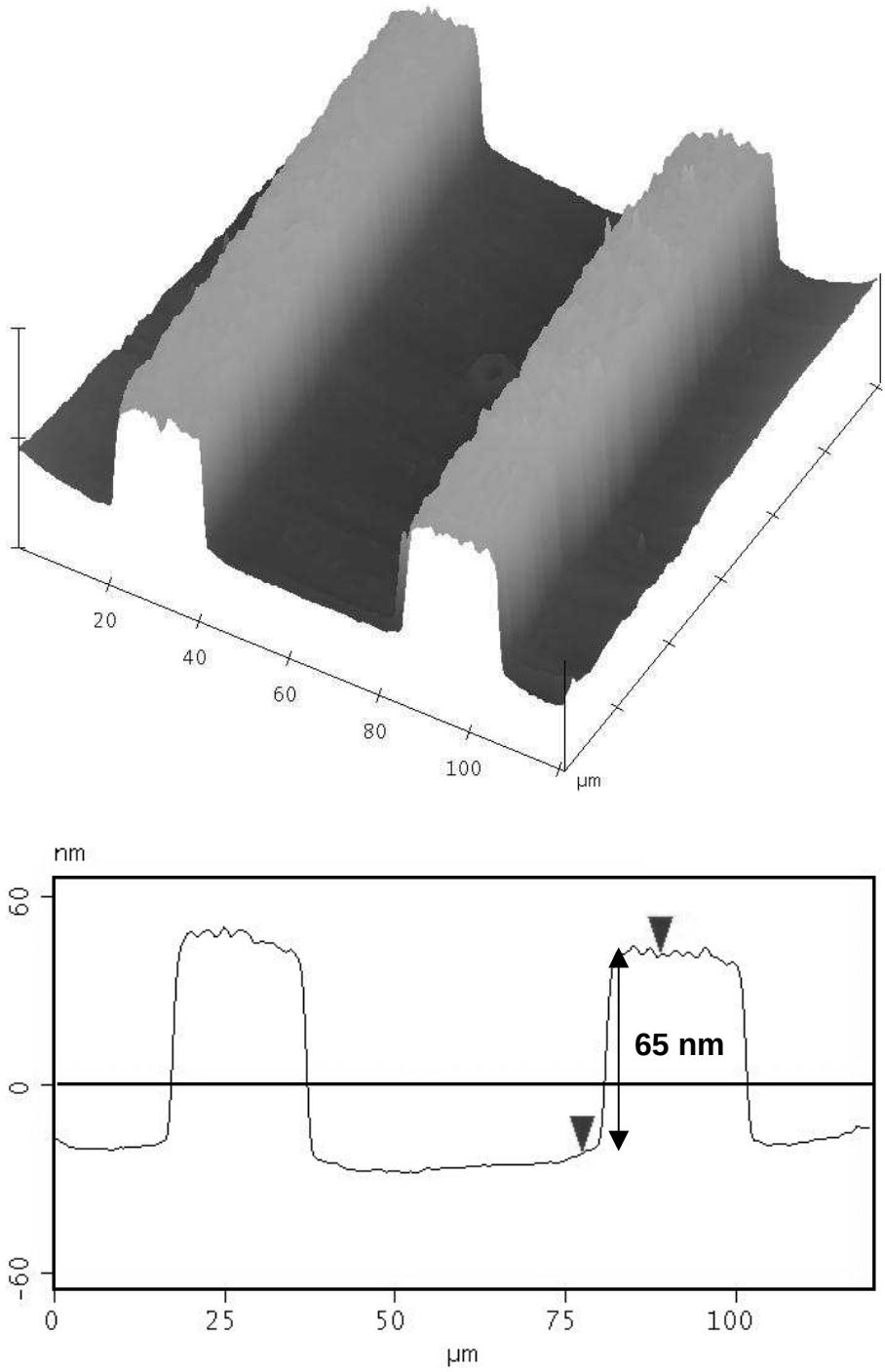

Figure 7.3. Tapping mode AFM image of a sample with patterned 20 µm lines of PHEMA film growth. PHEMA film thickness is 65 nm, with the film only growing in regions where the initiator was patterned.

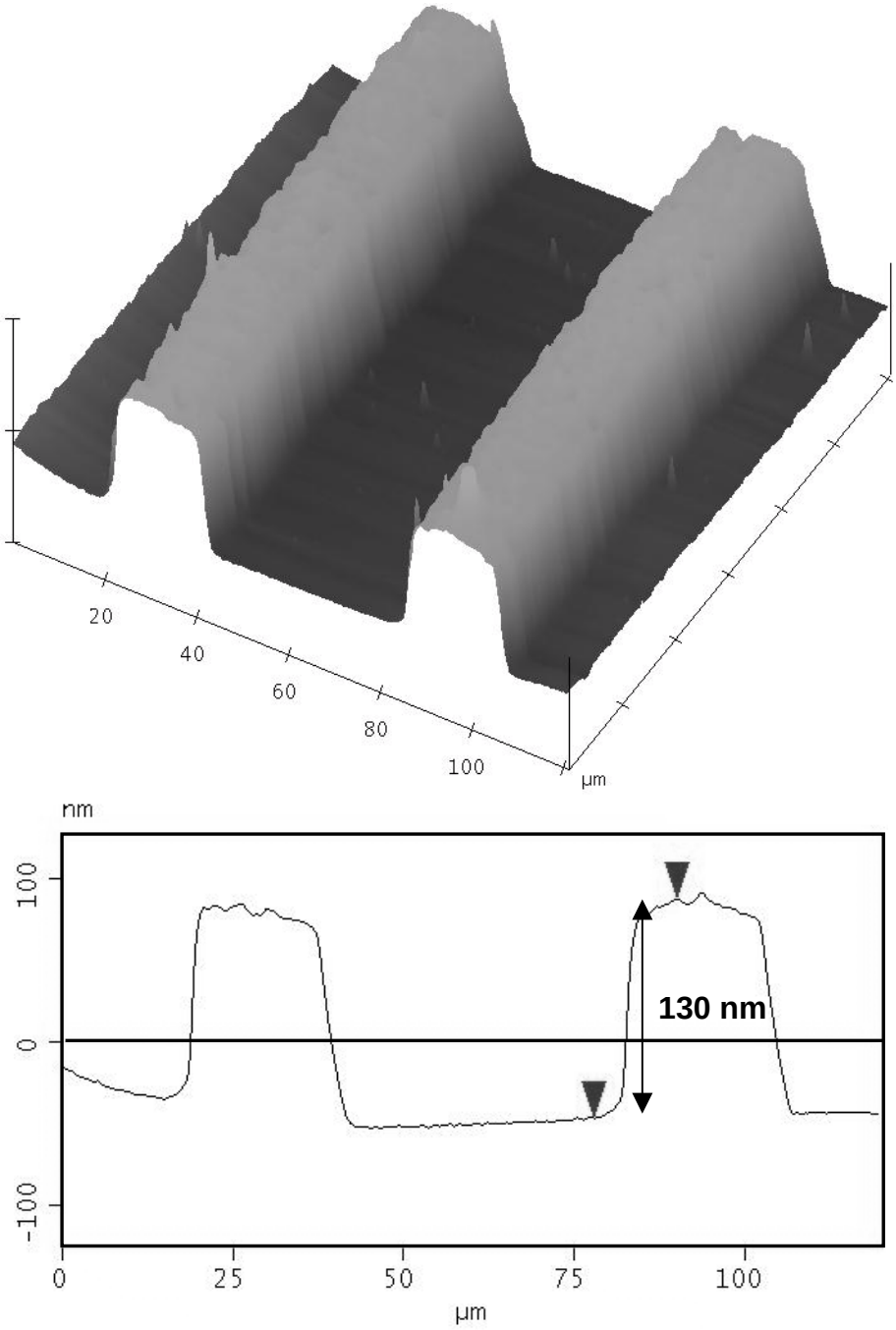

Figure 7.4. Tapping mode AFM image of a sample with patterned 20 µm lines of PHEMA film growth that were subsequently derivatized to form F7 in the same pattern. F7 film thickness is 130 nm, or approximately double the thickness of the starting PHEMA film.

thickness increase of ~140% based on traditional, non-patterned films of PHEMA to F7. Absolute film thickness for the patterned PHEMA film was 65 nm, but from the same batch the corresponding ellipsometric thickness for a 12 h PHEMA film on fully-initiated bare gold was ~210 nm. While the thickness difference is quite large, Farhan and Huck[19] noted similar behavior in the growth of poly(N-isopropyl acrylamide) on bare silicon and poly(ethylene terephthalate) where a homogeneous film yielded an ellipsometric thickness of 185 nm but an initiator-patterned film yielded an AFM thickness of 65 nm. They attributed the mismatch to differences in surface roughness since they patterned a relatively rough substrate but used smooth bare silicon as the control. Similarly, since the gold-coated silicon wafers used in our work are not atomically flat and are likely much rougher even than the base silicon wafers, we attribute some of our thickness mismatch to roughness as well. μCP onto a rough substrate hinders the amount of contact between the PDMS stamp and the surface, which is required to transfer the initiator onto the surface. Furthermore, creation of a homogeneous PHEMA film by dipping the entire substrate in solution overnight allows a complete initiator layer to be formed on the gold surface, no matter its roughness. It may also be unreasonable to expect close agreement between ellipsometry and AFM since the two methods are measuring and utilizing different film aspects, namely optical or mechanical film properties, to estimate thickness.

Mixed Fluorocarbon/Hydrocarbon Polymer Films

Modification of PHEMA with Fluorocarbons and Hydrocarbons

As greater engineering control over polymer film properties has become more desirable, an interest in self-assembling films that spontaneously or with minimal effort

form compositional domains has increased.[23,24] Fluorocarbons are known to phase separate in the presence of all other chemical compositions, including hydrocarbon chains.[25-27] In an effort to create modified PHEMA films having microdomains of fluorocarbon, we attempted to use the derivatization approach already demonstrated in Chapters IV and V to modify a single PHEMA film with both fluorocarbon and hydrocarbon side chains simultaneously. PHEMA films were reacted with solutions containing various ratios of palmitoyl and pentadecafluorooctanoyl chlorides (60 mM overall acid chloride concentration) in an attempt to form a random copolymer film, H15/F7.

F7 was generally formed much faster than H15 in homopolymer films, so palmitoyl chloride was used in excess of the fluorocarbon acid chloride in the reaction mixture. While results varied widely from run to run, typically even a small change in palmitoyl chloride:pentadecafluorooctanoyl chloride ratio from 12:1 to 14:1 resulted in markedly different compositions. The 12:1 reaction mixture (55.4 mM palmitoyl:4.6 mM pentadecafluorooctanoyl) gave an entirely fluorocarbon F7 film, whereas the 14:1 reaction mixture (56.0 mM palmitoyl/4.0 mM pentadecafluorooctanoyl) gave an entirely hydrocarbon H15 film, as demonstrated by the RAIR spectra in Figure 7.5. This figure is only meant to convey the difficulty in creating mixed fluorocarbon/hydrocarbon films via reactive modification. The exact reactant ratios where this composition inversion occurred tended to fluctuate over different independent preparations but were consistently observed within a <1 mM reactant concentration change. Out of approximately sixty derivatized films, only two were created that actually incorporated significant quantities of both H15 and F7 functionality. Several films contained <5% of one of the species and

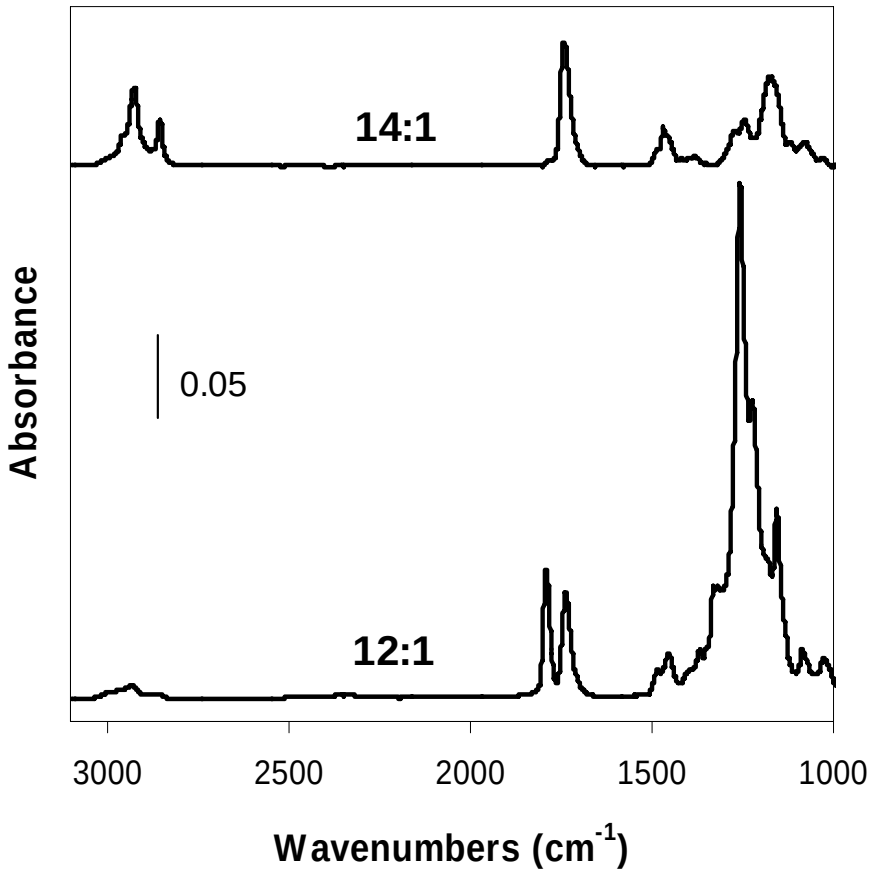

Figure 7.5. RAIR spectra for PHEMA films derivatized with a 60 mM acid chloride solution having either a 12:1 or 14:1 ratio of palmitoyl chloride: pentadecafluorooctanoyl chloride. At 12:1, the resulting derivatized film is all fluorocarbon (F7), while at 14:1, the derivatized film is all hydrocarbon (H15). The small window of reactant ratio-film composition change is indicative of phase separation phenomenon between fluorocarbon and hydrocarbon chains.

many others were entirely homopolymers. The variability of this process suggests that phase separation and, by extension, kinetics play a significant role in this random copolymer film modification. While there is more than sufficient acid chloride of either composition to modify the entire film, whichever chemical composition is the first to incorporate into the film generally dominates the entire film composition. This is presumably a product of phase separation (both in the liquid reaction mixture and in the film itself during reaction) between hydrocarbons and fluorocarbons. A film having either compositional extreme tends to preferentially partition more of the same groups into the film and ultimately yields homopolymers. Figure 7.5 thus demonstrates fluorocarbon/hydrocarbon phase separation in a convincing and concise manner.

Directed Growth of PHEMA and Polymethylene Films

Since fluorocarbon/hydrocarbon patterns cannot be reliably created by simultaneous functionalization of PHEMA, we sought alternative approaches to combine F7 with hydrocarbon polymer films by taking advantage of bare gold regions that remain after initiator-patterned growth of PHEMA. Since these mixed surfaces cannot be created through growth and modification of PHEMA, a separate processing step can be utilized to introduce hydrocarbon functionality for the purposes of creating patterned fluorocarbon/hydrocarbon microdomains and to investigate the interfacial behavior of the two polymers. As already shown in Figures 7.3 and 7.4, PHEMA growth and derivatization results in a film on a portion of the surface but leaves a large proportion of bare gold area. The unmodified bare gold is ideal for further processing steps to add surface functionality. Patterned 12 h PHEMA growth and modification to create a

fluorocarbon film was followed by surface-catalyzed growth of polymethylene (PM) from bare gold sites to create F7/PM.

Figure 7.6 shows the RAIR spectrum for F7/PM. The presence of PM is indicated primarily by increased peak intensity for CH_2 stretching modes at ~2850 and ~2920 cm^{-1}. Various peaks from 1000 to 1800 cm^{-1} indicate the presence of F7 functionality, as discussed in Chapter IV. F7/PM demonstrates the ability to create a single film containing both fluorocarbon and hydrocarbon groups using μCP. If the PHEMA film is not derivatized before PM growth, a route to create patterned PHEMA/PM hydrophilic/hydrophobic surfaces is possible. These types of patterned films are potentially useful in a variety of applications, including microfluidic devices,[7] dewetting phenomenon,[4] etch resists,[8] or cell/biological attachment[28,29] where the presence of fluorocarbon/hydrocarbon or hydrophobic/hydrophilic groups directs surface events to preferentially occur on one of the regions.

Tapping mode AFM images of PHEMA/PM and F7/PM are presented in Figures 7.7 and 7.8, respectively. The most noticeable aspect of the PHEMA/PM film evident from the AFM image in Figure 7.7 is the presence of what appears to be an interfacial gap between the hydrophobic PM and the hydrophilic PHEMA. The overall thickness difference between the two polymer regions is only ~50 nm, but the trench present between them is at least 30 nm deep when compared to the PHEMA film. Based on the results of Figure 7.3, we would expect the PHEMA film to be ~65 nm thick (or perhaps a bit thicker if PM grows underneath PHEMA, as discussed in the next two paragraphs), so the trench presumably does not extend all the way to the surface, although this cannot be verified. The ability of AFM to probe this gap is limited, but it consistently appears on

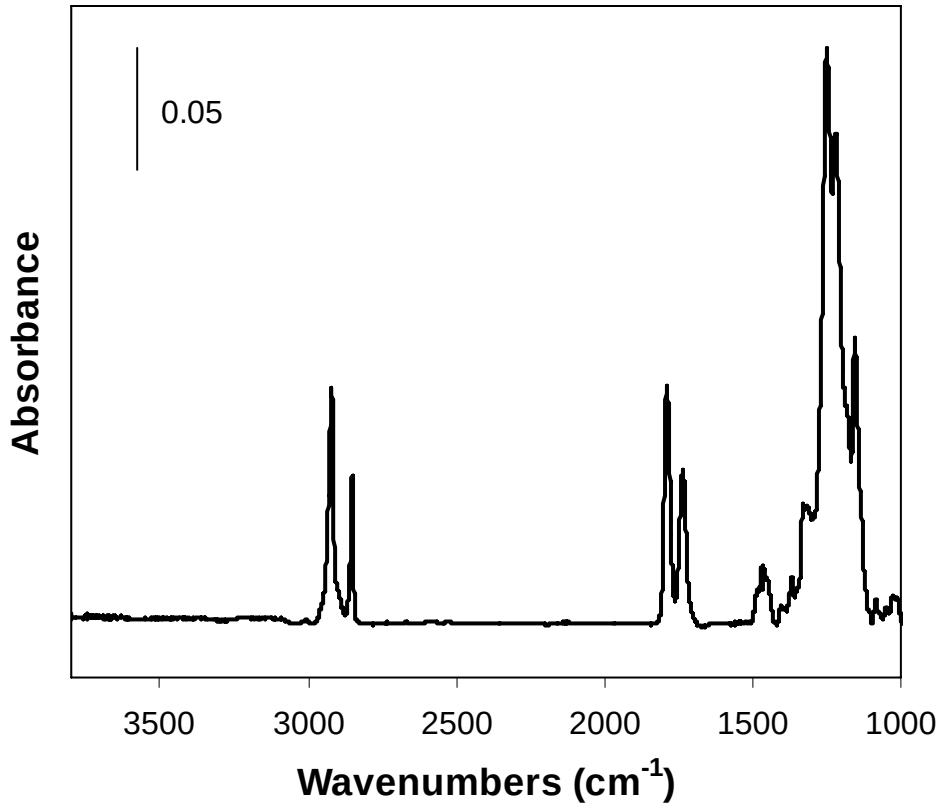

Figure 7.6. RAIR spectrum for F7/PM. Peak assignments are the same as for a homogeneous F7 film except for intense CH_2 bending and stretching modes around 1450 and 2900 cm^{-1}, respectively, due to PM. F7/PM contains both fluorocarbon and hydrocarbon functionality.

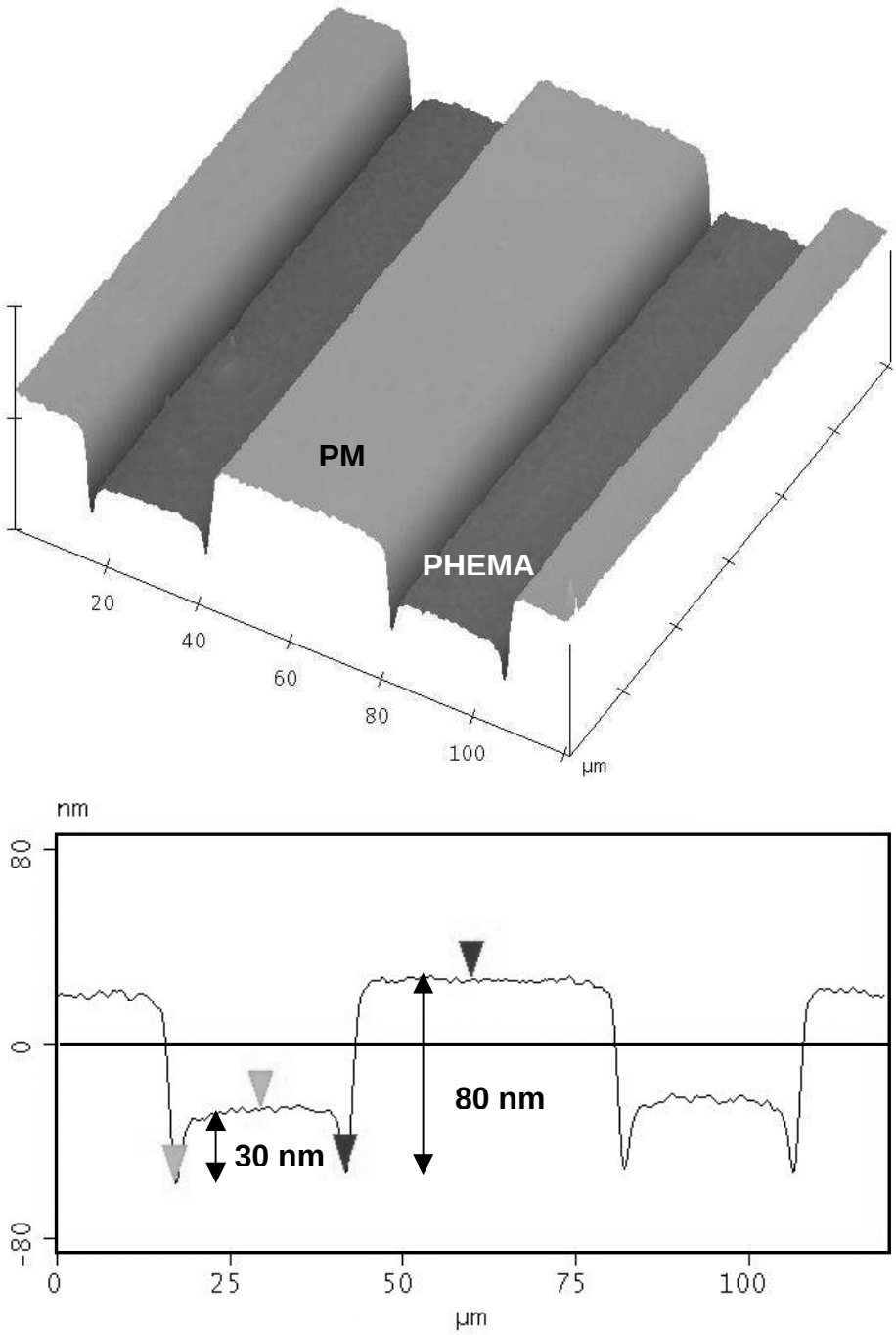

Figure 7.7. Tapping mode AFM image of a sample with patterned 20 μm wide lines of PHEMA film growth and 40 μm wide stripes of PM grown from intermediate bare gold spaces. A cross-section of the film, indicating differences in thickness between the PHEMA and PM regions, is presented in the lower portion of the figure.

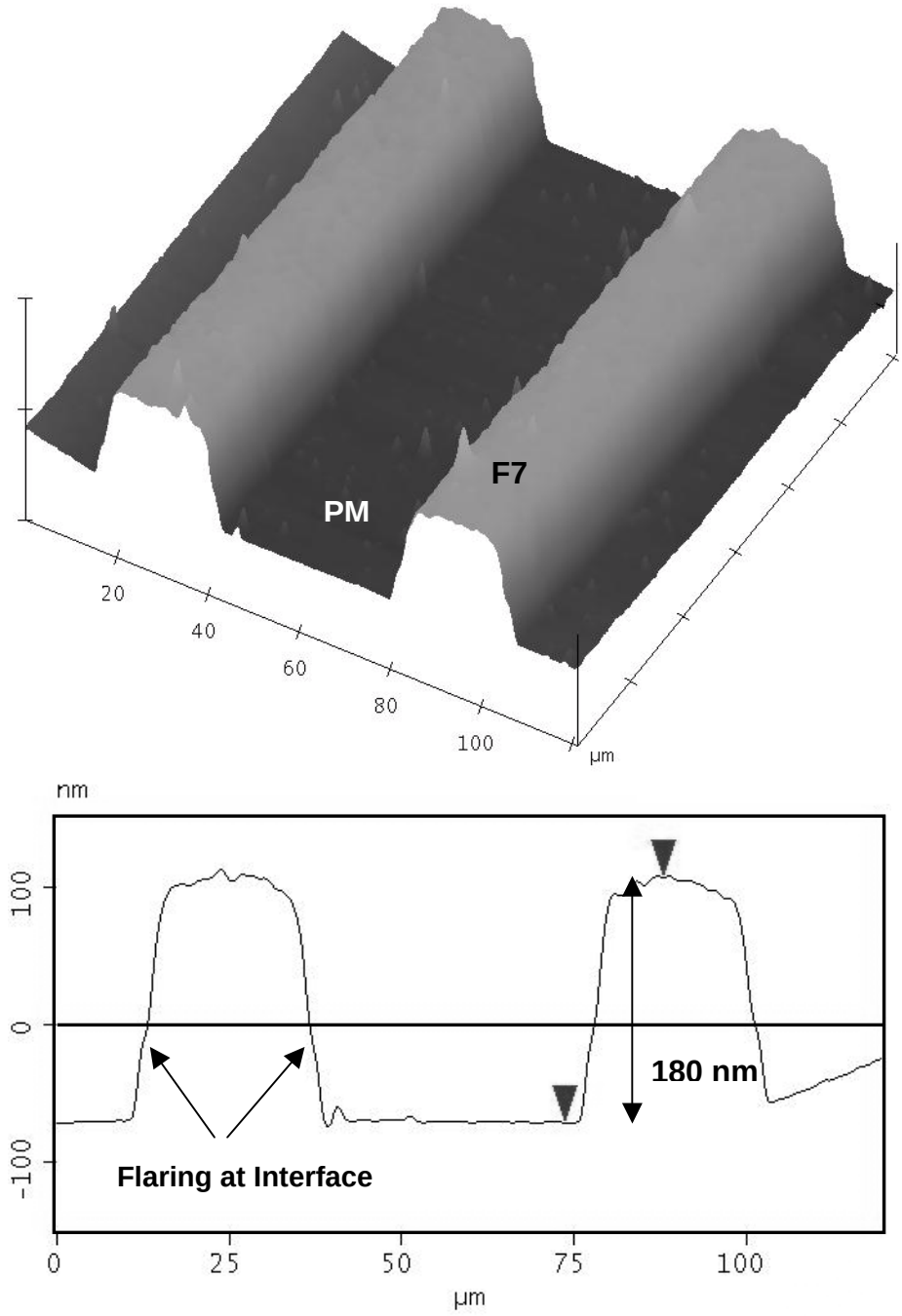

Figure 7.8. Tapping mode AFM image of a sample with patterned 20 µm wide lines of PHEMA film growth that was subsequently derivatized to F7 before growth of PM from intermediate bare gold spaces. A cross-section of the film, indicating the difference in thickness between the F7 and PM regions, is presented in the lower portion of the figure. Regions at the interface that exhibit "flaring," likely explained by the PM growth mechanism, are also indicated.

AFM images of PHEMA/PM only. For both ATRP of PHEMA and surface-catalyzed growth of PM, the termination of active, growing chains increases at longer polymerization times (thicker films), such that the polymer chain density decreases as the distance from the surface becomes greater. The result of decreased polymer chain density in regard to patterned films is a tendency for the features to shrink in dimension as the distance from the underlying surface is increased. Hence, we observed a sloped sidewall on each patterned region in PHEMA/PM. Since PHEMA and PM features are adjacent, but each feature becomes thinner as distance from the surface increases, the final result in the PHEMA/PM patterned film is an apparent interfacial gap that forms between the two polymer regions. The horizontal distance from the lowest measured point in the gap to the top edge of the sidewall for either PHEMA or PM features is ~2-3 μm, resulting in a total maximum distance across the gap of ~5 μm. With the feature size of the AFM tip being <10 nm, the observed phenomenon is apparently not an artifact of AFM measurement but exists as a real feature of these films.

The tapping mode AFM image of F7/PM in Figure 7.8 does not exhibit the interfacial gap between the PM and F7 regions, but the interface between PM and F7 does flare out at the base of the F7 patterned region. This feature is apparently not an artifact of AFM imaging either since the unfiltered version (not shown) of the AFM image in Figure 7.8 contains distinctly recognizable steps about 2-3 μm wide at the interface between the two regions; processing the image partially washed out these features, but the flared regions are still evident in Figure 7.8. A possible explanation for the two distinct interfacial phenomena occurring between the PHEMA and PM phases lies in the mechanism of the surface-catalyzed growth of PM. Guo and Jennings[11]

previously showed that the presence of a SAM actually enhances the growth of PM on gold substrates. Similarly, when homogeneous PHEMA and F7 films (0.5 h polymerization or ~35 nm thick PHEMA and ~85 nm thick F7) were exposed to PM growth conditions (4 mM DM in ether at 0 ºC overnight), PM was incorporated into the film (Figure 7.9) to form PM-*b*-PHEMA and PM-*b*-F7, respectively. The presumed PM growth mechanism is based on insertion of adsorbed methylene at gold sites that is enhanced by and pushes up a SAM.[21] In this case, the PHEMA-based films contain an initiator SAM along with the tethered polymer film. Presumably, the entire film is pushed up during PM growth such that a block-like copolymer film having lamellar PM and PHEMA (or F7) domains is formed. In the homogeneous cases, PM growth on F7 was significantly greater than that on PHEMA. Compared to the growth of PM under the same conditions on bare gold,[21] F7 enhanced the growth whereas PHEMA stunted PM growth. A thicker F7 barrier film apparently allows DM into the film and to the underlying gold substrate more readily than does a thinner, loosely-packed PHEMA film. A possible explanation for these observations is that the hydroxyl groups present in greater abundance in PHEMA react with DM and quench the reaction.

The extent of PM growth on homogeneous PHEMA and F7 films offers insight into the interfacial behavior exhibited between PHEMA and PM regions in the AFM images. The gap, or trench, between phases is only observed in PHEMA/PM because of the quenching effect exerted by PHEMA on PM growth, where PM is physically unable to grow near regions dominated by PHEMA to the extent that it can grow in open bare gold spaces. If significant PM growth were to occur underneath PHEMA, a gap would not be observed since the entire PHEMA layer would be pushed above a homogeneous

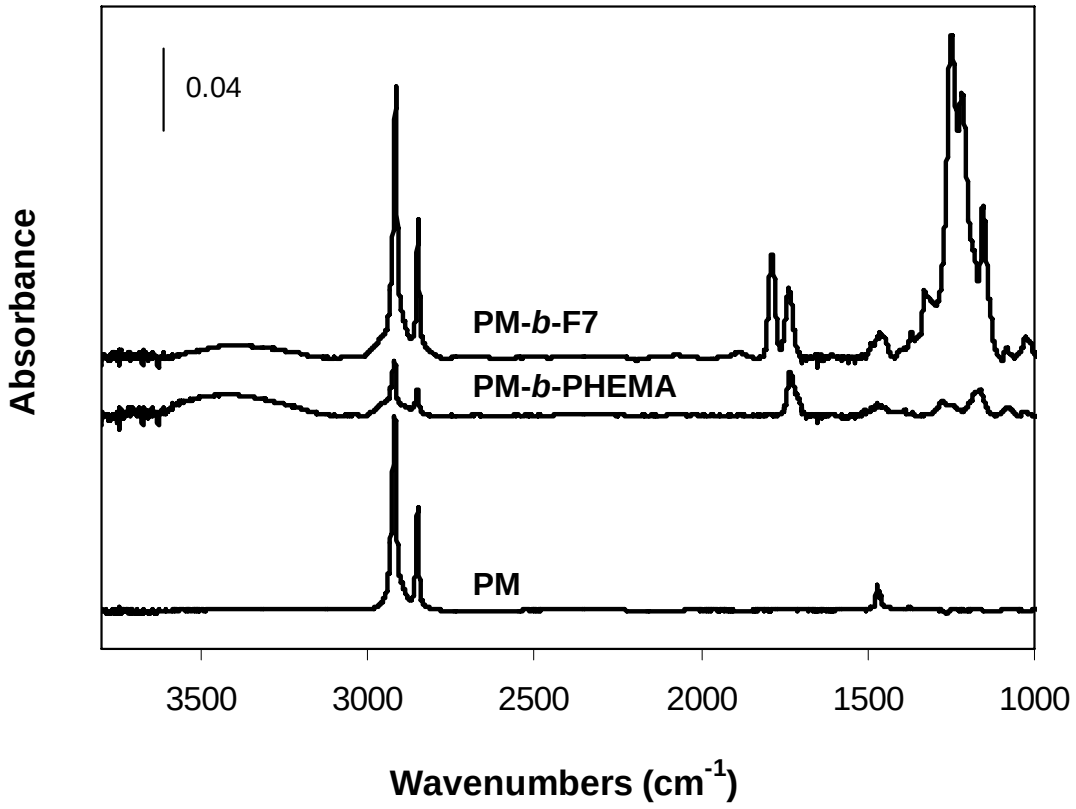

Figure 7.9. RAIR spectra for PM, PM-*b*-PHEMA, and PM-*b*-F7 films created by exposing PHEMA and F7 films to PM growth conditions. Presumably PM grows underneath the PHEMA-based films by an insertion mechanism, pushing the initiator and polymer films up as it grows. The resulting films likely have a lamellar block copolymer structure. PM grown on bare gold is shown as a reference.

PM layer and the two regions would no longer be adjacent. A greater understanding of the interfacial behavior (particularly the presence of gaps such as the one observed here) of patterned films may open up new routes to patterned submicron features.

The flaring behavior observed in F7/PM at the interface between the two regions, in similar manner, is likely the result of PM growth enhancement offered by F7. The large difference in thickness (230 nm) for the PHEMA-patterned areas found by comparing Figures 7.7 and 7.8 (and assuming PM growth in bare gold regions is consistent) can likely be explained by the greater degree of "pushing-up" exerted on F7 by PM. The flared region in F7/PM exhibits a height of ~60 nm. This flared region is most likely PM growing underneath the F7 that inflates the height changes in favor of F7. Furthermore, from Figure 7.9, we would expect even more PM to grow in the presence of F7 than grows on bare gold, so that the height of PM underneath the F7 region should be slightly greater than that in bare gold regions. If the 60 nm tall flared region is actually just PM, the corresponding height of F7 in Figure 7.8 is 120 nm, which is in good agreement with a F7 film height of 130 nm from Figure 7.4. The lack of an interfacial gap in F7/PM is, therefore, consistent with significant PM growth underneath the F7 film. Since the entire F7 film is pushed above the adjacent PM film, there are no regions where the two films are directly adjacent to one another. A homogeneous PM film dominates the entire lower layer, with F7 lying above that. In the cases of both PHEMA/PM and F7/PM, the interfacial behavior exhibited is a direct result of the control over PM growth kinetics offered by the two distinct functionalities (PHEMA or F7) patterned onto the surface. PHEMA/PM likely also includes some (but much less) PM growth underneath

PHEMA that makes a direct comparison of height changes between PHEMA/PM and F7/PM nontrivial.

Hydrolytic Patterning of Fluorocarbon-Modified PHEMA

A more novel aspect of patterning modified PHEMA films lies in the remarkable ability to partially hydrolyze fluorinated esters on the side chains. Since base (KOH) has been shown to easily hydrolyze esters having α or β fluorines, stamping basic solution onto a surface consisting entirely of fluorinated PHEMA would hydrolyze the surface in accordance with the pattern. However, unlike traditional μCP followed by surface-initiated polymerization, a polymer film remains over the entire substrate. The stamped regions would maintain PHEMA functionality while the unstamped portions retain fluorocarbon functionality—a hydrophilic region surrounded by hydrophobic, oleophobic walls, as the film thickness should decrease upon hydrolysis (see Chapter IV).

Complete hydrolysis of fluorocarbon-modified PHEMA films was demonstrated in Chapter IV, while controlled hydrolysis of these films was exploited in Chapter VI to create block-like copolymer films. Combining hydrolysis and μCP may be accomplished by inking a PDMS stamp with a reactive species, KOH. It was expected that base would be delivered to the surface at the features and begin cleaving fluorocarbon ester side chains upon contact. The only related work found in the literature was conducted by Grzybowski and coworkers,[15] who used an agarose stamp to apply potassium dichromate to PDMS or polystyrene to oxidize the surfaces, making hydrophilic regions in a patterned arrangement.

Macroscale Demonstration

As demonstration of a concept for hydrolytic patterning, a fluorocarbon-modified PHEMA film was patterned on the macroscale. A paintbrush was first soaked in a 0.1 M KOH in ethanol solution and then subsequently used to "paint" a pattern on a F7 film. Areas where KOH was introduced by the paintbrush were readily hydrolyzed, regenerating hydroxyl groups and yielding hydrophilic, oleophilic surface regions. Upon rinsing with either water or ethanol, liquid wets the hydrolyzed regions, maintaining the pattern that was painted on. Without even using a liquid to test wettability, the painted regions are visibly altered due to a stark contrast in refractive index for F7 and PHEMA (~1.38 vs. ~1.50). Figure 7.10 shows an example of a macropatterned F7 film, where a "VU" image was created on a F7 film using a paintbrush and then was rinsed with water. As expected, water remained only in the hydrophilic "VU" region but avoided the extremely hydrophobic surrounding areas. Hydrolytic patterning of fluorocarbon-modified PHEMA films is feasible for use in macroscale applications where patterned surface energy is desirable, such as directing the flow of water droplets on surfaces.[30]

Microscale Hydrolytic Patterning

Several issues were determined to be of utmost importance in the micropatterned cleaving of fluorocarbon ester side chains in derivatized PHEMA films. One of the most significant obstacles to patterning polymer films on the microscale is the behavior of solvent from the stamp upon contact with the surface. If the solvent spreads across the surface, the resulting hydrolysis will give a distorted pattern. Furthermore, the solvent would ideally be transported linearly down into the film with little to no lateral diffusion and completely hydrolyze the fluorocarbon-modified film in the patterned region only.

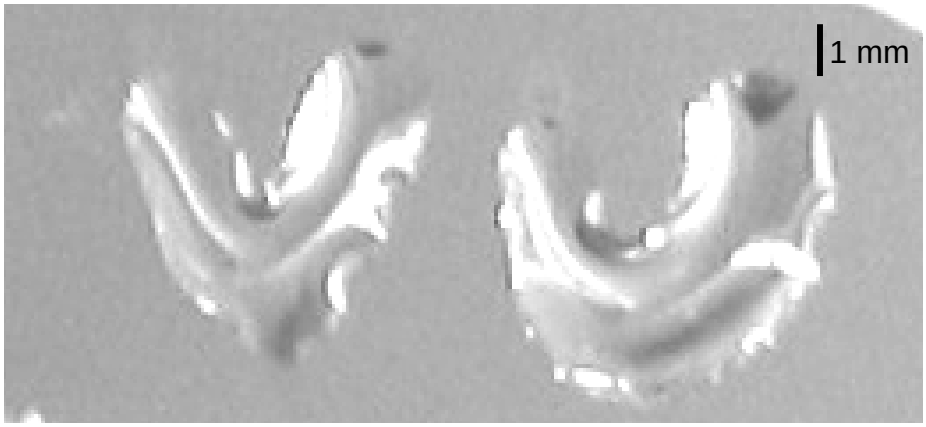

Figure 7.10. F7 film with a macropatterned “VU” painted onto it with a paintbrush soaked in 0.1 M KOH in ethanol. While feature size shown here is rather large (~0.6 cm), it demonstrates the potential feasibility of patterning fluorocarbon-modified PHEMA films on the microscale.

So in addition to solvent effects, a sufficient amount of base must be transferred to completely hydrolyze a several hundred nm thick film. To further complicate the process, the film thickness should immediately shrink once hydrolysis starts and potentially result in a loss of stamp-film surface contact. The specific factors that govern these behaviors are the following: surface energy of the film being patterned, surface tension of the liquid used to ink the PDMS stamp, and concentration of base in the inking solution. Ultimately, inking the PDMS stamp with a solution of 0.5 M KOH in ethanol and μCP onto a F1 surface proved to be the most reliable conditions for hydrolytic patterning.

Initial attempts at μCP fluorocarbon-modified PHEMA focused on F7 and a PDMS stamp inked with ethanol solutions having KOH concentrations ranging from 0.1 to 0.5 M. Optical microscope images of these attempts (not shown) revealed entirely unpredictable patterns that appeared to result from solvent spreading across the F7 surface, as a small amount of residual solvent (ethanol in this case) aids in transport of the KOH into and across the film upon stamp contact. Additionally, higher KOH concentrations resulted in more overall hydrolysis, so 0.5 M KOH solutions were used subsequently for all experiments in attempts to completely hydrolyze the fluorocarbon-modified films in patterned regions. To keep solvent spreading from occurring as readily, water was used as the solvent since it has a much higher surface tension and thus, exhibits a much higher contact angle on F7 than ethanol.

In order to use water as the solvent for μCP, a PDMS stamp was made hydrophilic by placement in a UV/ozone cleaner for 1 h. Longer exposure times were observed to crack the PDMS stamp and make it essentially unusable for reliable patterns.

The PDMS surface was confirmed to be hydrophilic since water completely wetted it immediately after removal from UV/ozone. The stamp was stored in water to ensure that it remained hydrophilic for an extended period of time. The PDMS stamp was inked with an aqueous 0.5 M KOH solution, dried, and applied to a F7 film. Similar results occurred as before, with optical microscope images of the patterns being highly irregular (not shown).

The primary unchanged variable up to this point was the film surface itself. Since F7 presents an extremely hydrophobic and well-packed barrier film, the KOH solutions likely have difficulty penetrating the film and then transporting cleaved material out of the film. To evaluate this issue, we attempted μCP of 0.5 M KOH solutions in both ethanol and water on F1. FBZ has similar wettability to F1 but is more stable towards hydrolysis, so it was not considered an option. Overall results with F1 were still found to be somewhat irregular and not entirely faithful to the original PDMS pattern, as solvent still spreads across the surface. Nonetheless, we were able to produce an improved pattern when F1 was used as the base film instead of F7. Figure 7.11 shows a tapping mode AFM image of a F1 surface microcontact printed with a PDMS stamp having 20 μm line features and inked with a 0.5 M KOH in ethanol solution. The F1 film shown in Figure 7.11 was based on a PHEMA film that was only grown for 0.5 h to produce a film thickness of ~35 nm. The hydrolysis pattern is wavy and does not render pattern features crisply, and the hydrolysis pattern depth is only 6 nm. We would expect a ~18 nm deep feature based on the expected difference in thickness exhibited by F1 for a 35 nm PHEMA film (Table 4.1). The shallow depth arises from two possibilities: insufficient amounts of base can be delivered into the film to completely hydrolyze the film at the

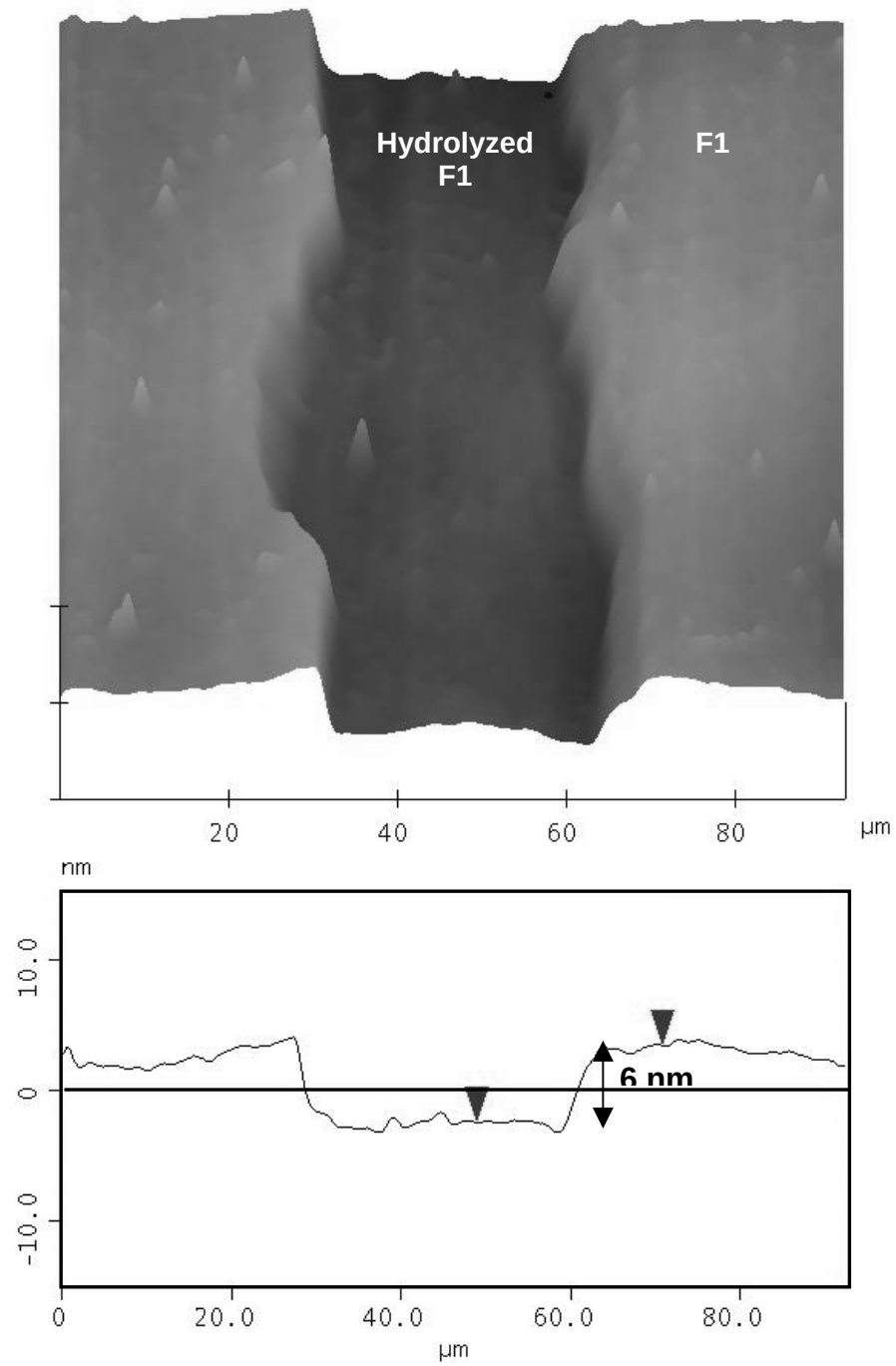

Figure 7.11. Tapping mode AFM image of a F1 film microcontact printed with a PDMS stamp having 20 µm line features and inked with 0.5 M KOH in ethanol. The hydrolyzed region has a depth of 6 nm and does not faithfully reproduce the line pattern. The increased feature width (up to 40 µm) likely results from solvent spreading across the surface.

points of contact and/or the F1 film does not exhibit as large a film thickness change upon hydrolysis as does F7.

Conclusions

Numerous methods exist for the creation of micropatterned polymer films through the use of microcontact printing. We have demonstrated two straightforward methods to grow PHEMA (and derivatized PHEMA) films on gold in a patterned fashion—μCP of an inert alkanethiol followed by backfilling with an ATRP initiator or direct μCP of the initiator onto gold. Because of its simpler processing, μCP the initiator directly onto gold is more desirable, and it also maintains bare gold functionality between regions of patterned PHEMA growth. Bare gold can then be used to conduct a variety of additional processes. In this work, we have exploited the unmodified gold regions to grow entirely hydrocarbon PM films via surface-catalyzed polymerization. We were thus able to create mixed films having both fluorocarbon and hydrocarbon microdomains, which we were previously unable to achieve through the reactive modifications discussed in previous chapters. AFM images of the PHEMA/PM and F7/PM films indicated interesting behavior at the interface between the regions, with PHEMA/PM exhibiting a noticeable gap and F7/PM exhibiting flared growth. We believe these behaviors result from a quenching effect observed for growth of PM on homogeneous PHEMA films and a growth kinetics enhancement observed for PM on homogeneous F7.

Since the fluorinated esters present in fluorocarbon-modified PHEMA films may be hydrolyzed by exposure to base, these films have the potential to be patterned hydrolytically by μCP basic solution. A demonstration of this process on the macroscale

for these films verified the potential to use the hydrolysis reaction on the microscale. Various efforts, mainly centered on controlling solvent spreading during stamping and supplying a sufficient amount of base to the surface to effect hydrolysis, were made to micropattern fluorocarbon-modified PHEMA films hydrolytically. Ultimately this approach is relatively unreliable and, on the microscale, unable to fully meet the expectations offered by the macroscale success.

References

1. Xia, Y. N.; Whitesides, G. M. "Soft Lithography," *Annual Review of Materials Science* **1998**, *28*, 153-184.

2. Wallraff, G. M.; Hinsberg, W. D. "Lithographic Imaging Techniques for the Formation of Nanoscopic Features," *Chemical Reviews* **1999**, *99*, 1801-1821.

3. Seemann, R.; Brinkmann, M.; Kramer, E. J.; Lange, F. F.; Lipowsky, R. "Wetting Morphologies at Microstructured Surfaces," *Proceedings of the National Academy of Sciences of the United States of America* **2005**, *102*, 1848-1852.

4. Fan, F. Q.; Stebe, K. J. "Assembly of Colloidal Particles by Evaporation on Surfaces with Patterned Hydrophobicity," *Lanmguir* **2004**, *20*, 3062-3067.

5. Böltau, M.; Walheim, S.; Mlynek, J.; Krausch, G.; Steiner, U. "Surface-Induced Structure Formation of Polymer Blends on Patterned Substrates," *Nature* **1998**, *391*, 877-879.

6. Ciobanu, M.; Kincaid, H. A.; Jennings, G. K.; Cliffel, D. E. "Photosystem I Patterning Imaged by Scanning Electrochemical Microscopy," *Langmuir* **2005**, *21*, 692-698.

7. Zhao, B.; Moore, J. S.; Beebo, D. J. "Pressure-Sensitive Microfluidic Gates Fabricated by Patterning Surface Free Energies inside Microchannels," *Langmuir* **2003**, *19*, 1873-1879.

8. Zhou, F.; Liu, Z. L.; Li, W. N.; Hao, J. C.; Chen, M.; Liu, W. M.; Sun, D. C. "Selective Electrodeposition and Etching on Polymer Brush Template Prepared by Patterned Monolayer Surface Initiated Polymerization," *Chemistry Letters* **2004**, *33*, 602-603.

9. Xia, Y. N.; Whitesides, G. M. "Soft Lithography," *Angewandte Chemie-International Edition* **1998**, *37*, 551-575.

10. Kumar, A.; Biebuyck, H. A.; Whitesides, G. M. "Patterning Self-Assembled Monolayers - Applications in Materials Science," *Langmuir* **1994**, *10*, 1498-1511.

11. Guo, W. F.; Jennings, G. K. "Directed Growth of Polymethylene Films on Atomically Modified Gold Surfaces," *Advanced Materials* **2003**, *15*, 588-591.

12. Jeon, N. L.; Finnie, K.; Branshaw, K.; Nuzzo, R. G. "Structure and Stability of Patterned Self-Assembled Films of Octadecyltrichlorosilane Formed by Contact Printing," *Langmuir* **1997**, *13*, 3382-3391.

13. Yang, K. L.; Cadwell, K.; Abbott, N. L. "Contact Printing of Metal Ions onto Carboxylate-Terminated Self-Assembled Monolayers," *Advanced Materials* **2003**, *15*, 1819-1823.

14. Delamarche, E.; Donzel, C.; Kamounah, F. S.; Wolf, H.; Geissler, M.; Stutz, R.; Schmidt-Winkel, P.; Michel, B.; Mathieu, H. J.; Schaumburg, K. "Microcontact Printing Using Poly(Dimethylsiloxane) Stamps Hydrophilized by Poly(Ethylene Oxide) Silanes," *Langmuir* **2003**, *19*, 8749-8758.

15. Campbell, C. J.; Smoukov, S. K.; Bishop, K. J. M.; Grzybowski, B. A. "Reactive Surface Micropatterning by Wet Stamping," *Langmuir* **2005**, *21*, 2637-2640.

16. Shah, R. R.; Merreceyes, D.; Husemann, M.; Rees, I.; Abbott, N. L.; Hawker, C. J.; Hedrick, J. L. "Using Atom Transfer Radical Polymerization to Amplify Monolayers of Initiators Patterned by Microcontact Printing into Polymer Brushes for Pattern Transfer," *Macromolecules* **2000**, *33*, 597-605.

17. Dyer, D. J. "Patterning of Gold Substrates by Surface-Initiated Polymerization," *Advanced Functional Materials* **2003**, *13*, 667-670.

18. Tu, H.; Heitzman, C. E.; Braun, P. V. "Patterned Poly(N-Isopropylacrylamide) Brushes on Silica Surfaces by Microcontact Printing Followed by Surface-Initiated Polymerization," *Langmuir* **2004**, *20*, 8313-8320.

19. Farhan, T.; Huck, W. T. S. "Synthesis of Patterned Polymer Brushes from Flexible Polymeric Films," *European Polymer Journal* **2004**, *40*, 1599-1604.

20. Kratzmuller, T.; Appelhans, D.; Braun, H.-G. "Ultrathin Microstructured Polypeptide Layers by Surface-Initiated Polymerization on Microprinted Surfaces," *Advanced Materials* **1999**, *11*, 555-558.

21. Guo, W. *Atomic Scale Modification of Metal Surfaces to Impact the Surface-Catalyzed Growth of Polymethylene Films*. Doctoral Thesis, Chemical Engineering, Vanderbilt University, 2003.

22. Bai, D.; Jennings, G. K. "Surface-Catalyzed Growth of Polymethylene-Rich Copolymer Films on Gold," *Journal of the American Chemical Society* **2005**, *127*, 3048-3056.

23. Hosoi, A. E.; Kogan, D.; Devereaux, C. E.; Bernoff, A. J.; Baker, S. M. "Two-Dimensional Self-Assembly in Diblock Copolymers," *Physical Review Letters* **2005**, *95*.

24. Tsai, I. Y.; Kimura, M.; Russell, T. P. "Fabrication of a Gradient Heterogeneous Surface Using Homopolymers and Diblock Copolymers," *Langmuir* **2004**, *20*, 5952-5957.

25. Lonostro, P. "Phase-Separation Properties of Fluorocarbons, Hydrocarbons and Their Copolymers," *Advances in Colloid and Interface Science* **1995**, *56*, 245-287.

26. Hirano, K.; Suzuki, K.; Nakano, K.; Tosaka, M. "Phase Separation Structure in the Polymer Blend of Fluorocarbon Elastomer and Hydrogenated Nitrile Rubber," *Journal of Applied Polymer Science* **2005**, *95*, 149-156.

27. Gudipati, C. S.; Greenlief, C. M.; Johnson, J. A.; Prayongpan, P.; Wooley, K. L. "Hyperbranched Fluoropolymer and Linear Poly(Ethylene Glycol) Based Amphiphilic Crosslinked Networks as Efficient Antifouling Coatings: An Insight into the Surface Compositions, Topographies, and Morphologies," *Journal of Polymer Science Part a-Polymer Chemistry* **2004**, *42*, 6193-6208.

28. Houseman, B. T.; Mrksich, M. "The Microenvironment of Immobilized Arg-Gly-Asp Peptides Is an Important Determinant of Cell Adhesion," *Biomaterials* **2001**, *22*, 943-955.

29. Drumheller, P. D.; Hubbell, J. A. "Polymer Networks with Grafted Cell-Adhesion Peptides for Highly Biospecific Cell Adhesive Substrates," *Analytical Biochemistry* **1994**, *222*, 380-388.

30. Chaudhury, M. K.; Whitesides, G. M. "How to Make Water Run Uphill," *Science* **1992**, *256*, 1539-1541.

CHAPTER VIII

CONCLUSIONS AND FUTURE WORK

Conclusions

The overall work presented herein demonstrates a variety of tools available to engineer the architecture and physicochemical properties of polymeric films and structures. Surface-initiated growth of PHEMA via water-accelerated ATRP provides a great deal of control over film thickness. This hydroxyl-laden polymer can then be used as a base film for the addition of numerous functionalities, namely perfluoroalkyl, perfluoroaryl, and alkyl side chains via an acylation reaction, to dramatically alter film structuring and surface and barrier properties. Extremely hydrophobic and even oleophobic surfaces can be created by modifying PHEMA with long perfluoroalkyl and alkyl groups. Film barrier properties, which are up to five orders of magnitude higher than the base PHEMA film, are highly dependent on conversion of hydrophilic hydroxyl groups to hydrophobic fluorocarbon and hydrocarbon side chains but also depend to a lesser degree on overall film structuring and surface hydrophobicity. Utilizing a wide range of chain lengths for both alkyl and perfluoroalkyl modifications allows film properties, especially surface energy and film structuring, to be tuned simply by the choice of modifying species.

Hydrolysis of perfluoroaryl-modified PHEMA films can be performed in a controlled fashion to create block-like copolymer films by regenerating and subsequently rederivatizing hydroxyl groups in a surface region of the film. Since the effects of a

variety of modifying species on film properties are known, hydrolysis may be combined with a surface modification choice to engineer surface wettability while maintaining a bulk fluorocarbon barrier film. Film barrier properties can be boosted an order of magnitude beyond those of the base homopolymer film upon addition of hydrophobic surface modifications. An even greater degree of engineering control over film properties is demonstrated by the creation of block copolymer films in this manner.

Microcontact printing can be used to extend film modifications to the microscale. μCP of the ATRP disulfide initiator directly onto gold to create a micropatterned PHEMA or modified PHEMA film leaves bare gold regions throughout the surface, which can subsequently be used for further processing. An inert hydrocarbon film, PM, can be grown via surface-catalyzed polymerization in these gold regions to create microdomains of hydrophilic/hydrophobic or fluorocarbon/hydrocarbon composition on the surface, which cannot be made using reactive modification steps. Hydrolysis of fluorocarbon-modified PHEMA was attempted via μCP, but it was unsuccessful for the formation of well-defined patterns.

The techniques described here hold promise for the application-specific engineering of polymer films and coatings. The fluorocarbon- and hydrocarbon-rich films described here could find use as dielectrics, etch resists, water- and oil-repellent coatings, and ultrathin membrane skins.

Future Work

Dependence of Film Properties on Thickness

The polymers discussed throughout this work were based almost exclusively on a PHEMA film that was grown for 12 h and had a thickness of ~220 nm. In many applications, it is advantageous to minimize film thickness while maintaining desirable surface and barrier properties. Altering polymerization time to decrease PHEMA film thickness would provide an additional aspect of film control (demonstrated in Figure 3.2) that has yet to be explored in regard to post-polymerization modification schemes. Upon modification of thinner PHEMA films with fluorocarbon and hydrocarbon side chains, many film properties would be expected to remain the same. However, barrier properties of the films should gradually decrease until the initiator monolayer becomes a more dominant barrier at low frequency. Since these same types of films have already found use in membranes,[1,2] where flux as well as selectivity are of importance, the dependence of barrier properties on film thickness would be useful in system design. As film thickness decreases, the polymer films may also structure differently or even exhibit dynamic or stimulus-responsive behavior that is often observed in thinner polymer films.[3,4]

Probing the Hydrolysis Interface of Block-like Copolymer Films

The interface resulting from hydrolysis of perfluoroaryl-modified PHEMA in the creation of block-like copolymer films appears to be confined to a region near the film surface. Based on overwhelming circumstantial evidence, the reaction appears to exhibit

diffusion-limited behavior. However, the interface created during this process could be more completely and accurately characterized using neutron reflectivity, which is often a tool of choice for the evaluation of polymer interfaces.[5] Since fluorocarbons and hydrocarbons have vastly different scattering lengths, the presence of fluorocarbon below the interface and only hydrocarbon above it creates an excellent natural point of contrast within these samples.[6] Furthermore, neutron reflectivity is capable of resolving nanometer distances over penetration depths of 100 nm or greater,[7] which would yield a sufficient depth profile to capture the interfacial behavior for controlled hydrolysis of perfluoroaryl-modified PHEMA. Using this technique, one could characterize diffusion-like behavior of the hydrolysis reaction and subsequently the copolymer interface.

Probing PHEMA/PM and F7/PM Interfacial Regions

The mixed PHEMA and PM films created in this work exhibited interesting interfacial behavior, particularly the existence of a gap between PHEMA and PM regions resulting from the growth mechanics of patterned polymer films. Creation of submicron patterned features may be possible by taking advantage of the gap present in PHEMA/PM. To further probe the extent of this gap, EIS may be used to investigate the film barrier properties. Although the PHEMA film is already a poor barrier, the gap should create a less-obstructed path to the underlying gold surface. Based on the results already presented in this work, we would expect a very thin film of PM and perhaps a layer of initiator in this gap near the surface. Compared to the remainder of the substrate area, however, these gaps comprise a very limited area, should offer even less of a barrier to transport of various materials, and could prove to be ideal sites for performing

chemistry on much smaller scales. It may even be possible to create stamps for μCP that have relief features mimicking the gap of PHEMA/PM by curing an elastomer solution on top of one of these patterned surfaces.

Hydrolytic Patterning of Fluorinated PHEMA Using Hydrogel Stamps

The hydrolytic patterning of fluorocarbon-modified PHEMA films was successfully demonstrated on the macroscale but encountered solvent spreading and base concentration issues when attempts were made to apply it to the microscale. The work of Grzybowski and coworkers[8] demonstrated the use of agarose and polyacrylamide hydrogel stamps for reactive patterning of substrates. They delivered potassium dichromate to various polymer surfaces to oxidize the surface, making it hydrophilic. This procedure is similar to our attempts to hydrolytically pattern fluorinated PHEMA with KOH. The use of a hydrogel would allow aqueous solutions of KOH to be used, and KOH has a much higher solubility in water than in ethanol. Furthermore, the hydrogel should absorb significantly more of the aqueous inking solution than the PDMS stamp could absorb the ethanolic inking solution. The one limitation present for hydrolytic patterning (that they did not encounter and that may ultimately be the most important factor in utilizing the process for fluorocarbon-modified PHEMA films) is the shrinking of film thickness upon hydrolysis, which may inhibit continuous contact of the stamp and surface. If prolonged contact is not possible, either a sufficient amount of KOH must be applied upon initial contact or only partial patterned film hydrolysis will be accomplished.

References

1. Balachandra, A. M.; Baker, G. L.; Bruening, M. L. "Preparation of Composite Membranes by Atom Transfer Radical Polymerization Initiated from a Porous Support," *Journal of Membrane Science* **2003**, *227*, 1-14.

2. Sun, L.; Baker, G. L.; Bruening, M. L. "Polymer Brush Membranes for Pervaporation of Organic Solvents from Water," *Macromolecules* **2005**, *38*, 2307-2314.

3. Granville, A. M.; Boyes, S. G.; Akgun, B.; Foster, M. D.; Brittain, W. J. "Thermoresponsive Behavior of Semifluorinated Polymer Brushes," *Macromolecules* **2005**, *38*, 3263-3270.

4. Granville, A. M.; Boyes, S. G.; Akgun, B.; Foster, M. D.; Brittain, W. J. "Synthesis and Characterization of Stimuli-Responsive Semifluorinated Polymer Brushes Prepared by Atom Transfer Radical Polymerization," *Macromolecules* **2004**, *37*, 2790-2796.

5. Zhang, Y. M.; Li, W.; Tang, B.; Ge, S.; Hu, X.; Rafailovich, M. H.; Sokolov, J. C.; Gersappe, D.; Peiffer, D. G.; Li, Z.; Dias, A. J.; McElrath, K. O.; Lin, M. Y.; Satija, S. K.; Urquhart, S. G.; Ade, H. "Interfacial Properties of Elastomer Blends as Studied by Neutron Reflectivity," *Polymer* **2001**, *42*, 9133-9141.

6. Traiphol, R.; Smith, D. W.; Perahia, D. "Surface Ordering in Thin Films of Liquid-Crystalline Polymers Containing Fluorinated and Protonated Segments: Neutron-Reflectometry Study," *Journal of Polymer Science Part B-Polymer Physics* **2002**, *40*, 2817-2824.

7. Penfold, J. "Neutron Reflectivity and Soft Condensed Matter," *Current Opinion in Colloid & Interface Science* **2002**, *7*, 139-147.

8. Campbell, C. J.; Smoukov, S. K.; Bishop, K. J. M.; Grzybowski, B. A. "Reactive Surface Micropatterning by Wet Stamping," *Langmuir* **2005**, *21*, 2637-2640.

APPENDIX A

SURFACE-INITIATED ATRP PROCEDURE

1. Initiation of Surface

    a) The disulfide initiator $(S(CH_2)_{11}OC(O)C(CH_3)_2Br)_2$ was prepared according to literature procedures to give a viscous yellow liquid.
    b) The tip of a glass pipette was dipped directly into the initiator to collect a small volume.
    c) Ethanol was squirted into the top of the pipette and the resulting initiator/ethanol solution was collected in a glass vial.
    d) Ethanol was poured into the vial until approximately half full.
    e) At most, eight gold samples were placed into a single vial for at least 2 h (but generally for 24 h) to give initiated gold samples.
    f) Upon initiation, samples were removed from the solution, rinsed with ethanol, and dried with nitrogen.

2. Apparatus

    a) The following was set up in a fume hood with clamps: a vacuum pump connected with hose directly to a vacuum trap that was, in turn, connected to a vacuum manifold.
    b) Before each polymerization, the manifold was checked for cracks and all valves were placed into the closed position.
    c) Into a clean Schlenk flask, the appropriate weighed amounts of bipyridine, $CuBr_2$, and CuCl were placed along with a stir bar. Please note that the Schlenk flask should never be much more than half full, as it may explode during processing if overly full. Keep this in mind while planning for the volume of solution (and accordingly, these solids) to be added during polymerization.
    d) A large rubber septum was pulled down over the top opening of the Schlenk flask to seal it off. The fitting for the sidearm of the flask was screwed in to a closed position.
    e) Two pieces of copper (or other suitably malleable but strong) wire were twisted together and then used to tie down the rubber septum. Pliers were used to hold both ends of the wire, pull it tightly around the septum, and twist it.
    f) The sealed Schlenk flask was clamped into place and connected to the manifold using rubber hose.

g) The vacuum pump was turned on with both the manifold and flask valves closed. The manifold valve in line with the flask was opened slowly. Then, the flask valve was opened slowly until the flask was evacuated, as evidenced by the rubber septum being sucked down tightly onto the flask opening.
h) Upon flask evacuation, the flask valve was closed and nitrogen was introduced to the flask through the rubber septum via a needle connected to a hose from a nitrogen gas cylinder. The nitrogen flow through the needle should be very small (i.e. you should just lightly feel the flow if you direct it toward your arm). The needle was removed from the flask once the rubber septum popped back up (or no more than 5-10 sec). Continuing gas flow in this state too long presents a hazard, as the pressure builds up within the flask.
i) Evacuation and filling with nitrogen were repeated twice, ending with a moderately nitrogen-filled flask.
j) A 1:1 v:v mixture of hydroxyethyl methacrylate (or other monomer):water was measured out using a graduated cylinder and poured into a beaker.
k) A needle and syringe were used to introduce the monomer/water solution into the flask through the rubber septum. If the pressure in the flask is too low initially, the liquid will be drawn out of the syringe and into the flask. If the pressure is too high, the liquid will need to be forced into the flask. Under this latter condition and after emptying the syringe, simply suck air into the syringe and discharge into the hood after removal from the flask. Repeat until the flask is no longer over-pressurized. The entire volume of solution was added to the flask.
l) The solution was stirred for about 10 sec using a magnetic stirrer to get the solids and liquids mixed together. Then the stirrer was turned off.
m) A dewar was filled with liquid nitrogen and the vacuum trap was placed down into the dewar. This is most easily accomplished by sitting the dewar on an adjustable stand and raising/lowering it.
n) Once the trap was cool, the valve to the flask was opened to evacuate it. Note that the trap should always be in liquid nitrogen when the potential exists to pull a liquid from the flask. When small bubbles began forming at the top of the solution in the flask, the valve of the Schlenk flask was closed. The rubber septum should again be depressed at the top of the flask.
o) Nitrogen was added to the flask via needle as before until the septum popped back up.
p) The evacuation/filling steps were repeated twice before ending with a final evacuation step to leave the flask halfway-filled with solution and at reduced pressure.
q) The connection of the rubber hose from the manifold to the Schelnk flask was wrapped with parafilm. Also the rubber septum atop the flask was wrapped with parafilm to minimize air introduction to the flask.

3. Freeze-Pump-Thaw Cycles

    a) The liquid nitrogen dewar was removed from the vacuum trap and the lower portion of the Schlenk flask was submerged into liquid nitrogen. Liquid nitrogen only needs to come up to the level of liquid in the flask. Again, the flask should not be much more than half full, as it may explode during the freezing process.
    b) Once the liquid in the flask was frozen (typically ~ 5min), the liquid nitrogen dewar was transferred back to the vacuum trap. The flask valve was opened to begin pumping down the flask while the vacuum trap remained under liquid nitrogen.
    c) The flask continued to be pumped down until the top of the solution began to liquefy (typically ~10-15 min).
    d) The flask valve was closed. Using an adjustable stand, the partially frozen flask was placed in a room temperature water bath to thaw it out (typically ~30 min).
    e) The water bath was removed and the bottom of the flask was dried with a paper towel.
    f) The freeze, pump, and thaw steps were repeated twice more (for a total of three cycles). Additional cycles may be run if desired but three cycles are most often used in the literature.
    g) At the conclusion of the third (or last) thaw cycle, the flask was filled with nitrogen gas via needle as before.
    h) The solution was stirred with a magnetic stirrer until a homogeneous brown solution formed (at least 10 min). It does not hurt, however, to leave the solution stirring for a couple of hours.

4. Preparation of samples in vials

    a) A line was made with permanent marker on the outside of clean vials to denote the fill level for the desired volume (typically 8mL). Samples were placed into these marked vials. Generally up to eight samples may be placed in each vial. It is important that the gold side of samples do not touch, as this could introduce scratches and may limit possible film growth in the confined areas.
    b) Once the desired samples were placed in the vial, a small rubber septum was pulled down over the top opening of the vial to seal it off. As with the Schlenk flask, pliers and two wires twisted together were then used to tie off the septum.
    c) A rubber hose with a needle attachment on one end was connected to the side of the manifold under vacuum. The valve corresponding to this attached hose was opened.
    d) Each vial was degassed by carefully inserting the needle from this new attachment into flask through the rubber septum.

e) The vials were subsequently backfilled with nitrogen using a needle as before. Care must be taken when degassing/backfilling the vials (particularly backfilling a vial with numerous samples) to ensure that the samples are not knocked around and fall atop one another.
f) The degassing/backfilling procedure was performed two more times for each vial, ending with backfilling the vial with nitrogen.

5. Transfer of reaction mixture to vials

a) To transfer the reaction mixture into the vials without exposure to oxygen, nitrogen was introduced to the flask via needle as before. Once the rubber septum popped up and the flask was filled with nitrogen, one end of a cannula was also inserted into the flask. It is important that the nitrogen flow and amount of nitrogen in the flask be such (over-pressurized) that when the cannula is inserted, nitrogen is vented out through the cannula. The cannula should NOT be inserted into the liquid at this point.
b) The other end of the cannula was inserted into a degassed/backfilled vial. Once the vial filled with nitrogen (typically ~1-2 sec), a needle attached to a bubbler was also inserted into the vial. Nitrogen should immediately be vented through the bubbler, resulting in a steady rate of bubbles through the mineral oil of the bubbler.
c) Stirring of the reaction mixture was stopped at this point, and the cannula was dipped into the reaction mixture in the flask. After approximately 10 sec, the brown liquid began flowing from the other end of the cannula into the sample vial. Nitrogen flow may be adjusted slightly to slow or speed up flow of the reaction mixture through the cannula. Few or no bubbles were present in the bubbler at this point.
d) Once the reaction mixture level in the vial was approximately halfway to the marked volume line, polymerization time was recorded starting at this point.
e) The mixture continued to be fed into the vial until the volume reached the marked line. At this point, the end of the cannula in the Schlenk flask was pulled up out of the reaction mixture, and flow into the vial correspondingly ceased after a few seconds. Nitrogen began flowing through the bubbler again.
f) To seal the vial off for polymerization, the end of the cannula in the vial was first removed, followed by removal of the needle to the bubbler.
g) The vial was subsequently wrapped completely in parafilm and set aside to polymerize for the desired period of time.
h) To ensure homogeneity of the reaction mixture, the solution was stirred again for a few seconds. The process for introducing the reaction mixture was repeated for each vial.

6. Clean-up

    a) After finishing all vials, the vacuum pump and nitrogen gas flow were turned off.
    b) The manifold was slowly opened to atmospheric pressure by opening one of the valves on the side of the manifold not under vacuum.
    c) All waste was disposed of properly.
    d) The cannula was cleaned by filling the Schlenk flask with water and putting nitrogen on it with the cannula inserted. The cannula was dipped into the water and allowed to purge with water directly into the waste container for several minutes.
    e) The Schlenk flask was cleaned with soap and water to prepare it for the next use.